Dissertation

submitted to the

Combined Faculty of Mathematics, Engineering and Natural Sciences

of the

Heidelberg University, Germany

for the degree of

Doctor of Natural Sciences

Put forward by

Carlos Fabian Jaramillo Gracia

born in Quito, Ecuador

Oral examination: 18 October 2023

A new production mechanism for Sterile Neutrino Dark Matter by varying Yukawa couplings

1st Referee: *Prof. Dr. Dr. h.c. Manfred Lindner*

2ndReferee: *Prof. Dr. Tilman Plehn*

Author: *Carlos F. Jaramillo G.*

In Gedenken an Julia Schäfer
⋆ 26.11.1992 · † 24.10.2021

Ich vermisse dich jeden Tag
und werde dich immer lieben...

Abstract

In this thesis, a new production mechanism for sterile neutrino dark matter is proposed, which, in contrast to previous research, relies neither on the oscillations between active and sterile neutrinos, nor on the decay of heavier additional degrees of freedom, nor on new exotic neutrino interactions beyond the Yukawa coupling to the Standard Model. Instead, we generate the abundance of sterile neutrinos by decoupling from thermal equilibrium, as is typical for WIMPs. This type of production mechanism is usually not viable for sterile neutrinos, because the longevity requirement mandates that the neutrino Yukawa coupling be very tiny, which prevents the dark matter neutrinos from reaching thermal equilibrium. We resolve this conflict by invoking varying Yukawa couplings, going from sizeable values at early times, thus enabling the sterile neutrinos to thermalize, and then becoming suppressed during a phase transition, thereby forcing the sterile neutrinos to decouple and stay quasi-stable thereafter. We formulate an implementation of varying Yukawa couplings based on a Froggatt-Nielsen model, where the vacuum expectation value of the flavon changes during a phase transition, thereby dynamically driving the suppression of the Yukawa couplings and inducing the decoupling of the sterile neutrinos. We show that our mechanism successfully generates 100% of the observed dark matter in the form of sterile neutrinos with masses in the keV range. The necessary phase transition is provided by the spontaneous breaking of the electroweak symmetry. Furthermore, the active neutrino oscillation parameters are reproduced and simultaneously the flavour hierarchy in the lepton sector is alleviated.

Zusammenfassung

In dieser Dissertation wird ein neuer Produktionsmechanismus für Dunkle Materie in Form von sterilen Neutrinos vorgebracht. Im Gegensatz zu früheren Arbeiten, welche Oszillationen zwischen aktiven und sterilen Neutrinos, Zerfälle schwererer zusätzlicher Teilchen oder neue exotischen Neutrino-Wechselwirkungen jenseits des Standardmodells benötigen, erzeugen wir die Menge der Dunkle-Materie-Neutrinos durch das Entkoppeln vom thermischen Gleichgewicht, wie es für WIMPs typisch ist. Dieser Produktionsmechanismus ist normalerweise nicht möglich, da die Stabilität von Dunkler Materie auf kosmologischen Zeitskalen eine sehr kleine Neutrino-Yukawa-Kopplung erfordert, welche wiederum eine thermische Produktion durch das primordiale Plasma verhindert. Wir lösen diesen Konflikt, indem variierende Yukawa-Kopplungen postuliert werden, welche im frühen Universum anfänglich große Werte annehmen, durch einen auftretenden kosmologischen Phasenübergang im Folgenden jedoch stark unterdrückt werden. Dies ermöglicht eine Thermalisierung steriler Neutrinos vor dem Phasenübergang sowie eine Entkopplung vom thermischen Plasma bei gleichzeitiger Quasi-Stabilität danach. Das vorliegende Mechanismus variierender Yukawa-Kopplungen basiert auf einem Froggatt-Nielsen-Modells, in welchen die Veränderung des Flavon-Vakkumerwartungswertes die Unterdrückung der Yukawa-Kopplungen dynamisch antreibt und die Entkopplung der sterilen Neutrinos induziert. Es wird im Folgenden gezeigt, dass dieser Mechanismus eine vollständige Produktion der beobachteten Menge an Dunkler Materie in Form von sterilen Neutrinos im keV-Massenbereich erlaubt, wenn der notwendige Phasenübergang durch die spontane Brechung der Elektroschwachen Symmetrie induziert wird. Gleichzeitig werden die beobachteten Parameter der aktiven Neutrino Oszillationen reproduziert und die Flavour-Hierarchie im Leptonsektor abgemildert.

Contents

Chapter 1

Introduction

"There are more things in heaven and earth, Horatio,
Than are dreamt of in your philosophy."
- William Shakespeare in *Hamlet*

These lines, written by the great poet William Shakespeare around the year 1600, could well be said today to describe the state of our understanding of nature and the Universe. Since Galileo Galilei pointed his telescope to the night sky and became the first person to discover some of the wonders of our solar system, we have made astonishing progress in our scientific pursuit to understand the world around us. Just in the recent decades, we have discovered that space itself is expanding, i.e. all galaxies are receding away from each other; we came to understand how the light chemical elements were formed in the early Universe, and how heavier metals are produced by stars; we measured and analysed the cosmic microwave background (CMB), which can rightly be called the afterglow of the big bang; and we have detected gravitational wavesx (GW) and black holes (BHs). With the discovery of the Higgs boson [1, 2] at CERN's large hadron collider (LHC) in 2012, the last missing piece of the Standar Model of particle physics (SM) was detected. It can be argued that the SM is one of the most successful scientific theories that have ever been formulated, as its predictions have been confirmed to impressive levels of accuracy and it has withstood all tests with great precision.[1] The extent to which our knowledge and understanding about the Cosmos has grown is truly mind-boggling. As Albert Einstein is credit with saying, *"The most incomprehensible thing about the universe is that it is comprehensible"*. And yet, whats is even more exciting, we know that our theories are still incomplete. Although some of the remaining open questions can be said to be only of aesthetic nature, two particular

[1] Of course, there have been and still are some anomalies that need explaining, but as of the date of writing of this thesis, none have been conclusively confirmed to disprove the SM or indeed indicate new physics, see for example Ref. [3].

puzzles clearly indicate that we still have a lot to discover:

1. **The Origin of the mass of neutrinos.** For many years, physicists were puzzled by the so called *atmospheric-* and *solar neutrino problems*. The puzzle consisted in a mysterious discrepancy between the predicted and measured (flavour specific) neutrino fluxes produced by cosmic rays interacting with our atmosphere and by nuclear interactions in the sun [4]. It soon became apparent that this puzzle could be resolved by the phenomenon of *neutrino oscillations*, whereby neutrinos of one flavour transform back and forth into a different neutrino flavour during propagation. This phenomenon is only possible if the neutrinos are not massless.[2] However, within the SM, neutrinos were thought to be massless because the theory does not include *right-handed* neutrinos, which would be necessary for the SM neutrinos to acquire mass by the same means as the other fermions in the theory. And even if right-handed (RH) neutrinos were added *a posteriori* by hand, the mass scale of the neutrinos would be $\sim$ 6 orders of magnitude smaller that that of the electron, the lightest fermion in the SM. When neutrino oscillations were finally confirmed by the SNO and Super-Kamiokande experiments, for which the 2015 Novel Prize in Physics was awarded [5], it became clear that the SM would have to be amended or modified to accommodate a mechanism to generate neutrino masses.

2. **The nature of Dark Matter.** Astronomical and astrophysical observations strongly suggest the existence of a non-baryonic substance that permeates the Universe and interacts gravitationally with common matter. This mysterious substance was first postulated by the Swiss astronomer Fritz Zwicky, who noted that the observable mass in the Coma Cluster was insufficient to keep the galaxies bound in the cluster; for this invisible massive substance he coined the term *Dark Matter* [6]. Later observations on other galaxy clusters and also single galaxies confirmed the necessity for dark matter (DM) to explain the dynamics of these systems. Initially, dark astrophysical objects were thought to be responsible for these puzzling observations, but the failure to detect them even with modern sophisticated instruments, such as the Hubble Space Telescope, ruled them out as a viable explanation (with the exception of a quite narrow window for sub-planetary masses) [7]. Additional cosmological evidence for DM was later obtained by observations from gravitational lensing, the Large-Scale Structure (LSS) of the Universe and the Cosmic Microwave Background. While there have been attempts to explain these observations by modified theories of gravity, none have been convincingly successful. Various current constrains also disfavour the idea that Primordial Black Holes (PBHs) contribute significantly to the bulk of the Dark Matter density. Thus, the dominating current consensus in the

[2] More precisely, it is the mass squared differences of the neutrino mass eigenstates that may not vanish, i.e. $\Delta m_{ij}^2 = m_i^2 - m_j^2 \neq 0$, implying that the masses of the neutrinos must be finite and non-degenerate.

scientific community is that a new particle exists, the Dark Matter particle, which is massive and, beyond gravitationally, only interacts very weakly (or perhaps not at all) with the SM particles and is responsible for the aforementioned phenomena. However, very little is known about the properties of the DM particle or how it came to be produced in the early Universe. Nevertheless, one thing seems certain: whatever the answer to these questions is, it will most probably involve some form of new physics.

It is intriguing to think about the possibility, that the solutions to these problems might actually be related to each other. Not only that, but they might also help to answer other open questions in fundamental physics, such as origin of the matter-antimatter asymmetry, the wide mass differences in the fermion sector and the hierarchy problem.

Many particles have been proposed to serve as DM candidates and explain the observations mentioned above. Accordingly, a great deal of effort and resources have gone into building experiments and detectors to search for these DM candidates. Similarly, many models have been formulated to extend the SM and implement some mechanism to generate masses for the neutrinos. Most of these models introduce new beyond the Standard Model (BSM) particles, some of which could be viable DM candidates. A prime example of this are RH Majorana neutrinos, which are SM-singlets and can couple to the left-handed (LH) neutrinos of the SM through the usual Yukawa terms in the Lagrangian. We often refer to these RH neutrinos as *sterile neutrinos*. Their presence in the Lagrangian permits the generation of Dirac masses for the neutrinos and, as we will see in section 3.3, the Majorana properties of the sterile neutrinos neatly explain the tiny size of the active neutrino masses.

Our main aim in this doctoral thesis will be to investigate a class of models where sterile neutrinos simultaneously play the role of the DM particle. As will be discussed later, one of the main challenges when proposing a viable DM candidate, is the fact that one must deliver a computable mechanism by which the DM particles are produced in the early Universe, and the result of this computation must agree with the observed Dark Matter density. This requirement constrains the available parameter space of many, otherwise very appealing, DM models. And this is precisely where the focus of this work will be: we will propose a new concept by which sterile neutrinos are produced in the early Universe and after their production "go on to live their lives" as DM particles. Furthermore, we will see that particular realisations of this new concept can shed light on the so-called flavour puzzle, i.e. the origin of the peculiar hierarchy in the fermion masses. Of course, sterile neutrinos have been considered as Dark Matter candidates for a long time already, but as we will later see in detail, constrains on their stability have ruled out the most straightforward production mechanisms.

In a nutshell, the starting point for us in this work will be the extension of the SM to include three RH neutrinos and the Type I *Seesaw Mechanism*. Adding RH neutrinos to the SM makes it possible to write Yukawa terms for the neutrinos, which after electroweak symmetry breaking (EWSB) generate a Dirac mass for the

neutrinos. Also, because the sterile neutrinos are SM singlets, it is possible to write a Majorana mass term for them. Then, through the well-known Seesaw Mechanism, one ends up with three very light mass eigenstates, mostly aligned with the LH neutrinos, and a certain number of very heavy mass eigenstates that are mostly composed of the RH or sterile states. The main idea and scientific contribution of this doctoral thesis can be summarised as follows: by promoting the Yukawa couplings to dynamic variables which change in value during a brief period in the early Universe, we will be able to simultaneously guarantee the cosmological longevity of the sterile neutrinos while also successfully achieving the thermal production of the right amount of sterile neutrinos so that the may account for the observed DM density.

Before diving into the details and subtleties of this new production mechanism for sterile neutrino Dark Matter, in what is left of this chapter, we give a very short presentation of the relevant aspects of the SM, so as to introduce some of the necessary vocabulary. The subject matter of this work touches on three important topics of particle physics: the flavour puzzle, neutrinos and DM. Therefore, the flavour puzzle will be introduced in the second chapter, along with a popular model to address it. In the third chapter, we discuss the phenomenon of neutrino oscillations and the problem of neutrino masses. In chapter four we start by reviewing the evidence for the existence of DM and present some of the most common DM candidates before diving into the freeze-out mechanism and sterile neutrinos as DM candidates. Chapter five is the heart of this thesis, where we introduce and study the new production mechanism for sterile neutrino DM proposed here. For the reader who is already familiar with the material presented in the previous chapters, or who is simply in a hurry, we strongly recommend reading the introduction to chapter five. Finally, we conclude with with a summary and some closing remarks in chapter six.

1.1 The Standard Model in a Nutshell

To set the stage for the following chapters, we will here very briefly introduce the portions of the SM that are most relevant for this thesis; and for more details on the SM we refer to the standard book by Schwartz [8] or any other textbook or review available in the literature. The SM is a gauge theory invariant under the group $\mathrm{SU}(3)_\mathrm{c} \times \mathrm{SU}(2)_L \times \mathrm{U}(1)_Y$, equipped with the associated gauge bosons G^a_μ, W^a_μ and B_μ respectively, where a is the $\mathrm{SU}(2)_L$ group-generator index and μ is a Lorentz index. The theory further contains fermionic matter fields that are charged under the SM-group according to table 1.1 and a complex scalar $\mathrm{SU}(2)_L$ doublet H, that contains *the Higgs boson*,

$$H = \begin{pmatrix} H^+ \\ H^0 \end{pmatrix}. \tag{1.1}$$

Table 1.1. Standard Model fermions in their $\mathrm{SU}(2)_L$ representation and their charges under the SM group $\mathrm{SU}(3)_\mathrm{c} \times \mathrm{SU}(2)_L \times \mathrm{U}(1)_Y$. The α index stands for the fermion generations. All fermions have spin 1/2, while all gauge bosons (which are not included in the table) have spin 1 and exist in the adjoint representation of their respective subgroups. The Higgs H is a complex scalar and its SM-representation is $(\mathbf{1}, \mathbf{2}, 1)$.

Field		Charge under $\mathrm{SU}(3)_\mathrm{c} \times \mathrm{SU}(2)_L \times \mathrm{U}(1)_Y$
Quark doublets	$Q_\alpha = \begin{pmatrix} u_L \\ d_L \end{pmatrix}, \begin{pmatrix} c_L \\ s_L \end{pmatrix}, \begin{pmatrix} t_L \\ b_L \end{pmatrix}$	$(\mathbf{3}, \mathbf{2}, 1/3)$
up quark singlets	$u_\alpha = (u_R,\, c_R,\, t_R)$	$(\mathbf{3}, \mathbf{1}, 4/3)$
down quark singlets	$d_\alpha = (d_R,\, s_R,\, b_R)$	$(\mathbf{3}, \mathbf{1}, -2/3)$
Lepton doublets	$L_\alpha = \begin{pmatrix} \nu_{eL} \\ e_L \end{pmatrix}, \begin{pmatrix} \nu_{\mu L} \\ \mu_L \end{pmatrix}, \begin{pmatrix} \nu_{\tau L} \\ \tau_L \end{pmatrix}$	$(\mathbf{1}, \mathbf{2}, -1)$
Lepton singlets	$e_\alpha = (e_R,\, \mu_R,\, \tau_R)$	$(\mathbf{1}, \mathbf{1}, -2)$

The Higgs potential, which is responsible for the spontaneous symmetry breaking (SSB) of the electroweak symmetry, enters the Lagrangian as

$$\mathcal{L}_\mathrm{Higgs} = \mu^2\, H^\dagger H - \lambda (H^\dagger H)^2, \tag{1.2}$$

with the mass parameter μ^2 and the Higgs self-coupling λ. Provided that $\mu^2 > 0$, the field configuration with $|H| = \mu/\sqrt{\lambda}$ minimizes the potential and is thus the energetically preferred configuration; this defines the vacuum expectation value (vev) of the Higgs $v = \mu/\sqrt{\lambda}$.

The $\mathrm{SU}(2)_L$ bosons $W_\mu^{1,2}$ build linear combinations to form the physical states

$$W_\mu^\pm = \frac{1}{\sqrt{2}} \left(W_\mu^1 \mp i\, W_\mu^2 \right),$$

while the other gauge bosons W_μ^3 and B_μ are rotated into the mass basis as

$$\begin{pmatrix} Z_\mu \\ A_\mu \end{pmatrix} = \begin{pmatrix} \cos(\theta_W) & -\sin(\theta_W) \\ \sin(\theta_W) & \cos(\theta_W) \end{pmatrix} \begin{pmatrix} W_\mu^3 \\ B_\mu \end{pmatrix},$$

where θ_W is the Weinberg angle. The interactions between the gauge bosons and the fermions can be separated into so-called neutral- and charged currents (NC and CC respectively). For the neutral- and electromagnetic currents the interaction Lagrangian reads

$$\mathcal{L} \supset g_\mathrm{w}\, Z_\mu\, J_Z^\mu + e\, A_\mu\, J_\mathrm{EM}^\mu, \tag{1.3}$$

with the weak coupling $g_{\rm w} = e/\sin(\theta_W)$ and the respective currents defined as

$$J_Z^\mu = \sum_\alpha \left[\cos(\theta_W)\, \overline{\psi}_L^\alpha\, \gamma^\mu\, T^3\, \psi_L^\alpha - \frac{\sin^2(\theta_W)}{\cos(\theta_W)} \left(Y_\alpha^L\, \overline{\psi}_L^\alpha\, \gamma^\mu\, \psi_L^\alpha + Y_\alpha^R\, \overline{\psi}_R^\alpha\, \gamma^\mu\, \psi_R^\alpha \right) \right], \tag{1.4}$$

$$J_{\rm EM}^\mu = \sum_\alpha Q_\alpha \left[\overline{\psi}_L^\alpha\, \gamma^\mu\, \psi_L^\alpha + \overline{\psi}_R^\alpha\, \gamma^\mu\, \psi_R^\alpha \right], \tag{1.5}$$

where $\psi = Q,\, L,\, u, \ldots$ stands for any specific type of fermion from table 1.1, T^3 is the third $\mathrm{SU}(2)_L$ generator and $Y_\alpha^{L/R}$ stands for the hypercharge of the fermion $\psi_{L/R}^\alpha$. Furthermore, Q_α is the electric charge of the fermion ψ^α, and is defined as $Q_\alpha = T_\alpha^3 + Y_\alpha/2$. Notice that the neutral- and electromagnetic currents are flavour diagonal, i.e. only involve fermions of the same type. For the charged currents we have the interaction Lagrangian

$$\mathcal{L} \supset \frac{g_{\rm w}}{\sqrt{2}} \left(W_\mu^+\, J_+^\mu + W_\mu^-\, J_-^\mu \right), \tag{1.6}$$

where the charged currents for the leptons are given by

$$J_+^\mu = \sum_\alpha \left[\bar{\nu}_L^\alpha\, \gamma^\mu\, e_L^\alpha + \bar{u}_L^\alpha\, \gamma^\mu\, d_L^\alpha \right], \qquad J_-^\mu = \sum_\alpha \left[\bar{e}_L^\alpha\, \gamma^\mu\, \nu_L^\alpha + \bar{d}_L^\alpha\, \gamma^\mu\, u_L^\alpha \right], \tag{1.7}$$

and analogously for quarks. It is important to emphasise that the charged current interactions act only on LH fermions. However, in contrast to the neutral currents eq. (1.3) which diagonally couple fermions of the same type, the charged currents eq. (1.7) couple only the two different components of the $\mathrm{SU}(2)_L$ doublets with each other. At this point, these couplings are also diagonal, but as we will see later, they turn non-diagonal when we rotate into the mass basis. The SM group $\mathrm{SU}(3)_{\rm c} \times \mathrm{SU}(2)_L \times \mathrm{U}(1)_Y$ also allows for renormalizable terms involving one LH fermion, one RH fermion, and the Higgs boson - these are the Yukawa couplings. To write them down, we define the dual Higgs field $\widetilde{H}$ which is given by

$$\widetilde{H} = i\sigma_2\, H^\star = \begin{pmatrix} H^0 \\ -H^- \end{pmatrix}, \tag{1.8}$$

which transforms as an $\mathrm{SU}(2)_L$ doublet and carries a hypercharge of -1. The Yukawa terms then read

$$\mathcal{L}_{\rm Y} = -\, y_{\alpha\beta}^d\, \overline{Q}_L^\alpha\, H\, d_R^\beta \;-\; y_{\alpha\beta}^u\, \overline{Q}_L^\alpha\, \widetilde{H}\, u_R^\beta \;-\; y_{\alpha\beta}^e\, \overline{L}_L^\alpha\, H\, e_R^\beta \;-\; \text{h.c.} \tag{1.9}$$

where $y_{\alpha\beta}^\psi$ stands for the components of the 3×3 complex Yukawa matrix for the fermions of type ψ. Notice that there is no Yukawa term for the neutrinos; the reason for that is that there are only LH neutrinos in the SM, but no RH ones. Due to the SSB of the $\mathrm{SU}(3)_{\rm c} \times \mathrm{SU}(2)_L \times \mathrm{U}(1)_Y$ group, and after choosing the *unitary gauge* (see e.g. Ref. [8]), the masses of the fermions are generated after the

Higgs assumes its vacuum expectation value (vev),

$$\langle H \rangle = \frac{1}{\sqrt{2}} \begin{pmatrix} 0 \\ v \end{pmatrix}, \qquad \langle \widetilde{H} \rangle = \frac{1}{\sqrt{2}} \begin{pmatrix} v \\ 0 \end{pmatrix}, \tag{1.10}$$

resulting in the fermion mass Lagrangian

$$-\mathcal{L}^{\text{ferm}}_{\text{mass}} = \frac{y^d_{\alpha\beta}\, v}{\sqrt{2}}\, \bar{d}^\alpha_L\, d^\beta_R \;+\; \frac{y^u_{\alpha\beta}\, v}{\sqrt{2}}\, \bar{u}^\alpha_L\, u^\beta_R \;+\; \frac{y^e_{\alpha\beta}\, v}{\sqrt{2}}\, \bar{e}^\alpha_L\, e^\beta_R \;+\; \text{h.c.} \tag{1.11}$$

The mass matrix for the fermion ψ arises as

$$m^\psi_{\alpha\beta} = \frac{y^\psi_{\alpha\beta}\, v}{\sqrt{2}}. \tag{1.12}$$

The mass basis is the one in which the mass matrices are diagonal, or in other words, in which the Yukawa matrices are diagonal. The Yukawa matrices can always be diagonalised by a biunitary transformation, e.g.

$$y^u = U_u\, (y^u_D)\, W^\dagger_u, \qquad y^d = U_d\, (y^d_D)\, W^\dagger_d, \qquad y^e = U_e\, (y^e_D)\, W^\dagger_e, \tag{1.13}$$

with appropriate unitary matrices U_ψ and W_ψ and where y_D is diagonal with real entries. Now, by redefining the fermions as

$$u_L \to U_u\, u_L, \qquad u_R \to W_u\, u_R, \tag{1.14}$$
$$d_L \to U_d\, d_L, \qquad d_R \to W_d\, d_R, \tag{1.15}$$
$$e_L \to U_e\, e_L, \qquad e_R \to W_e\, e_R, \tag{1.16}$$

we can rewrite the mass Lagrangian in the mass basis, which then reads

$$-\mathcal{L}^{\text{ferm}}_{\text{mass}} = m^d_\alpha\, \bar{d}^\alpha_L\, d^\alpha_R \;+\; m^u_\alpha\, \bar{u}^\alpha_L\, u^\alpha_R \;+\; m^e_\alpha\, \bar{e}^\alpha_L\, e^\alpha_R \;+\; \text{h.c.} \tag{1.17}$$

These are Dirac mass terms, which mix the LH and RH components of the fermions. Again, notice that, due to the fact that RH neutrinos are not included in the SM, there is no Dirac mass term for the neutrinos. The field transformations that take us to the mass basis, i.e. eqs. (1.14) to (1.16), are also applied to other portions of the Lagrangian where the fermions appear. It is easy to see that while the neutral- and electromagnetic currents eq. (1.3) stays unchanged, the terms involving quarks in the charged currents eq. (1.7) do get modified, the result being

$$J^\mu_+ = \sum_\alpha \left[\bar{\nu}^\alpha_L\, \gamma^\mu\, e^\alpha_L + \bar{u}^\alpha_L\, \gamma^\mu\, (V_{\text{CKM}})^{\alpha\beta}\, d^\alpha_L \right], \tag{1.18}$$

$$J^\mu_- = \sum_\alpha \left[\bar{e}^\alpha_L\, \gamma^\mu\, \nu^\alpha_L + \bar{d}^\alpha_L\, \gamma^\mu\, (V^\dagger_{\text{CKM}})^{\alpha\beta}\, u^\alpha_L \right], \tag{1.19}$$

with $V_{\text{CKM}} = U^\dagger_u\, U_d$ as the famous Cabibbo-Kobayashi-Maskawa (CKM) Matrix [9,

10], which is responsible for all flavour changing effects in the quark sector.

This finalises our extremely short summary of the SM, whereby we restricted ourselves to the aspects of the SM that are most relevant for this thesis and left out a lot of important bits and parts such as the gauge sector, the Higgs potential and a more detailed discussion of EWSB. The reader is referred to [8] or any other SM textbook for a thorough discussion discussion of these topics.

Chapter 2

The Flavour Puzzle

As mentioned previously, the Higgs mechanism provides the mass terms for the fermions from the Yukawa terms in the Lagrangian. After diagonalizing the Yukawa matrices, the mass for the fermion ψ is given by

$$m_\psi = \frac{y_\psi\, v}{\sqrt{2}}. \tag{2.1}$$

The gauge couplings and the Higgs self coupling in the SM have all been measured to [8, 11]

$$g_\mathrm{s} \sim 1, \qquad g_\mathrm{w} \sim 0.6, \qquad g_\mathrm{y} \sim 0.4, \qquad \lambda \sim 0.1,$$

i.e. they all are of a comparable $\mathcal{O}(1)$ size. Thus, the first guess and naive expectation would be that the values of the Yukawa couplings are also of a similar size. Indeed, for the Yukawa coupling of the top quark, this is the case,

$$y_\mathrm{t} \sim 1,$$

leading to a top quark mass of $m_\mathrm{t} \approx 174\,\mathrm{GeV}$. However, all other Yukawa couplings turn out to have much different values - the smallest one being the Yukawa coupling of the electron, $y_\mathrm{e} \sim 10^{-6}$. It turns out that the values of the Yukawa couplings are spread out over six orders of magnitude in a hierarchical manner. This hierarchy manifests itself in the fermions masses, as can be seen in fig. 2.1. The hierarchy arises not only among the three fermion generations, but also within each fermion generation (with the exception of the first quark generation, where the down-quark is actually slightly heavier than the up-quark). Furthermore, if one assumes neutrinos to be Dirac particles and their masses to be generated by the SSB in the electroweak sector, then the hierarchy is even more severe - the Yukawa couplings would expand a range of more than twelve orders of magnitude, while leaving a huge mass gap of six orders of magnitude between the neutrinos and the charged leptons. This can be seen as a hint for a different mechanism existing behind the generation of neutrino masses.

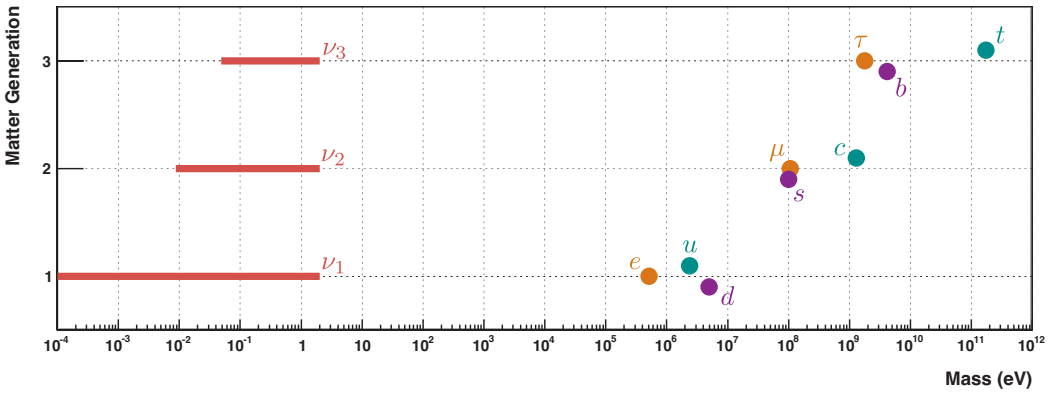

Figure 2.1. The masses of the three fermion generations, strangely spanning 6 orders of magnitude. It almost looks like each generation should form a cluster in this mass spectrum, although the masses of the top and charm quarks lie a little distant to their generation partners. In the figure, the ranges for the neutrino masses are shown too. If neutrinos are Dirac particles and their masses are generated by the SSB of the electroweak (EW) symmetry, like for all the other fermions, then the tininess of their masses exacerbate the puzzle, because it would mean that the values of the Yukawa couplings expand over more than 12 orders of magnitude. Image adapted from [12].

It is interesting to note that the SM possesses an enhanced accidental symmetry if the Yukawa terms vanish: the different fermion generations become indistinguishable - a fact which manifest itself through the invariance under the global symmetry [13]

$$G_{\text{global}}(y_\psi = 0) = \text{SU}(3)_q^3 \times \text{SU}(3)_l^2 \times \text{U}(1)^5, \tag{2.2}$$

with

$$\text{SU}(3)_q^3 = \text{SU}(3)_Q \times \text{SU}(3)_u \times \text{SU}(3)_d \tag{2.3}$$
$$\text{SU}(3)_l^2 = \text{SU}(3)_L \times \text{SU}(3)_e \tag{2.4}$$
$$\text{U}(1)^5 = \text{U}(1)_B \times \text{U}(1)_L \times \text{U}(1)_Y \times \text{U}(1)_{PQ} \times \text{U}(1)_e, \tag{2.5}$$

where the individual SU(3) symmetries transform the fermions from one generation to another. The first four U(1) symmetries can be identified with Baryon number-, Lepton number-, Hypercharge-, and Peccei-Quinn symmetries, and the last one, namely $\text{U}(1)_e$ describes rotations of the charged singlet fields e_R alone. It is the presence of the non-vanishing Yukawa terms that break this large global symmetry and leave as a remnant

$$G_{\text{global}}(y_\psi \neq 0) = \text{U}(1)_B \times \text{U}(1)_e \times \text{U}(1)_\mu \times \text{U}(1)_\tau, \tag{2.6}$$

which is responsible for baryon number conservation and the generation-wise conservation of lepton number. The $\mathrm{U}(1)_Y$ gauge symmetry remains unbroken too.

While it cannot be ruled out that the hierarchy pattern is just the result of chance and there is no deeper meaning to it,[1] it does beg the question: is there a cause or mechanism behind this pattern? This question is intriguing for a number of reasons. First of all, in the SM the principles of gauge invariance and renormalizability deliver a fully computable description of the strong and weak interactions for all fermions that relies on only three free parameters: the three gauge couplings g_s, g_w and g_y, which are all $\mathcal{O}(1)$. It is then plausible that in a more fundamental theory, perhaps a grand unified theory (GUT), the fermion masses become computable from first principles and that there are much fewer free parameters - indeed, many proposed solutions go in this direction, e.g. Refs. [14–16]. Other proposals also relate the flavour puzzle to other open problems such as the strong CP problem [17] or the hierarchy problem for the Higgs mass (which is only an issue if the SM is seen as an effective field theory (EFT) valid below a certain cut-off scale). Prominent examples of the latter are the frameworks of *Partial Compositeness* [18] and models with compactified extra dimensions [19]. A different approach to resolving the flavour puzzle, is given by the *Froggatt-Nielsen* mechanism [20], which we discuss in the following.

2.1 The Froggatt-Nielsen Mechanism

With the Froggatt-Nielsen (FN) mechanism [20], instead of postulating a fundamental theory in which the fermion masses can be computed from first principles with a reduced number of free parameters, one follows a much more agnostic, bottom-up approach. See also e.g. Refs. [21, 22]

The SM is taken as an EFT of a more fundamental theory which respects a global flavour symmetry, usually $U(1)_\mathrm{FN}$, and includes a multitude of additional heavy fermions, the so called Froggatt-Nielsen fermions or Froggatt-Nielsen messengers, and a scalar field called the *flavon* Θ. The flavon is a SM singlet but is charged under the $U(1)_\mathrm{FN}$ symmetry, or in other words, it has a flavour charge f_Θ, whereby one usually sets $f_\Theta = -1$, as we will do here. Similarly, the heavy FN fermions and the individual $\mathrm{SU}(2)_L$ representations of the SM fermions, i.e. the doublets and singlets, also carry a flavour charge, which we denominate as f_ψ. Some of the heavy FN fermions couple to the SM fermions, and thus have the same SM quantum numbers as the SM fermions that they couple to. One usually assumes that the FN fermions have all a similar mass which defines a high energy scale Λ_FN, which we will denote as the flavour scale. Below the flavour scale Λ_FN the FN fermions can be integrated out, resulting in the SM EFT. While the gauge interactions are left unchanged by the introduction of the $U(1)_\mathrm{FN}$ symmetry, the

[1] It should be noted that, in the SM,1 the Yukawa couplings are technically natural, meaning that their tiny size can be justified by the fact that setting them to zero increases the symmetry of the theory. The corresponding fermions would then be kept exactly massless, as their vanishing masses are protected by the additional symmetry

effective Yukawa terms have to be modified to be $U(1)_{\mathrm{FN}}$ invariant:

$$y^d_{\alpha\beta}\,\overline{Q}_\alpha\,H\,d_\beta \quad \longrightarrow \quad y^d_{\alpha\beta}\,\overline{Q}_\alpha\,H\,d_\beta\left(\frac{\Theta}{\Lambda_{\mathrm{FN}}}\right)^{f_{\overline{Q}_\alpha}+f_{d_\beta}+f_H} \tag{2.7}$$

$$y^u_{\alpha\beta}\,\overline{Q}_\alpha\,\widetilde{H}\,u_\beta \quad \longrightarrow \quad y^u_{\alpha\beta}\,\overline{Q}_\alpha\,\widetilde{H}\,u_\beta\left(\frac{\Theta}{\Lambda_{\mathrm{FN}}}\right)^{f_{\overline{Q}_\alpha}+f_{u_\beta}+f_{\widetilde{H}}} \tag{2.8}$$

$$y^e_{\alpha\beta}\,\overline{L}_\alpha\,H\,e_\beta \quad \longrightarrow \quad y^e_{\alpha\beta}\,\overline{L}_\alpha\,H\,e_\beta\left(\frac{\Theta}{\Lambda_{\mathrm{FN}}}\right)^{f_{\overline{L}_\alpha}+f_{e_\beta}+f_H} \tag{2.9}$$

and analogously for the hermitian conjugated terms, whereby in each case the sum of the charges in the exponent is such that the powers of the flavon, with its flavour charge $f_\Theta = -1$, compensate the flavour charges of the SM fields to ensure flavour invariance. When the flavour charge of the Higgs is set to zero, $f_H = f_{\widetilde{H}} = 0$ as is usually done, the flavon exponents simplify to $f_{\overline{\psi}_L} + f_{\psi_R}$, where ψ_L and ψ_R stand for the $\mathrm{SU}(2)_L$ doublets or singlets of the fermion ψ respectively.

Within the FN framework, the bare Yukawa couplings are all allowed to be $\mathcal{O}(1)$, so that in the fundamental theory there is no inherent hierarchy, although the different fermion representations are distinguishable by the different flavour charges. Then, it is assumed a that some point in the early history of the Universe the flavour symmetry gets spontaneously broken when the flavon acquires a vev. The symmetry breaking parameter is

$$\lambda := \frac{\langle\Theta\rangle}{\Lambda_{\mathrm{FN}}}, \tag{2.10}$$

and is expected to have values $\lambda < 1$, thus implying that the breaking of the flavour symmetry is the origin of the mass hierarchy in the fermions, because the Yukawa couplings become effectively suppressed by powers of the symmetry breaking parameter according to the flavour charges of the fermions involved,

$$y^\psi_{\alpha\beta} \longrightarrow y^\psi_{\alpha\beta}\,\lambda^{f_{\overline{\psi}_L}+f_{\psi_R}}. \tag{2.11}$$

Here we see how the FN framework does not make the SM Yukawa couplings computable or predictable from more fundamental principles, nor does it really reduce the number of free parameters in the theory - it simply maps the hierarchical Yukawa couplings to a set of $\mathcal{O}(1)$ flavour charges and explains the drastic hierarchy as a result of the exponentiation of those charges. Initially, it was thought that the symmetry breaking parameter could be related to related to the Cabibbo angle of the CKM matrix, i.e. $\lambda \approx 0.22$, and many concrete models were proposed to explain the hierarchy in the masses and mixing angles in the quark sector, e.g. [23]. Soon, models that aim to explain all of the flavour data, i.e. in the quark as well as in the lepton sector were developed, e.g. [22, 24] and even attempts to formulate a complete UV theory can be found, e.g. [25, 26].

Chapter 3

Neutrinos oscillations and masses

Neutrinos were first proposed by Wolfgang Pauli in his famous letter to the "*radioactive Ladies and Gentlemen ...*"[1] participating in a conference in Tübingen in 1930 [27]. This was Pauli's attempt to explain the continuous spectrum of β-decay without giving up on the principle of the conservation of energy. The neutrino hypothesis was confirmed in 1956 when Cowen and Reines experimentally detected neutrinos for the first time [28]. They observed an inverse β-decay reaction in their detector, wherein a proton p absorbs an electron-antineutrino $\bar{\nu}_e$ and turns into a neutron n and a positron e^+, i.e. $\bar{\nu}_e + p \to n + e^+$. To achieve this, they used a nuclear reactor in South Carolina as a $\bar{\nu}_e$ source, with a flux of $\sim 10^{13}\,\mathrm{cm}^{-2}\,\mathrm{s}^{-1}$.

Today we know that neutrinos are ubiquitous: they are copiously produced by weak interactions in the sun (and all other stars), in the atmosphere by cosmic rays, in the earths interior, in nuclear reactors and particle accelerators, in Supernova explosions (where they carry an enormous amount of the energy of the explosion) and in the Big Bang. With a number density of $\sim 336\,\mathrm{cm}^{-3}$, primordial relic neutrinos [29], i.e. those produced during the big bang, are the most abundant matter particle in the Universe. And yet, their interaction strength with other particles is so weak that their mean free path in lead is, dependent on their energy, of the order of multiple light years [30]. Physicists are rightly fascinated by neutrinos not only because they provide a unique probe of particle physics, nuclear physics, astrophysics and cosmology, but more importantly because the discovery of neutrino oscillations [31, 32] counts as the first convincing piece of evidence for the existence of BSM physics.

3.1 Neutrino Oscillations

The idea of neutrino oscillations was first imagined by Pontecorvo [33, 34] in 1957 as oscillations between neutrinos and antineutrinos. In 1962 Maki, Nakagawa and

[1] translated from the original German.

Sakata introduced the idea of transitions between neutrino flavour and mass eigenstates [35], which then prompted Pontecorvo to discuss neutrino flavour oscillations [36].

A straightforward and simplified way to derive the master formula for neutrino oscillation that requires only a few assumptions and is based on a quantum mechanic treatment goes as follows. As we will see, the phenomenon is only possible if neutrinos are massive. In section 3.2 on we will elaborate on some of the most popular mechanisms to generate neutrino masses in extensions of the SM. The neutrino states that couple to the weak interactions define the interaction basis and are called flavour states. To sketch a quick and general overview of the phenomenon of neutrino oscillations, we start by assuming the existence of n neutrino flavours ν_α with $\alpha = \{a_1, a_2, \ldots, a_n\}$ (even though the SM only has three flavours ν_α, with $\alpha = \{e, \mu, \tau\}$). We further assume that there are n neutrino mass eigenstates, denominated as ν_i with $i = \{1, 2, \ldots, n\}$. In general, this mass basis will not coincide with the interaction basis. Assuming that both sets of eigenstates $|\nu_\alpha\rangle$ and $|\nu_i\rangle$ form a complete basis for the neutrino Hilbert space, we can transition from one basis to the other by a unitary transformation,

$$|\nu_\alpha\rangle = U^*_{\alpha i}\,|\nu_i\rangle, \qquad |\nu_i\rangle = U_{\alpha i}\,|\nu_\alpha\rangle \tag{3.1}$$

with the unitary matrix $U_{\alpha i}$, which is known as the PMNS matrix[2] and is the leptonic analog to the CKM matrix. As a unitary complex matrix, the PMNS matrix has a priory n^2 real independent parameters. However, just like in the quark sector, some of these parameters can be eliminated by field redefinitions: in the case of Dirac fields, one can eliminate $(2n-1)$ complex phases, while in the case of Majorana fields n phases can be eliminated, leaving us with $n(n-1)/2$ rotation angles and $(n-1)(n-2)/2$ complex phases in the Dirac case or $n(n-1)/2$ complex phases in the Majorana case respectively.

Although neutrinos are created as flavour eigenstates, their time evolution and propagation in vacuum is determined by the action of the time evolution and propagation operators. Thus, for a neutrino being produced at $t = 0$ and $\vec{x} = 0$ we have as a flavour eigenstate $|\nu_\alpha\rangle$, the propagated state will read

$$|\nu(\vec{x}, t)\rangle = \exp\left[-i(H\,t - Px)\right]|\nu_\alpha\rangle, \tag{3.2}$$

where H stands and the free Hamiltonian and P is the momentum operator. From the relativistic energy-momentum relationship it is clear that the energy eigenvalues will also be the mass eigenvalues; therefore, it is useful to change the basis to the mass basis, where we then have

$$|\nu(\vec{x}, t)\rangle = U^*_{\alpha i}\,\exp\left[-i(E_i\,t - p_i x)\right]|\nu_i\rangle. \tag{3.3}$$

[2]The matrix $U_{\alpha i}$ is equal to the PMNS matrix only in the basis in which the charged lepton mass matrix is diagonal. More generally, the PMNS matrix is the product of the transformation matrices between flavour and mass basis of both neutrinos and charged leptons.

What we are mainly interested in are the transition probabilities for finding a certain neutrino flavour at a detector located at $(\vec{x}, t)$ after $|\nu_\alpha\rangle$ was emitted, i.e. we want to compute $P_{\alpha\to\beta} = |\langle\nu_\beta|\nu(\vec{x},t)\rangle|^2$ for which we must re-express the mass eigenstates in eq. (3.3) in therms of the flavour eigenstates to obtain

$$|\nu(\vec{x},t)\rangle = U^*_{\alpha i} U_{\beta i}\, \exp\left[-i(E_i\, t - p_i x)\right]|\nu_\beta\rangle. \tag{3.4}$$

At this point, the literature often suggests making the following simplifying assumptions (e.g. Ref. [37]): the produced neutrino state has a well defined momentum p which does not change during propagation and the energy of the neutrinos, which are ultra-relativistic due to their tiny masses, can be satisfactorily approximated by $E_i \approx p + m_i^2/2p$. Also, one can simplify things further by introducing the *baseline* L to replace t and x, i.e. $L := t = x$. Then, putting everything together and writing the summations explicitly, we find

$$\begin{aligned} P_{\alpha\to\beta} = |\langle\nu_\beta|\nu(\vec{x},t)\rangle|^2 &= \sum_{i,j} U^*_{\alpha i} U_{\beta i} U^*_{\beta j} U_{\alpha j}\, \exp\left[-i(\Delta m^2_{ij} L/2E)\right] \\ = \sum_i |U^*_{\alpha i} U_{\beta i}|^2 &+ 2\,\mathrm{Re}\left[\sum_{i<j} U^*_{\alpha i} U_{\beta i} U^*_{\beta j} U_{\alpha j}\, \exp\left[-i(\Delta m^2_{ij} L/2E)\right]\right], \end{aligned} \tag{3.5}$$

whereby the first constant term stands for the time-averaged flavour conversion, while the second term introduces the time- (or baseline) dependent oscillatory effect. Although the result above works for any number of neutrino generations - they are not restricted to three generations - the case of only two generations is particularly instructive. For $n = 2$ the PMNS matrix has only one mixing angle θ and zero Dirac phases. The oscillation probabilities then read

$$P_{\alpha\to\beta} = \sin^2(2\theta)\, \sin^2(\Delta m^2 L/4E), \qquad P_{\alpha\to\alpha} = 1 - P_{\alpha\to\beta}, \tag{3.6}$$

whereby Δm^2 is the difference of the squares of the two mass eigenstates, $\Delta m^2 = m_2^2 - m_1^2$. The factor of $\sin^2(2\theta)$ is constant in time and reflects the amplitude for the oscillations, which are driven by the factor $\sin^2(\Delta m^2 L/4E)$. One can also introduce the so-called oscillation length

$$l_{\mathrm{osc}} = 2\pi \left(\frac{\Delta m^2}{2E}\right)^{-1} \tag{3.7}$$

to rewrite eq. (3.6). Neutrino oscillations are only observable if the neutrino masses are non-degenerate (which implies that at least some of them are non-vanishing) and if the mixing angle is non-zero, i.e. $U \neq \mathbf{1}$.

In the case of three neutrino generations, as we have in the SM, the PMNS matrix has a total of four (six) independent parameters: three mixing angles θ_{ij} with $ij = \{12, 23, 13\}$ and one complex phase δ for Dirac neutrinos (and two

additional phases for Majorana neutrinos). A common parametrization is given by

$$\begin{aligned} U &= \begin{pmatrix} 1 & 0 & 0 \\ 0 & c_{23} & s_{23} \\ 0 & -s_{23} & c_{23} \end{pmatrix} \cdot \begin{pmatrix} c_{13} & 0 & s_{13}e^{-i\delta} \\ 0 & 1 & 0 \\ -s_{13}e^{i\delta} & 0 & c_{13} \end{pmatrix} \cdot \begin{pmatrix} c_{12} & s_{12} & 0 \\ -s_{12} & c_{12} & 0 \\ 0 & 0 & 1 \end{pmatrix} \\ &= \begin{pmatrix} c_{12}\,c_{13} & s_{12}\,c_{13} & s_{13}\,e^{-i\delta} \\ -s_{12}\,c_{23} - c_{12}\,s_{13}\,s_{23}\,e^{i\delta} & c_{12}\,c_{23} - s_{12}\,s_{13}\,s_{23}\,e^{i\delta} & c_{13}\,s_{23} \\ s_{12}\,s_{23} - c_{12}\,s_{13}\,c_{23}\,e^{i\delta} & -c_{12}\,s_{23} - s_{12}\,s_{13}\,c_{23}\,e^{i\delta} & c_{13}\,c_{23} \end{pmatrix} \end{aligned} \tag{3.8}$$

where we have defined $s_{ij} = \sin(\theta_{ij})$, $c_{ij} = \cos(\theta_{ij})$. The two additional Majorana phases can be introduced by multiplying U from the right with $\mathrm{diag}\big(1, e^{i\varphi_1/2}, e^{i\varphi_2/2}\big)$. These neutrino parameters have been measured by a multitude of experiments using solar, atmospheric, reactor and accelerator neutrinos. Global fit analysis are provided by the *neutrino global fit* group from Valencia [38] as well as from the *νfit* group. Results from the latter performed on the latest available data (i.e. November 2022) [39][3] reveals the 1σ values

$$\theta_{12} = 33.14^{\circ\,+0.75}_{-0.72} \qquad \theta_{23} = 49.1^{\circ\,+1.0}_{-1.3} \qquad \theta_{13} = 8.54^{\circ\,+0.11}_{-0.12} \qquad \delta = 197^{\circ\,+42}_{-25}$$

$$\Delta m^2_{21} = 7.41^{+0.21}_{-0.20} \times 10^{-5}\mathrm{eV}^2 \qquad \Delta m^2_{31} = 5.514^{+0.028}_{-0.027} \times 10^{-3}\mathrm{eV}^2$$

for normal ordering (NO), i.e. $m_1 < m_2 < m_3$, and

$$\theta_{12} = 33.45^{\circ\,+0.78}_{-0.75} \qquad \theta_{23} = 49.3^{\circ\,+1.0}_{-1.2} \qquad \theta_{13} = 8.61^{\circ\,+0.12}_{-0.12} \qquad \delta = 286^{\circ\,+27}_{-32}$$

$$\Delta m^2_{21} = 7.41^{+0.21}_{-0.20} \times 10^{-5}\mathrm{eV}^2 \qquad \Delta m^2_{32} = -2.497^{+0.028}_{-0.028} \times 10^{-3}\mathrm{eV}^2$$

for inverted ordering (IO), i.e. $m_3 < m_1 < m_2$. Neutrino oscillation measurements shed no light on the question of the absolute scale of the mass eigenvalues. To that purpose other dedicated experiments have been built and are being operated, most notably the KATRIN experiment, which aims for precision measurements of the high energy tail of the β-decay spectrum of tritium and currently delivers the most stringent upper bound on the mass of the electron antineutrino at 0.8 eV at 90% CL [40].

At this point it should be mentioned that the plane wave approximation and the assumptions made above in order to arrive at eq. (3.5), i.e. that the flavour states have a well defined momentum which does not change during propagation, are too simplistic but nevertheless lead to the correct solution. A more careful treatment would involve considering quantum mechanical wave packets instead of plane waves, and an even more rigorous approach would be to use quantum field theory (QFT), which would take the emission, propagation and detection of neutrinos properly into account, see e.g. [41–43].

Another very important and fascinating fact about neutrino oscillations, which we will only briefly discuss here, is that the phenomenon occurs differently in vac-

[3] For the latest results from recent datasets one should rather consult www.nu-fit.org.

uum and in matter. Wolfenstein first noticed that for neutrinos propagating in matter instead of in vacuum, the oscillation behaviour could be affected [44]. Shortly afterwards, Mikheyev and Smirnov realised that in certain circumstances the neutrino flavour transition amplitude could be resonantly enhanced; this is the famous MSW effect [45]. It occurs because neutrinos traveling through matter will interact with other leptons in that medium through NC and CC interactions, and while the NC processes treat all neutrino flavours equally, the CC processes do not. The forward scattering CC process $\nu_\alpha\, l_\alpha^\pm \to \nu_\alpha\, l_\alpha^\pm$, which occurs through the exchange of a $W^\pm$ boson, is indeed the most relevant process for the MSW effect. Since electrons are the only charged leptons that are usually available in ordinary matter, this process will occur for electron neutrinos but not for the other neutrino flavours. As a consequence the matter-Hamiltonian receives an additional contribution such that its eigenstates are different from those of the free Hamiltonian. This is easiest to see in the case of two neutrino generations, where the matter-Hamiltonian in the flavour basis $\hat{H}_\mathrm{m}^\alpha$ reads

$$\hat{H}_\mathrm{m}^\alpha = \begin{pmatrix} -\frac{\Delta m^2}{4E}\cos(2\theta) + \sqrt{2}G_F\, N_e & \frac{\Delta m^2}{4E}\sin(2\theta) \\ \frac{\Delta m^2}{4E}\sin(2\theta) & \frac{\Delta m^2}{4E}\cos(2\theta) \end{pmatrix}. \tag{3.9}$$

Here, θ is the vacuum mixing angle, G_F is the Fermi constant and N_e is the electron number density. It turns out that in a medium of constant density, i.e. $N_e = \text{const}$, the vacuum formula eq. (3.6) is still valid [46] if one replaces the oscillation length by an effective oscillation length in matter

$$l_\mathrm{osc} \to l_\mathrm{m} = \frac{2\pi}{\sqrt{\left(\frac{\Delta m^2}{2E}\,\cos 2\theta - \sqrt{2}\,G_F\,N_e\right)^2 + \left(\frac{\Delta m^2}{2E}\right)^2 \sin^2 2\theta}} \tag{3.10}$$

and the vacuum oscillation angle by an effective oscillation angle in matter, namely

$$\sin^2 2\theta_\mathrm{m} = \frac{\left(\frac{\Delta m^2}{2E}\right)^2 \sin^2 2\theta}{\left(\frac{\Delta m^2}{2E}\,\cos 2\theta - \sqrt{2}\,G_F\,N_e\right)^2 + \left(\frac{\Delta m^2}{2E}\right)^2 \sin^2 2\theta}. \tag{3.11}$$

Here we see that $\sin^2 2\theta_\mathrm{m}$ is saturated if the electron density and neutrino energy are such that

$$\frac{\Delta m^2}{2E}\,\cos 2\theta = \sqrt{2}\,G_F\,N_e, \tag{3.12}$$

which is known as the MSW resonance condition. When fulfilled, this leads to a greatly enhanced flavour conversion probability, even if the vacuum mixing angle was originally very small.

In more realistic scenarios, such as in the case of the sun, the electron density is not constant but it varies throughout the medium. Consider the following scenario: electron neutrinos are produced in a region of very high electron density, and that

density adiabatically decreases along the path of trajectory of the neutrinos until a very low density is reached, while on the way crossing through a region where the MSW condition is satisfied. Remarkably, one finds that for some values of the vacuum mixing angle, a nearly complete flavour conversion can occour after the propagation through the medium of adiabatically decreasing density [46, 47].

With this we conclude our short discussion of neutrino oscillations by emphasising that this phenomena definitely indicates that neutrinos are not massless, and that to explain the origin the of those masses we must look beyond the SM of particle physics.

3.2 The Problem of Neutrino Masses

We have now established that neutrinos must have non-vanishing masses. It is worthwhile to recapitulate the reasons why it is not possible to accommodate neutrino masses within the SM, whereby we closely follow the argumentation presented by Akhmedov in Ref. [46].

A Dirac fermion ψ is a four-component spinor that can always be decomposed into its right- and left-chirality components, $\psi = \psi_L + \psi_R$. Its mass term in the Lagrangian is

$$-\mathcal{L}_{\text{mass}}^{\text{Dirac}} = m\,\overline{\psi}\,\psi = m\,\overline{\psi_L}\,\psi_R + m\overline{\psi_R}\,\psi_L, \tag{3.13}$$

where it becomes obvious that Dirac masses require both chiral components of a fermion. Since the minimal SM does not contain RH neutrinos, no Dirac masses for them can be included. But what about the case of Majorana neutrinos? Majorana particles are those that are identical to their particle-antiparticle conjugates. Particle-antiparticle conjugation works as follows:

$$\psi \xrightarrow{c} \psi^c = C\,\overline{\psi}^T, \quad \text{with} \qquad C = i\gamma_2\gamma_0 \tag{3.14}$$

in the Dirac base, where γ_i stands for the gamma-matrices of the Clifford algebra. It follows then than $\overline{\psi^c} = \psi^T\,C$. Note also that for a chiral spinor, this transformation flips its chirality. A Majorana particle is defined as one that satisfies the relation

$$\psi^c = \eta^*\,\psi, \tag{3.15}$$

i.e. the particle is, up to a phase factor η^*, identical to its antiparticle, which can only ever occur with neutral particles. For a Majorana particle, its RH component is simply the particle-antiparticle conjugate of its LH component, i.e.

$$\psi_R = (\psi_L)^c = (\psi^c)_R. \tag{3.16}$$

Therefore, for LH Majorana particles, one can write mass terms without needing

independent RH partners, namely

$$-\mathcal{L}_{\text{mass}}^{\text{Maj}} = \frac{1}{2}\left[\overline{\psi_L^c}\, M\, \psi_L + \overline{\psi_L}\, M^\dagger\, (\psi_L)^c\right] = \frac{1}{2}\left[\psi_L^T\, C\, M\, \psi_L + \text{h.c.}\right]. \tag{3.17}$$

Crucially, we see that the Majorana mass term will violate any conservation laws associated with a U(1) symmetry under which the Majorana field ψ is charged. As the only neutral fermion in the SM, neutrinos are the only candidate in the theory that could be a Majorana fermion. So, could we just assign them Majorana masses? Not without violating gauge invariance, Lorentz invariance or renormalizability: A bare Majorana mass term of the form

$$\frac{1}{2}\overline{\nu_L^c}\, m_M\, \nu_L \tag{3.18}$$

is of dimension three and thus does not violate renormalizability, but it violates $\text{SU}(2)_L \times \text{U}(1)_Y$ invariance and is therefore forbidden. However, the operator in eq. (3.18) could be generated by the vev of the electrically neutral component of an $\text{SU}(2)_L$ scalar triplet Δ with a weak hypercharge of -2, whereby the gauge- and Lorentz invariant operator would then read

$$(L^T\, C\, i\sigma_2 \vec{\sigma}\, L)\Delta + \text{h.c.} \tag{3.19}$$

but there is no such $\text{SU}(2)_L$ scalar triplet in the SM. One could extend the SM to include the scalar triplet Δ, in which case the following comments are in place: if one demands that eq. (3.19) conserves lepton number, then Δ necessarily has to carry the lepton number -2, and then the vev of Δ would spontaneously break lepton number, resulting in additional Goldstone bosons. Furthermore, the presence of Δ would introduce new exotic lepton interactions and contribute to the masses of the gauge bosons, which is constrained by the experimental value of the ρ-parameter, defined as $\rho = m_W^2/\cos^2(\theta_W) m_Z^2$. This results in a bound imposed on the vev of the scalar triplet at the $\mathcal{O}(1)$ GeV level [48, 49].

An interesting alternative is to construct the scalar triplet as a composite state made of two SM Higgs instead of introducing it as a fundamental particle, namely

$$\Delta \to (H^T\, i\sigma_2 \vec{\sigma}\, H), \tag{3.20}$$

which has the correct quantum numbers. With this combination we can construct the dimension 5 operator,

$$\frac{f}{M}\, (L^T\, C\, i\sigma_2 \vec{\sigma}\, L)(H^T\, i\sigma_2 \vec{\sigma}\, H), \tag{3.21}$$

with the couplings f and the high mass scale M. This operator is a realization of the *Weinberg operator* [50], which is of the general form

$$\mathcal{O}_W^{(5)} \sim \frac{f}{M}\, LLHH. \tag{3.22}$$

It turns out that this 5-dimensional operator is the unique operator that generates neutrino masses and consists only of SM fields. After SSB this operator generates Majorana masses for the neutrinos,

$$m_M \approx \frac{f}{M}\, v^2. \tag{3.23}$$

However, being of dimension 5, the Weinberg operator is not renormalizable and therefore forbidden at the fundamental level. It also cannot arise at the loop level within the SM because it not only violates lepton number, but it also violates $B-L$, which in the SM is non-perturbatively conserved. Thus, we conclude that to accommodate neutrino masses we must go beyond the Standard Model, i.e. expand the particle content or the gauge group. Then, the Weinberg operator can arise as an effective operator after integrating out heavier states of a more fundamental theory. As discussed above, introducing $\mathrm{SU}(2)_L$ scalar triplets is an interesting option. An alternative is to introduce RH sterile neutrinos, which gives rise to the *type I seesaw mechanism*, which we will now discuss in more detail.

3.3 The Seesaw Mechanism

One of the simplest and most appealing extensions we could implement in the SM to generate neutrino masses is the addition of RH neutrinos, resulting in the well known *type I seesaw mechanism* [51–54]. Being SM singlets, any number of RH neutrinos can be added, i.e. the number of RH neutrinos does not necessarily have to match the number of LH neutrinos.[4] However, the most attractive extension - and indeed the most common - is by three RH neutrinos, since this would re-establish the symmetry between quarks and leptons, i.e. each LH lepton would have a RH lepton partner, just as is the case among charged leptons and in the quark sector. This is also a common feature of many GUTs and left-right-symmetric models [46]. The addition of sterile neutrinos ν_R to the SM, and their assignment of lepton number $L = +1$, immediately allows us to write neutrino Yukawa terms, which then generate Dirac masses via the Higgs mechanism, i.e.

$$-y_\nu\, \overline{L}\, \widetilde{H}\, \nu_R + \text{h.c.} \qquad \xrightarrow{\text{SSB}} \qquad -y_\nu\, \overline{\nu_L}\, m_D\, \nu_R + \text{h.c.} \tag{3.24}$$

where the generation indices (α, β) have been suppressed for clarity, so L and $\nu_{L/R}$ should be understood as representing all three generations and y_ν is a complex 3×3 matrix of neutrino Yukawa couplings. So, could this m_D be the final origin of neutrino masses? In principle, this is a possibility, but as mentioned previously, in order for it to explain the oscillation data, the Yukawa couplings would have to be extremely tiny, namely $y_\nu \sim 10^{-12}$. One could argue that this should not be a problem; after all, we readily accept that electrons have very small Yukawa couplings too, $y_e \approx 3 \cdot 10^{-6}$ (although this can be seen as puzzling in itself, c.f.

[4] At least two RH neutrinos are necessary for the seesaw mechanism to generate the masses of two active neutrinos, leaving one active neutrino massless.

chapter 2). However, this is a rather unsatisfactory explanation, because it would introduce a huge and unexplained hierarchy in the masses within each fermion generation - disregarding neutrinos, all fermions within each generation, e.g. the electron and the up- and down quarks, all have masses that are clustered within one or two orders of magnitude of each other, see fig. 2.1. Without a plausible mechanism that suppresses the masses of neutrinos, this pattern would be destroyed. A solution is offered by the fact that, since sterile neutrinos are SM singlets, we may add a Majorana mass term for them in the Lagrangian without violating gauge invariance. The term is of the form

$$-\frac{1}{2}\,\overline{\nu_R^c}\,M_R\,\nu_R + \text{h.c.}, \tag{3.25}$$

and violates lepton number by two units, $\Delta L = 2$. Previously, we established that L is an accidental symmetry of the standard model, but it is only an accidental and not an imposed symmetry of the model, so we willingly give up this accidental symmetry in exchange for the right to include Majorana masses for the RH neutrinos.

Thus, following the treatment in Refs. [46, 55], we extend the SM Lagrangian by the following terms

$$-\mathcal{L}_\nu = i\bar{\nu}_R\,\partial\!\!\!/\,\nu_R + y_\nu\,\bar{L}\,\tilde{H}\,\nu_R + \frac{1}{2}\,\overline{\nu_R^c}\,M_R\,\nu_R + \text{h.c.}, \tag{3.26}$$

where, by the Higgs mechanism, the Yukawa term generates the Dirac mass matrix after SSB, $m_D = y_\nu\,v/\sqrt{2}$. The neutrino mass Lagrangian is then

$$-\mathcal{L}^\nu_{\text{mass}} = y_\nu\,\overline{\nu_L}\,m_D\,\nu_R + \frac{1}{2}\,\overline{\nu_R^c}\,M_R\,\nu_R + \text{h.c.} \tag{3.27}$$

After some algebra, and assuming that neutrinos are indeed Majorana particles, i.e. $(\nu_R)^c = \nu^c{}_L$, we can change into the six-dimensional basis defined by

$$\nu_{\mathcal{M}} = (\nu_L,\,\nu_R{}^c)^T = (\nu_L,\,\nu^c{}_L)^T = (\nu_{L,e}, \nu_{L,\mu}, \nu_{L,\tau}, \nu_{R,1}{}^c, \nu_{R,2}{}^c, \nu_{R,3}{}^c)^T, \tag{3.28}$$

where the neutrino mass Lagrangian then reads

$$-\mathcal{L}^\nu_{\text{mass}} = \frac{1}{2}\,\overline{\nu^c_{\mathcal{M}}}\,\mathcal{M}_\nu\,\nu_{\mathcal{M}} + \text{h.c.} = \frac{1}{2}\,\overline{\nu^c_{\mathcal{M}}}\begin{pmatrix} 0 & m_D \\ m_D^T & M_R \end{pmatrix}\nu_{\mathcal{M}} + \text{h.c.}. \tag{3.29}$$

Here, $\mathcal{M}_\nu$ is the full 6×6 neutrino mass matrix, while m_D is an arbitrary 3×3 matrix and M_R is a symmetric 3×3 matrix. We aim to block-diagonalize $\mathcal{M}_\nu$ in the expectation that we will decouple the light from the heavy mass eigenstates. This is easy to do when $m_D \ll M_R$, which is actually a very reasonable assumption, because m_D is generated by the Higgs mechanism at the EW scale, and is thus not expected to be larger than the top mass. On the other hand, the scale of the Majorana mass M_R is a priori unrestricted - in principle, it could be as high as the GUT or the Planck scale. Particularly, it is conceivable that M_R is generated

by some mechanism similar to the Higgs mechanism at some BSM scale, which will necessarily be above the EW scale. Thus, in this context, the so-called seesaw condition $m_D \ll M_R$ is generically fulfilled and the block diagonalization of $\mathcal{M}_\nu$ is realized by the unitary 6×6 matrix

$$U = \begin{pmatrix} 1 & \theta \\ -\theta^\dagger & 1 \end{pmatrix}, \qquad \text{with} \qquad \theta = m_D\, M_R^{-1}\,. \tag{3.30}$$

The 3×3 matrix $\theta = m_D\, M_R^{-1}$ quantifies the mixing between the heavy and light neutrino degrees of freedom. The seesaw condition ensures that $\theta \ll 1$ and thus θ can be treated as a small perturbation. The result is the diagonalized 6×6 neutrino mass matrix

$$\mathcal{M}'_\nu = \begin{pmatrix} m' & 0 \\ 0 & M' \end{pmatrix}, \qquad \text{with} \qquad m' \approx m_D\, M_R^{-1}\, m_D^T, \qquad M' \approx M_R. \tag{3.31}$$

Here we can best appreciate the seesaw effect: thanks to the seesaw condition $m_D \ll M_R$, the neutrino mass Lagrangian contains three very heavy states with masses in the matrix $M' \approx M_R$ that are mostly composed of the sterile states, and three very light neutrino states with masses in the light Majorana matrix $m' \approx m_D\, M_R^{-1}\, m_D^T$, that are mostly composed of the LH active neutrinos. Clearly, the reason for the smallness of m' is the much larger size of M_R - this is the seesaw. After block-diagonalization, the neutrino mass Lagrangian can be rewritten as

$$-\mathcal{L}^\nu_{\text{mass}} = \frac{1}{2}\, \overline{\nu^c_{\mathcal{M}}}\, \mathcal{M}_\nu\, \nu_{\mathcal{M}} + \text{h.c.} = \frac{1}{2}\, (\overline{\nu_L{}^c},\, \overline{\nu_R}) \begin{pmatrix} m' & 0 \\ 0 & M' \end{pmatrix} \begin{pmatrix} \nu_L \\ \nu_R{}^c \end{pmatrix} + \text{h.c.} \tag{3.32}$$

$$= \frac{1}{2}\, \nu_L{}^T\, C\, m'\, \nu_L + \frac{1}{2}\, \nu_R{}^T\, C\, M'\, \nu_R + \text{h.c.} \tag{3.33}$$

whereby we have neglected the mixing between LH and RH neutrinos, which is of the order of $\theta \ll 1$. Now, both matrices m' and M' can be further diagonalized by the appropriate transformations, i.e.

$$m = V_L^T m' V_L = \begin{pmatrix} m_1 & & \\ & m_2 & \\ & & m_3 \end{pmatrix}, \; M = V_R^T M' V_R = \begin{pmatrix} M_1 & & \\ & M_2 & \\ & & M_3 \end{pmatrix}, \tag{3.34}$$

and we will refer to the light mass eigenstates as $\nu = (\nu_1, \nu_2, \nu_3)$ and to the heavy ones as $N = (N_1, N_2, N_3)$, or in other words

$$\nu = (V_L)^T\, \nu_L, \qquad N = (V_R)^T\, \nu_R. \tag{3.35}$$

Note that here, in principle, it is possible to start in a basis in which the Majorana mass matrix M_R is already diagonal, because that would simply amount to a field redefinition of $\nu_R = (\nu_{R,1}, \nu_{R,2}, \nu_{R,3})$.

As discussed previously, there are also other ways to generate the Weinberg operator, eq. (3.21), namely: at three level, besides introducing RH neutrinos, which

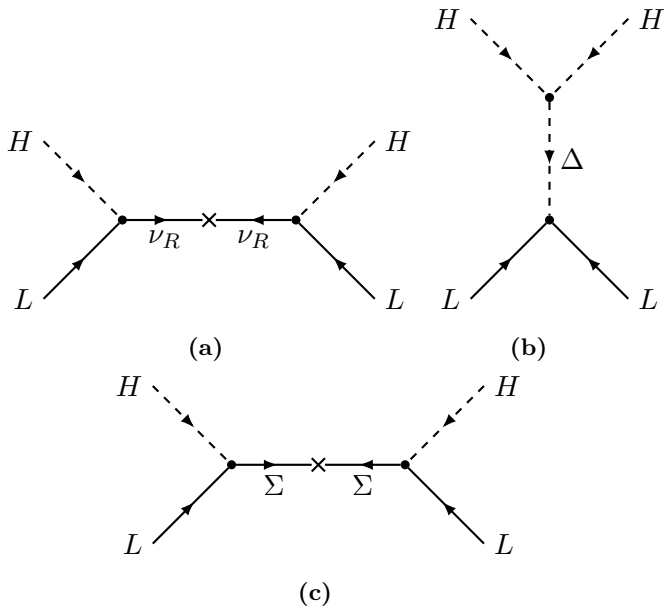

Figure 3.1. Diagrams in minimal SM extensions that generate the Weinberg operator at tree level. (a) Type-I seesaw extension - The RH neutrinos ν_R, i.e. Majorana fermions that are SM singlets, form the usual Yukawa vertices that we are familiar with from the SM. (b) Type-II seesaw extension - A massive $\mathrm{SU}(2)_L$ triplet scalar Δ with a hypercharge of -2 couples to LL and HH, and obtains a vev from its coupling to the Higgs. (c) Type-III seesaw extension - Massive $\mathrm{SU}(2)_L$ triplet fermions Σ whose middle component mixes with the left-handed neutrino and has no hypercharge couple to LH.

are $\mathrm{SU}(2)_L$ singlets, one can introduce an $\mathrm{SU}(2)_L$ scalar triplet Δ (as discussed at the end of section 3.2), which is then referred to as the *type II seesaw mechanism* [56–58], or one can add a set of $\mathrm{SU}(2)_L$ fermions triplets, an extension which is referred to as the *type III seesaw mechanism* [59, 60]. Diagramms for all three types of seesaw variants are shown in fig. 3.1. A very different possibility is to generate neutrino masses radiatively through loop processes, which would also explain their suppressed values. Some of the most prominent examples of this approach are the *scotogenic model* [61] and the *Zee-Babu* model [62–64]. Further, there are many other models to choose from in the literature [65].

Chapter 4

Dark Matter

Dark matter (DM) is one of the fundamental pillars of the standard model of cosmology. In this chapter we start by presenting some of the most important pieces of evidence in favour of the existence of DM, which, as we will see, are very diverse and complementary. We then introduce some of the most popular DM candidates, most of which are BSM particles, although we also mention some non-particle candidates. The process of *freeze-out* to generate relic densities is discussed in more detail, as it is the basis for the production mechanism for sterile neutrinos that is the core of this thesis. For similar reasons we also spend some extra time discussing sterile neutrinos as DM candidates at the end of this chapter.

4.1 The evidence for the existence of Dark Matter

Since Zwicky first noticed the "missing mass" in the Coma cluster [6, 66], evidence has been mounting from a multitude of different sources and scales that point in the same direction: there exists a mysterious substance, i.e. non-ordinary matter, that interacts gravitationally with ordinary matter but is not subject to the electromagnetic interaction. Zwicky himself coined the term *Dark Matter* for this puzzling substance. The extensive body of evidence that has been built by now is very compelling; it is based on independent astrophysical and cosmological observations. On the astrophysical side, the rotation curves of galaxies, the dynamics of galaxy clusters, collisions of galaxy clusters and the effects of gravitational lensing all point to the existence of Dark Matter. The cosmological evidence is just as strong; it comes from the analysis of the CMB, the predicted and measured abundance of light elements that were created right after the Big Bang, i.e. the so called big bang nucleosynthesis (BBN), the observation of baryon acoustic oscillations (BAO), as well as the process of large scale structure formation in the Universe. In this section, we will briefly discuss the most important pieces of evidence for the existence of DM.

Virially bound Galaxy Clusters

For a self-gravitating system in a stable dynamical equilibrium, such as a galaxy cluster, the *Virial theorem* relates the kinetic and potential energy of the system as $E = -U/2$, where E stands for the former and U for the latter, respectively. While observing the Coma Cluster and measuring the peculiar velocities of the galaxies in the Cluster, Zwicky was able to estimate that the mass in the cluster should be ~ 160 times larger than one would expect by judging from the luminosity [6] - the velocities of the galaxies were so large that, without DM, the cluster could not be kept gravitationally bound, but would instead expand and eventually blow apart. The initially estimated factor of ~ 160 overestimated the amount of DM because, at that time, X-ray emitting gas and infrared emitting dust could not be accounted for. Nevertheless, modern observations of the Coma Cluster and other galaxy clusters agree with the DM interpretation [67–70].

Galactic Rotation Curves

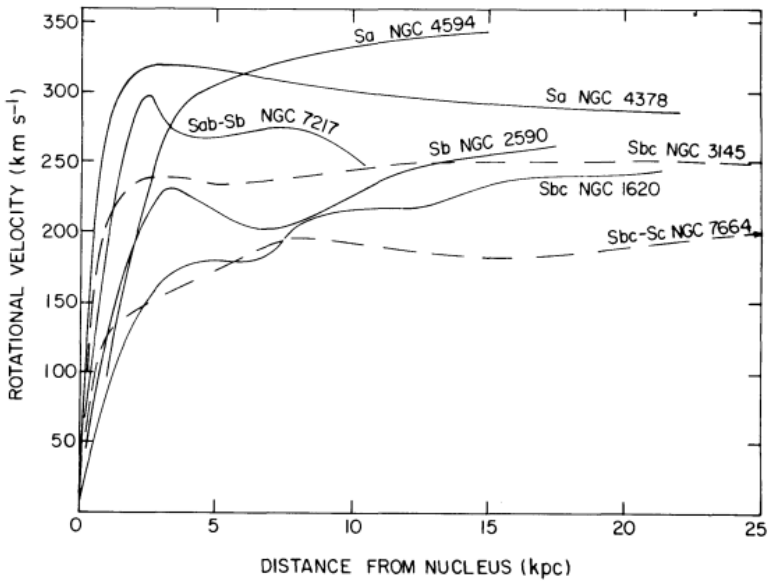

Figure 4.1. Rotation curves of several galaxies as observed by Rubin, Ford, and Thonnard in 1978. The expected $1/\sqrt{r}$ decline is not seen. Figure taken from [71].

Observations of the circular velocities of stars in galaxies, as first made by Rubin and Ford in 1970 [72] on the Andromeda galaxy M31, delivered unexpected results. The known relationship between circular velocity v, distance to the galactic axis r

and mass responsible for the gravitational attraction felt by the star is

$$v = \sqrt{\frac{G_N\, M(r)}{r}}, \tag{4.1}$$

with the gravitational constant G_N and the mass contained within a sphere of radius r around the galactic axis $M(r)$. For the outmost stars, nearly all of the visible mass in the galaxy will be contained within the sphere of radius r, so that the circular velocity is expected to keep decreasing as

$$v \sim \frac{1}{\sqrt{r}}. \tag{4.2}$$

However, in the observations by Rubin and Ford v stayed constant even for the largest values of r for which the rotation curve could be measured. This discrepancy has been consistently verified in essentially all galaxies observed [73] since then. A workable explanation was then proposed by Freeman in 1970 [74]: galaxies are enclosed in a halo of invisible matter, which extends far beyond the visible matter in the galaxy and has a mass density profile $\rho(r) \sim 1/r^2$ such that $M(r) \sim r$ and therefore $v \sim$ const. Of course, at some distance the Halo density will start decreasing more pronouncedly, but at that distance there are no observable stars nor hydrogen to track the rotation curve. Some early rotation curves indicating the existence of DM can be seen in fig. 4.1.

Gravitational Lensing

General relativity tells us that space-time itself is curved in the presence of a mass distribution. We also know that light travels in geodesics, which in curved space are themselves curved trajectories. It follows then that light will travel in curved paths around a mass distribution, resulting in the well known *gravitational lensing effect*. One distinguishes three different types of gravitational lensing:

Strong lensing: The light from a source passes and gets deflected by a dense mass distribution, such as the center of a galaxy or cluster, and finally gets redirected to the observer, resulting in one or multiple highly distorted images of the source. The most remarkable manifestation of strong gravitational lensing is the so called *Einstein ring*, whereby the source, lens and observer are aligned in such a way that the image seen by the observer resembles a ring surrounding the lens, as can be appreciated in fig. 4.2. Analysing strong lensing images from the Sloan digital sky survey (SDSS), cosmological parameters could be constrained and it was found that $\Omega_{\mathrm{M}} = 0.26^{+0.07}_{-0.06}$, while the baryon density of the Universe is known to be $\Omega_{\mathrm{b}} = 0.0493(6)$ [11]. One thus concludes that the total mass density of the universe is ~ 5 times larger than the contribution from baryonic matter [75, 76].

Weak lensing: The conditions necessary for strong lensing, i.e. a very dense mass distribution at the right distance along the line of sight between source and

Figure 4.2. Strong lensing. Right: Einstein ring generated by the red galaxy LRG 3-757 acting as lens for the image of a much more distant blue galaxy. Left: In the center the galaxy cluster CL0024+1654 acts as a gravitational lens, around which several blue images of the same source galaxy can be seen. Images from: ESA/Hubble & NASA, H. Lee & H. Ford (Johns Hopkins U.).

observer, are only rarely realized. Most frequently the mass distribution acting as a lens is not very dense and the light from the source galaxy might not pass directly through its center. Nevertheless, the light from background galaxies will get slightly distorted, or in other words, lensed. The effect is much more subtle than strong lensing - the images get compressed or elongated when propagating through an over- or underdense region respectively. Remarkably, four independent research groups in the year 2000 were successful in probing the average distribution of DM by analysing weak lensing images [77–80]. Further, in 2007 another group succeeded in constructing a 3D map of the DM distribution in a certain region of space [81].

Microlensing: For distant astronomical observations, this effect occurs due to the relative motion between a source and lens confined to a relatively small volume of space. When such a small lens passes through the line of sight between source and observer, the image of the source can be brightened for a period of time in the order of days or weeks. Through this method it was possible to rule out that the DM in our galaxy could be accounted for by Massive Compact Halo Objects (MACHOs) [76].

As we have now seen, gravitational lensing observations offer a convincing and direct probe for the existence of DM. One particularly fascinating case study indicating DM, which employs weak lensing observations, is that of the *Bullet Cluster*, which we will discuss next.

The Bullet Cluster

Colliding galaxy clusters offer a spectacular indication in favour of the DM hypothesis and a rare probe into its properties. Perhaps the most famous example of this is

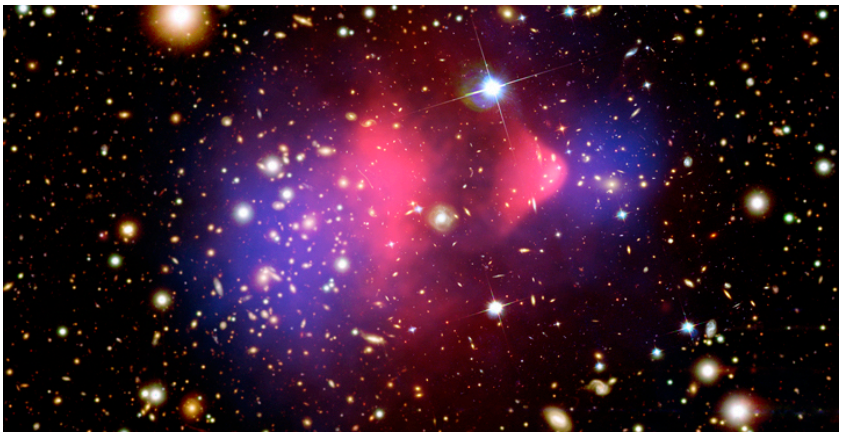

Figure 4.3. Cluster 1E 0657-56, better known as the *Bullet Cluster*, is the result of a collision between two galaxy clusters that occurred around 150 million years ago. As a result of the merger, the distribution of galaxies, intra-cluster gas and the bulk of the mass of both clusters dissociated: the galaxies followed their ballistic trajectories largely unbothered by the collision, while the gas was heated, shocked and decelerated by the violence of the collision and now emits X-rays as a consequence, which are visualized in this figure as red/magenta clouds; the shock front is easy to identify. On the other hand, the bulk of the mass distribution, being composed of collisionless DM, also survived the collision undisturbed, and is also visualized in the figure by blue blobs. The mass distribution was mapped by analysing the weak lensing images of background galaxies. The obvious separation of baryonic gas and the bulk of the mass in the merged cluster is a direct indication of the existence of non-baryonic massive matter in the system. Image credit: X-ray: NASA/CXC/CfA/M.Markevitch et al.; Optical: NASA/STScI; Magellan/U.Arizona/D.Clowe et al.; Lensing Map: NASA/STScI; ESO WFI; Magellan/U.Arizona/D.Clowe et al.

the galaxy cluster 1E 0657-56, better known as the *Bullet Cluster*, which is actually a merger of two clusters that collided some 150 million years ago [82–84]. What is fascinating about this merger is the segregated distribution of galaxies, intra-cluster gas, and mass [76]. Galaxies within the cluster are very widely spaced out and thus will mostly follow ballistic trajectories during cluster mergers without colliding with other galaxies. On the other hand, the intra-cluster gas uniformly spread in both clusters will experience a lot of friction during the collision, be shocked and as a consequence emit X-rays. The mass distribution is mapped by analysing the weak lensing of background galaxies. The result shows that while the gas was decelerated by the collision and the shock front is visible, the bulk of the mass of both clusters ghostly passed through each other undisturbed. This allowed to set a stringent upper limit on the DM self interaction cross section of $\sigma/m < 1.25\,\mathrm{cm}^2\mathrm{g}^{-1}$ at 1σ

confidence level [85]. The vast spacial separation between the center of mass of the X-ray emitting baryonic matter and the center of mass of the collisionless mass distribution, mapped by the weak lensing effect, has a statistical significance of 8σ, and serves as compelling direct evidence for the existence of DM [86]. It had been objected, that the collision velocities of the two clusters appeared too large, thereby making the collision highly improbable according to N-body simulations [87], but newer findings have ruled out this possibility as a challenge to the DM interpretation [88]. Cluster mergers like the Bullet Cluster are rare, and only a few others have been observed, such as the *Train Wreck cluster* (Abell 520) [89] and the so called *Baby Bullet Cluster* (MACSJ0025-12) [90], both of which also exhibit a spacial separation between the distributions of the hot gas and the lensing matter. Nevertheless, the Bullet Cluster remains the most spectacular example for a cluster collisions.

The Cosmic Microwave Background

The cosmic microwave background (CMB) was first predicted by Gamow, Alpher and Herman in 1948 [91, 92] as a result of the hot and dense beginnings of the Universe, i.e. what we today might call *the Big Bang theory*. At early times in cosmological history, when the temperature was still higher than the ionization energy of hydrogen, the Universe was composed of - besides neutrinos and presumably DM particles - light nuclei (mainly hydrogen and helium nuclei), electrons and photons. These were kept in thermal equilibrium by Thomson- and Compton scattering and by the ionization and recombination of hydrogen. While these interactions are in thermal equilibrium, the cosmic plasma is tightly coupled and photons cannot propagate freely - the Universe is opaque. However, as the Universe expands and cools, a temperature will be reached at which most photons do not have enough energy to ionize hydrogen atoms. This event is called *recombination*, and it occurred at a temperature of $\sim 0.3\,\mathrm{eV}$, which corresponds to a redshift of ~ 1100. At the moment of recombination, the mean free path of the photons increased abruptly to above the size of the observable Universe [93]. These are the CMB photons which we measure today. For the most part, they have been traveling to us undisturbed since their emission from the so-called *surface of last scattering* at the moment of recombination.

Since the accidental discovery of this radiation by Penzias and Wilson in 1965 [94, 95], many experiments have been built to measure it, most notably the satellites COBE, WMAP and Planck. The spectrum is at first sight that of a perfect black body radiator, homogeneous and isotropic with a temperature of $T_{\mathrm{CMB}} = 2.726\,\mathrm{K}$ [96], but bellow the level of $\Delta T/T \sim 10^{-4}$ one can appreciate an interesting pattern of anisotropic temperature fluctuations; a full sky map as measured by the Planck Satellite can be seen in fig. 4.4. The fluctuations are caused mainly by differences in the local gravitational potential on the surface of last scattering: photons emitted from regions where the gravitational potential is stronger get redshifted as they

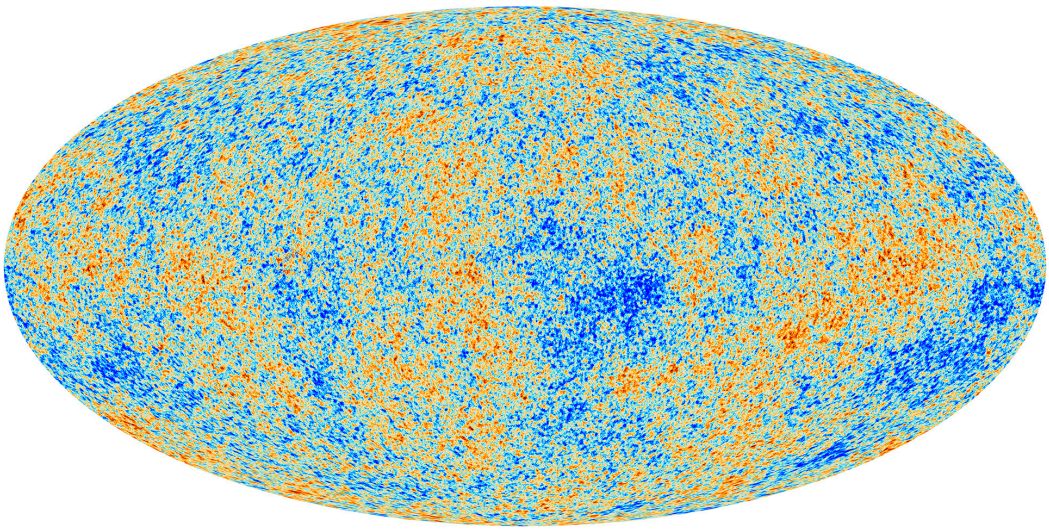

Figure 4.4. Full sky map at high resolution of the CMB indicating the fluctuations from the mean temperature $T_{\rm CMB} = 2.726\,\mathrm{K}$ at a level of $\Delta T/T \sim 10^{-5}$, where blue stands for colder spots and red for hotter. Image credit: ESA and the Planck Collaboration.

propagate away. This is the so-called *Sachs-Wolfe effect*.[1] Another important effect is that of acoustic oscillations [97]: density fluctuations in the radiation fluid generate gravitational potential wells in which the baryonic matter tends to fall in. Because of the strong coupling between the baryons and photons, the latter accumulate in the potential wells too. Thus, there is a build-up of radiation pressure in potential wells which pushes the fluid outwards and dilutes it. Then, the baryonic matter starts to fall in again and the process begins a new cycle. These are the baryon acoustic oscillations, and they occur on all density fluctuations of sizes within the sound horizon. The dynamics of these oscillations are largely determined by the geometry and content of the Universe: it matters how large the sound horizon is, what is the density of baryons, what is the density ratio of baryons to photons, and, if there is DM present, it will contribute to potential wells but not to the oscillating mass [98].

The temperature anisotropy data is analysed by first expanding it into spherical harmonics, i.e. $T(\theta,\varphi) = \sum_{l,m} a_{lm}\, Y_{lm}(\theta,\varphi)$, and then computing the two-point correlation function to obtain the power spectrum,

$$C_l = \frac{1}{2l+1} \sum_{m=-l}^{l} a_{lm}^{*}\, a_{lm}. \tag{4.3}$$

[1] There is also the *integrated Sachs-Wolfe effect*, which acts on photons as they propagate through over- or underdense regions of space whose gravitational potential is distorted due to the expansion of the Universe during the passage of the photons.

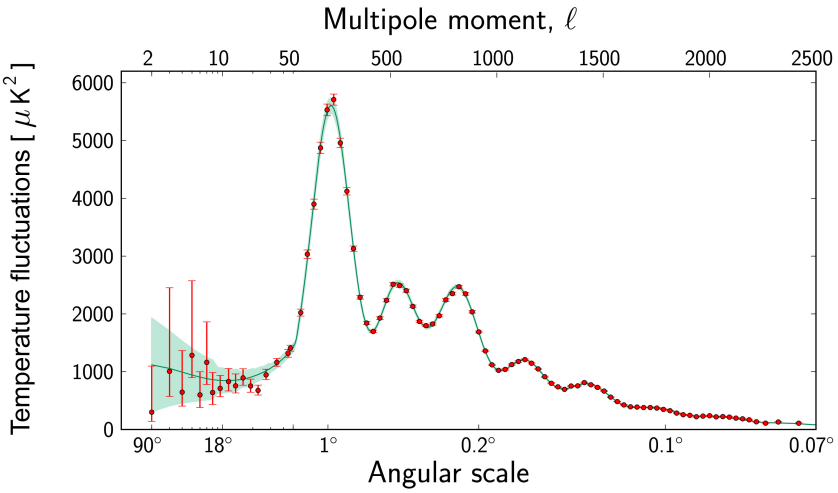

Figure 4.5. Power spectrum of the temperature fluctuations of the CMB as measured by the PLANCK COLLABORATION. The global fit delivers precise values for the parameters of the cosmological model and indicates, among other things, that the baryonic matter accounts for only a fraction of the total mass density in the Universe.
Image credit: ESA and the Planck Collaboration.

This power spectrum is presented in fig. 4.5. It exhibits a multitude of acoustic oscillation peaks, whose amplitude and l-position are highly sensitive to the content and geometry of the Universe, which are parameters of the underlying cosmological model [97]. For instance, the amplitude of the first peak determines the baryon to photon ratio, while the relative heights of the first and second peaks are sensitive to the ratio of the baryon density Ω_b to the DM density Ω_DM [98]. Here, the density parameter for baryons is defined as $\Omega_\mathrm{b} = \rho_\mathrm{b}/\rho_\mathrm{c}$, with the *critical density* ρ_c as the energy density necessary today to close the flat Universe; the density parameter for DM or other components is defined analogously.

The global fit by the PLANCK COLLABORATION to the ΛCDM cosmological model with the latest data (from the year 2018) [96] resulted in

$$\Omega_\mathrm{b} = 0.0493(6), \qquad \Omega_\mathrm{DM} = 0.265(7), \tag{4.4}$$

The simple fact that the CMB delivers the result $\Omega_\mathrm{b} \neq \Omega_\mathrm{DM}$ tells us that there is a large DM component to the Universe that is more abundant than baryonic matter.

Structure Formation and Large Scale Structures

The formation and development of structures, i.e. galaxies, clusters, filaments and voids, relies heavily on DM. The proper description of structure formation is delivered by *cosmological perturbation theory* [101], which is quite extensive and well beyond the scope of what we intend to discuss here. To motivate how structure for-

mation supports, and in fact requires the DM hypothesis, the following comments shall suffice. The seeds for structure formation are the primordial density fluctuations, which provide the primitive gravitational potential wells which can then be populated by matter. These primordial fluctuations can begin to grow due to the clustering of DM from the epoch of matter-radiation equality onwards. Meanwhile, the baryonic matter undergoes acoustic oscillations due to its coupling to photons and can only begin to contribute to the growth of structure after recombination. By that time, the primordial fluctuations have had plenty of time to accumulate mass from the DM infall, which would not be the case in the absence of DM [29]. This illustrates the fact that structure formation proceeds in very different ways in a Universe with versus without DM. Both cases can be studied in cosmological perturbation theory and compared to measurements from galaxy surveys. From this comparison, Dodelson showed in Ref. [100] that the DM hypothesis is the most compelling explanation for structure formation as we observe it. His argument is summarized in fig. 4.6. Simply stated, without DM the density fluctuations could not have grown to produce structures with the density contrast that we see today.

Another way to study the processes of structure formation is through computer simulations. Over the last decades, impressive improvements on computing power and a better understanding of the most likely initial conditions for cosmic develop-

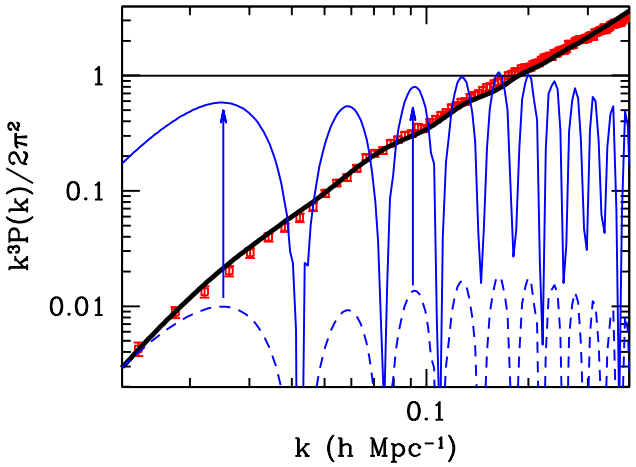

Figure 4.6. A portion of the matter power spectrum. In red we see the data from the SDSS [99]; the solid black line traced the power spectrum expected in the ΛCDM cosmological model with $\Omega_{\rm CDM} \sim 6\Omega_{\rm b}$; the dashed blue line stands for a model in which there is no DM and all the matter density is provided by baryonic matter at $\Omega_{\rm b} = 0.2$. Finally, the solid blue line stands for the modified theory of gravitation Tensor-Vector-Scalar (TeVeS), which obviates DM and amplifies the baryonic perturbations. Clearly, neither the TeVeS theory nor a standard cosmology without DM is able to explain the data. Image from [100].

ment - for example from the CMB - have allowed ever more complex and comprehensive computer simulations. Some have simulated very large volumes to probe physics on large cosmological scales, while other simulations have studied much smaller volumes to study the process of galaxy formation in detail. For instance, the MILLENIUM-XXL simulation used a cube with an edge length of more than 13 billion light years [103], while the AQUARIUS simulation used a cube with a side length of 137 Mpc to follow the evolution of a galactic halo for galaxies similar to the Milky Way [104]. Another distinction is the implementation of only DM or DM + baryonic matter, which increases enormously the complexity of the simulation.

A cosmological simulation starts by specifying a cosmological framework, which contains assumptions about: the underlying theory of gravity (i.e. Relativity or otherwise), the DM properties (warm/cold, fermionic/bosonic, self-interacting, etc.), the nature of Dark Energy (DE) (cosmological constant/inhomogeneous-/dynamic-/coupled DE), and it ideally includes the most important astrophysical processes governing the dynamics of baryonic matter, such as gas dynamics, star formation,

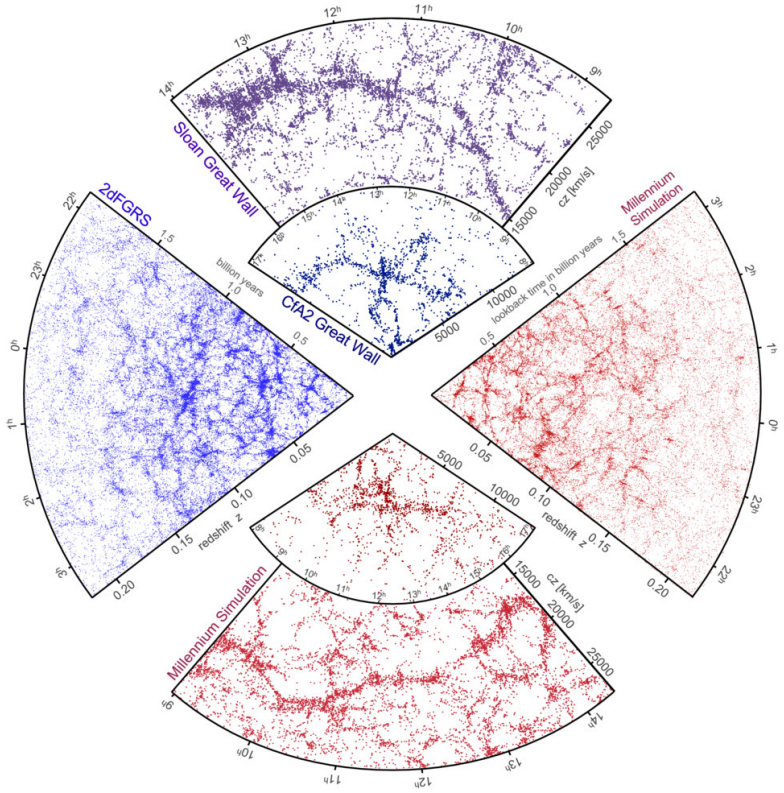

Figure 4.7. Galaxy distribution as measured by the galaxy surveys 2dF and SDSS in blue, and the distribution obtained from the Millennium simulation. The web-like structure, with voids, filaments and walls is well reproduced. Image from [102].

stellar feedback, magnetic fields, cosmic rays and black holes. The comparison of the results of large volume simulations with the distribution of galaxies measured by large galaxy surveys such as the SDSS has shown that the simulations with cold DM correctly predict the large scale structures of the Universe [105], as can be seen in fig. 4.7. On sub-galactic scales, there are some discrepancies between observations and simulations. These concern mainly the abundance of galaxy satellites and the true shape of DM galactic halo density profiles, and could be relieved if the DM was warm instead of cold. However, it is likely that these problems arise as a result of baryonic physics effects and baryonic-DM interactions that have not been accounted for in the simulations [105].

Baryon Acoustic Oscillations

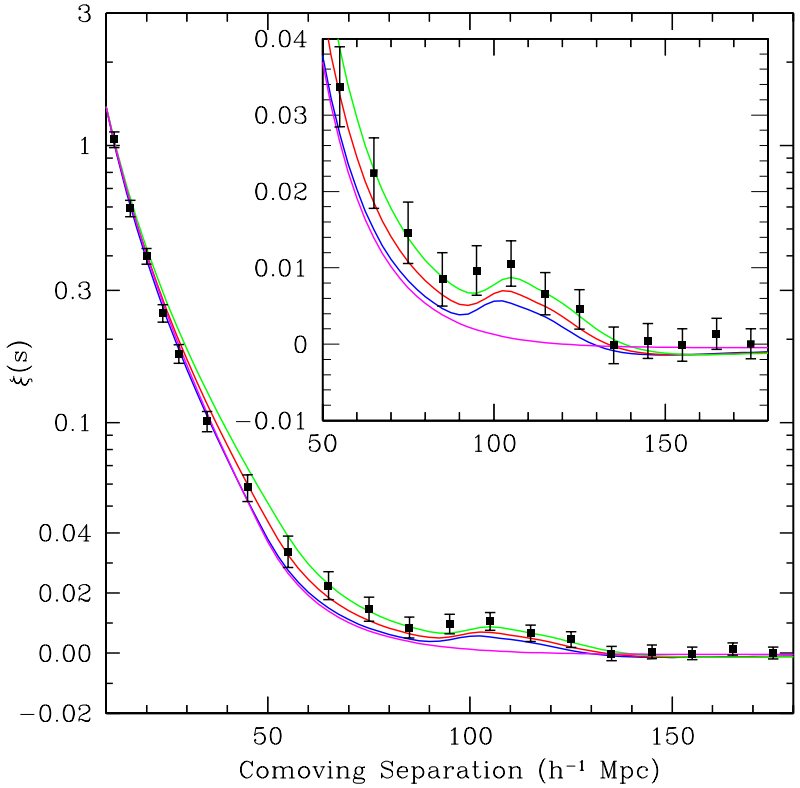

Figure 4.8. Space correlation function for a large sample of luminous red galaxies. The green, red and blue lines describe BAO models with different amounts of total matter, namely $\Omega_{\mathrm{M}}\,h^2 = 0.12,\ 0.13,\ 0.14$ respectively. The magenta line stands for a CDM model without BAO. The easily visible bump at $\sim 100h^{-1}\,\mathrm{Mpc}$ is precisely the expected result of BAO. Image from [106].

The BAOs mentioned above in our discussion about the CMB leave an important signature not only in the temperature fluctuations of the CMB but also on the matter power spectrum and therefore on the distribution of galaxies as observed today. As we saw, the CMB fluctuations reveal a snapshot of the cosmic plasma at the moment of recombination. Some of the acoustic modes were precisely in their phase of maximal compression or rarefaction at the moment of recombination. The BAO modes that were at maximal rarefaction form shells of baryon overdensity with a radius equal to the sound horizon at the moment of recombination. Then, these shells of baryon overdensity begin to gravitationally pull material towards them and thus act as late seeds for the formation of galaxies. These feature appears as a small bump in the spacial correlation function of the distribution of galaxies, as can be seen in fig. 4.8.

From the analysis of the impact of BAOs on the matter power spectrum, some parameters of the cosmological model can be extracted, such as the Hubble parameter and the matter density parameter. Indeed, assuming the ΛCDM model, the final data from the SDSS-III Baryon Oscillation Spectroscopic Survey found for the density fraction of matter (dark and baryonic) [107]

$$\Omega_{\mathrm{M}} = 0.310(6), \tag{4.5}$$

which is in good agreement with other probes and is consistently larger than the baryonic density fraction Ω_{b}.

4.2 Dark Matter Candidates

The evidence in favour of the existence of DM is extensive and compelling. But what physical entity is hiding behind what we call Dark Matter? Initially, it was thought that MACHOs, such as inert or otherwise very faint stars could account for the missing mass, but this hypothesis has since been ruled out, with the exception of a small window for non-baryonic objects of asteroid masses [108]. In the recent years, primordial black holes (PBH) have been claiming a lot of attention as a potential explanation [109], particularly since the detenction of GW [110], but these too have become strongly disfavoured by stringent constraints [111]. An alternative explanation could come in the form of a modified theory of gravity, such as the Modified Newtonian Dynamics (MOND) theory by Milgrom [112]. Although this type of theories have made a lot of progress in the recent decades, they still face major challenges in explaining cosmological observations [100, 113], which are more easily understood in the *particle* DM scenario. The point of view most widely accepted today is that there exists a massive BSM particle that is responsible for all the astrophysical and cosmological observations attributed to the "missing mass".

The possible DM candidates span a mass range of more than 80 orders of magnitude, from ultralight bosons with masses as tiny as $\sim 10^{-22}\,\mathrm{eV}$ that create macroscopic condensates of galactic size, or heavy BSM particles with masses at the EW scale and above, to PBHs of masses up to many times that of the sun [114]. The

fact that the mass range for candidates is so huge can be seen as a manifestation of our ignorance about the nature of DM. Nevertheless, impressive experimental efforts have gone into searching for DM candidates throughout this wide mass range, resulting in the constraining of the parameter spaces of individual candidates.

In this section we briefly introduce some of the proposed DM candidates, inevitably leaving many out - we do not intend to make a complete list here.

Fuzzy Dark Matter

A scalar field and the associated particles can play the role of the DM in the Universe if the assigned mass is extremely small. This type of DM, where the DM particles are bosons with masses $\sim 10^{-22}\,\mathrm{eV}$, is often called ultra light dark matter (ULDM) or also fuzzy dark matter. At such low mass scales, one finds that Bose-Einstein condensates of astronomical sizes can form, in which case the DM is in a coherent field state and can be described as a classical field [115].

The *de-Broglie* wavelength associated with the condensate can be related to the *Jeans length*, which is the length scale at which a cloud of massive particles finds itself in equilibrium between gravitational attraction and internal pressure (in this case, it is the *quantum pressure* related to the uncertainty principle that counteracts the gravitational pull) [115]. With masses in the region of $\sim 10^{-22}\,\mathrm{eV}$ one obtains wavelengths on kpc scales, i.e. galactic sizes. Thus, the Jeans condition ensures that fuzzy DM clouds form stable galaxy halos, and that the growth of structures on scales below the Jeans length is suppressed, which implies that the formation of halo-cusps and galactic satellites is inhibited, offering a solution to the small scale problems of the cold DM scenario [116]. Furthermore, the equations of motion of fuzzy DM show that at scales above the Jeans length the energy density of fuzzy DM and the power spectrum produced by it behave just like cold DM, so that the advantages of cold DM on large scales are retained in the fuzzy DM picture [117].

The production of fuzzy DM must occur non-thermally, since the DM would otherwise be highly relativistic, which is ruled out by structure formation. Viable non-thermal production mechanisms include out-of-equilibrium decays of parent particles, the decay of topological defects, and the misalignment mechanism [118], which can also be responsible for the production of axions, which we will mention next.

Axions and Axion-like Particles

Axions arise as a solution to the strong CP problem: the QCD Lagrangian can include a term of the form

$$\mathcal{L}_{\mathrm{QCD}} \supset \bar{\theta}\,\frac{g_s^2}{32\pi^2}\,G^a_{\mu\nu}\,\widetilde{G}^{a\mu\nu}, \tag{4.6}$$

where $G^a_{\mu\nu}$ stands for the gluon field strength and $\bar{\theta}$ is a parameter that gets two independent contributions, one related to the phase of the QCD vacuum and another

one related to the quark mass matrix. Crucially, both contributions come from seemingly unrelated sectors of the theory, i.e. the QCD vacuum on the one side and the Yukawa sector on the other. As it turns out, the term in eq. (4.6) violates CP invariance [119] and would induce a sizeable electric dipole moment for the neutron, which however has been experimentally constrained to $\lesssim 10^{-26}\, e\,\mathrm{cm}$ [120], implying that $\bar{\theta}$ must be itself rather tiny, namely $\bar{\theta} \lesssim 10^{-10}$. To explain the vanishing value of $\bar{\theta}$, Peccei and Quinn proposed to introduce a new global symmetry $\mathrm{U}(1)_{\mathrm{PQ}}$ and showed that when the symmetry is spontaneously broken, it dynamically drives the $\bar{\theta}$ parameter towards zero [121, 122]. The Nambu-Goldstone boson associated with the spontaneous symmetry breaking of the $\mathrm{U}(1)_{\mathrm{PQ}}$ symmetry is the axion a. However, the $\mathrm{U}(1)_{\mathrm{PQ}}$ is a chiral symmetry and is also explicitly broken by the term in eq. (4.6), so that the axion becomes a pseudo-Nambu-Goldstone boson and acquires a small mass $m_a \sim \Lambda_{\mathrm{QCD}}/f_a$, where Λ_{QCD} is the QCD scale and f_a stands for the energy scale at which the $\mathrm{U}(1)_{\mathrm{PQ}}$ is spontaneously broken and is also referred to as the axion decay constant [119, 123].

The axion is not inert - it couples feebly to SM particles, notably to the photon, a coupling which is exploited in experimental searches. Current bounds constrain the axion mass well into the sub eV range, where it could potentially be long-lived on cosmological time scales, such that it becomes an interesting DM candidate, if it can be produced to the correct amount in the early Universe [7]. The production has to occur non-thermally, for example through the *misalignment mechanism* [124].

Recently, particles with properties similar to those of the axion, arising as the pseudo-Nambu-Goldstone boson of a global U(1) symmetry and with very tiny masses but unrelated to the strong CP problem of QCD, have been found to be common features of many SM extensions. These so called *Axion-like particles* appear in many BSM models and could potentially play the role of the DM of the Universe, in which case they belong to the class of ultra light DM [117], and in some cases they may even play the role of the Dark Energy of the Universe [125].

Neutrinos

In the 1970s, physicists started investigating the role that neutrinos might play in cosmology [7]. Arguing that the energy density of neutrinos should not overclose the Universe, nor should it affect its expansion history too drastically, Gershtein and Zeldovich [126] and Cowsik and McClelland [127] were able to place bounds on the mass of SM neutrinos. At the time, the masses of the SM neutrinos were rather poorly constrained, and the question of whether there could be additional generations of more massive neutrinos was still open [7]. The idea that massive SM neutrinos could also account for the DM of the Universe was not contemplated until a couple of years later: Szalay and Marx estimated that if neutrinos had masses $\lesssim 13.5\,\mathrm{eV}$, then there should exist a neutrino relic abundance left over from the Big Bang that could explain the observations attributed to DM [128]. Shortly afterwards, Lee and Weinberg showed that if a much heavier neutrino existed, it could provide the missing energy density necessary to close the universe as long as

its mass was $\gtrsim 1 - 15\,\mathrm{GeV}$ [129]. Hereby, Lee and Weinberg showed that a heavy neutral lepton with mass in the GeV scale and weak interactions would decouple from equilibrium and its comoving density would *freeze-out* with a non-relativistic energy distribution. This represents an early version of what later came to be known as *the WIMP miracle*, which we will discuss in section 4.3. From then on, neutrinos were seriously considered as dark matter candidates, until by the mid 1980s the first computer simulations of the cosmological evolution of DM showed that a relativistic relic density of neutrinos (or in other words, a hot relic, as would be the case for eV neutrinos) could not match the observed structures of the Universe [7, 130]. The fourth, heavier neutrino imagined by Lee and Weinberg was also ruled out when it became definitively clear that there are only 3 LH neutrinos lighter than half of the mass of the Z boson in the standard model [131].

However, as we discussed in section 3.3, sterile neutrinos can be added to the theory to generate the tiny masses of LH neutrinos, and they could potentially be an excellent DM candidate. For that, the sterile neutrinos should have masses above the keV scale, be stable on cosmological time scales and be produced to the right amount in the early Universe by a plausible mechanism. Many attempts have indeed been made to realise these conditions, and we will discuss some of them at more length in section 4.4.

WIMPs

In cosmology, the concept of a bath of particles in thermal equilibrium as the state of the Universe in early times was well understood and exploited to compute and predict the CMB, the cosmic neutrino background (CνB) and the process of BBN. These relic densities are produced by the interplay between the interaction rate of the particles in the thermal bath and the expansion of the Universe itself, which dilutes the particle densities and cools the Universe [29]: in short, a particle species will stay in thermal (chemical) equilibrium as long as the rate of number-changing interactions Γ is larger than the expansion rate of the Universe H, each of which evolve differently as function of temperature. As the Universe expands and cools, a temperature is reached which violates the equilibrium condition, i.e. $\Gamma < H$. At that moment, the comoving number density of the particle species in question gets *frozen-out* of thermal equilibrium und stays nearly constant ever after (assuming that the particle species is stable) - this process is often referred to as *freeze-out*, and we will discuss it in more detail later in section 4.3.

One distinguishes between a cold relic density and a hot relic density: the word "cold" here refers to the momentum distribution that the relic particle had at the moment of freeze-out: if the particle was non-relativistic at freeze-out, then it is said to have a cold momentum distribution, whereas it is called "hot" if it was relativistic at freeze-out, and a "warm" momentum distribution is somewhere in between. As mentioned previously, large scale computer simulations rule out hot DM and favour cold DM.

So by the 1990s, when the consensus was reached that the bulk of the mass of the

Universe was contributed by a cold non-baryonic component, a natural assumption was that the relic density of the DM was also thermally produced, just like the other known relics [7]. It was soon realised that for the relic to be cold, the DM particle mass could not be too small, but it should lie in the MeV range and above, and furthermore, its self-annihilation cross section should be of a similar size to that of the SM weak interactions[2] [7]. These realisations were very encouraging, partly because there were many theoretical reasons besides DM to expect new physics to appear at the weak scale. Thus, particle DM candidates with masses in the MeV - TeV range and produced by thermal freeze-out through interactions of strength similar to the weak interactions became known as Weakly Interacting Massive Particles, or WIMPs, for short, and have become one of the most studied and searched for DM candidates [7]. The term "WIMP" should now be understood as a rather diverse class of BSM particles produced by thermal freeze-out: WIMP candidates can be found in supersymmetry (SUSY) theories, GUTs and many other models; they can be scalars, fermions, or vector particles and can couple to the SM either directly or through mediators or portal particles that can be themselves very diverse too [132]. Great efforts are invested into looking for such WIMPs, in direct detection experiments, collider searches and indirect astrophysical observations [132]. And although these searches have not yet found any DM WIMPs but placed strong constraints on them, they remain a very appealing class of DM candidates. Currently, the latest most stringent constraints from WIMP searches are those from the LZ experiment [133, 134], while the most competitive limits from a blind analysis are provided by the XENONnT experiment [135, 136].

WIMPZILLAS

WIMPZILLAS are a class of ultra heavy particles proposed as a DM candidate to offer an alternative to the WIMP paradigm [137]. WIMPZILLAS have masses around $\sim 10^{13}$ GeV and must therefore be produced non-thermally to avoid the unitarity bound [138]. They are assumed to be either exactly stable or very long-lived, with lifetimes comparable to the age of the Universe. In the latter case, they could be a source of ultra high energy cosmic rays (UHECR), even beyond the Greisen-Zatzepin-Kuzmin cut-off [139], but their existence and production does not necessarily rely on any couplings to the SM; WIMPZILLAS may have only gravitational interactions. A handful of possible production mechanism for such ultra heavy DM particles have been proposed, e.g. directly through the decays of the inflaton field in inflation scenarios that include a preheating period [140, 141] or at the end of inflation by gravitational effects acting on the vacuum, in a process similar to that which produces the primordial gravitational perturbations [137, 142].

[2] One of the earliest examples for such a particle as a DM candidate was the GeV neutrino by Lee and Weinberg [129]

Primordial Black Holes

Primordial Black Holes (PBHs) are BHs that formed in the early Universe as opposed to astrophysical black holes, which are the result of the gravitational collapse of very massive dying stars. If they exist, PBHs could provide a contribution to the DM density of the Universe, as Chapline pointed out already in 1975 [143]. Recently, this hypothesis has reclaimed a lot of interest since the first detection of gravitational waves from a BH binary merger in 2015 [110]. PBHs could have been produced in the early Universe by the gravitational collapse of primordial density perturbations after inflation [111], in which case a rough estimate of the mass M of the PBHs formed at a time t can be given by [111]

$$M \sim \frac{t}{G} \sim 10^{15} \left(\frac{t}{10^{-23}\mathrm{s}} \right) \mathrm{g},$$

which shows that from the Planck time $t_{\mathrm{pl}} = 10^{-43}\,\mathrm{s}$ until $t = 1\,\mathrm{s}$ the possible mass range for PBHs extends from $10^{-5}\,\mathrm{g}$ to $10^{38}\,\mathrm{g} \approx 10^{5}\,M_{\odot}$. While PBHs lighter than $10^{15}\,\mathrm{g}$ would have evaporated by now through the emission of Hawking radiation, heavier ones would still exist today, and would behave like cold DM with respect to structure formation [111]. However, many observations have placed stringent constraints on the masses of PBHs that could have formed in the early Universe and contribute meaningfully to the DM density. These constraints come from gravitational lensing observations, gravitational waves, evaporation times, effects on the CMB from the radiation emitted by the PBHs due to the accretion of gas, dynamical arguments related to the stability of dwarf galaxies and wide binary star systems, among others. These constraints currently only leave a small window of $10^{17}\,\mathrm{g} - 10^{22}\,\mathrm{g}$ where PBHs could be a significant fraction of DM. However, all constraints should be taken with a grain of salt, as they all involve important assumptions about the properties of BHs and astrophysical uncertainties [111].

An interesting question is: how could one distinguish astrophysical and primordial BHs? The Chandrasekhar mass $M_{\mathrm{Ch}} \approx 1.4\,M_{\odot}$ is the maximal mass that a white dwarf star can have before the degeneracy pressure in the star ceases to be enough to resist the gravitational pull and the star implodes, resulting in a neutron star or a BH. Detecting BHs with masses below the Chandrasekhar limit M_{Ch} would be solid evidence for the existence of PBHs, because BHs from star collapse should always be heavier than M_{Ch}. For BHs with masses above M_{Ch}, it has been argued that the distinction could be made by analysing the redshift of the merger rate from the GW background: astrophysical BHs would start to merge at a redshift corresponding to an epoch after star formation, while PBHs would start to merge long before the first stars were ever born [144].

4.3 WIMP production: Thermal Freeze-out

The SM plasma that populated the early Universe was in a hot and dense state of thermal equilibrium. As the Universe expands, its temperature decreases. The

process of decoupling from this cosmic thermal equilibrium, also called *freeze-out*, has been very successful at predicting the relic abundances of photons, i.e. the CMB, and of the light chemical elements. Other relics have also been predicted, such as the cosmic neutrino background (CνB), which has not yet been detected but whose existence is uncontroversial [29]. Thus, it appears very plausible that the DM relic abundance was also produced by this mechanism, which we now review. We start our discussion by first presenting an approximative approach to freeze-out, which gives us a chance to introduce some frequently encountered quantities in cosmological thermodynamics. We then continue to explore the more detailed treatment of freeze-out, which is based on the Boltzmann-equation.

The expansion rate of the Universe is described by the Hubble parameter H, which is governed by the Friedmann equation,

$$\left(\frac{\dot{a}}{a}\right)^2 \equiv H^2 = \frac{1}{3\,M_{\rm Pl}^2}\,\rho. \tag{4.7}$$

Here, we have assumed a flat Universe, $M_{\rm Pl} \simeq 2.4 \times 10^{18}\,\text{GeV}$ is the reduced Plank mass and ρ stands for the energy density of the Universe, which receives contributions from radiation, matter (dark and baryonic) and dark energy. At early times ρ was dominated by the radiation component, so that we may substitute

$$\rho \to \rho_{\rm r} = \frac{\pi^2}{30}\,g_\rho\,T^4, \tag{4.8}$$

where g_ρ stands for the number of degrees relativistic of freedom contributing to the energy density and is given by

$$g_\rho(T) = \sum_{i=\text{bosons}} g_i \left(\frac{T_i}{T}\right)^4 + \frac{7}{8}\sum_{i=\text{fermions}} g_i \left(\frac{T_i}{T}\right)^4. \tag{4.9}$$

During the radiation dominated era of the early Universe, particles were kept in thermal equilibrium by the frequent interactions occurring between the particles. For a specific particle species, say χ, we denote its rate of interactions with the plasma by Γ. Thermal equilibrium is maintained as long as the rate of interactions is larger than the rate of expansion of the Universe. This equilibrium condition can loosely be written as

$$\Gamma > H. \tag{4.10}$$

For thermal decoupling, the relevant interactions are usually the number changing interactions, e.g. annihilations, for which the rate is given by

$$\Gamma = \langle\sigma v\rangle\, n_\chi, \tag{4.11}$$

where $\langle\sigma v\rangle$ stands for the thermally averaged cross section of the interactions being considered [145] and n_χ is simply the number density of the χ particles. The expan-

sion of the universe dilutes the number densities of all species, thereby diminishing the interaction rate Γ.[3] As the universe expands and cools, a temperature will be reached at which the interaction rate can no longer keep up with the expansion rate - in other other words, the equilibrium condition will eventually be violated. Thus, the temperature at which $\Gamma \approx H$ occurs, gives us an approximation of the decoupling temperature $T_{\rm fo}$. Until freeze-out, the number density of χ is given by its equilibrium distribution, which for a non-relativistic species is

$$n_\chi^{\rm eq}(T) = g_\chi \left(\frac{m_\chi T}{2\pi}\right)^{3/2} e^{-m_\chi/T}, \tag{4.12}$$

with the internal number of degrees of freedom g_χ, which for a Majorana fermion is equal to 2. At freeze-out, one could simplistically say that n_χ decouples from the thermal bath and is no longer modified by number changing interactions - its evolution is determined only by the dilution due to the cosmic expansion. Therefore, it is convenient to define the relic density

$$y_\chi = \frac{n_\chi}{s}, \tag{4.13}$$

with the entropy density s. The relic density y_χ is just a proxy for the comoving number density, because the effect of dividing by the entropy density is to factor out the dilution of n_χ due to the expansion by using the fact that the total entropy is conserved, i.e. $S = s\,a^3 = \text{const}$. With this, we can already estimate the relic abundance of our WIMP, the particle species χ. For that, we first estimate the relic density at freeze-out by inserting eq. (4.11) into eq. (4.13) and using the freeze-out condition $\Gamma \approx H$ to eliminate Γ. We then obtain

$$y_\chi^{\rm fo} \approx \frac{\pi \sqrt{g_\rho}\, T_{\rm fo}^2}{\sqrt{90}\, \langle\sigma v\rangle\, M_{\rm Pl}\, s(T_{\rm fo})} \tag{4.14}$$

Next, we insert the entropy density

$$s = \frac{2\pi^2}{45}\, g_s\, T^3. \tag{4.15}$$

which contains the number relativistic of degrees of freedom that contribute to entropy,

$$g_s(T) = \sum_{i=\text{bosons}} g_i \left(\frac{T_i}{T}\right)^3 + \frac{7}{8} \sum_{i=\text{fermions}} g_i \left(\frac{T_i}{T}\right)^3. \tag{4.16}$$

We also introduce the dimensionless variable $z = M/T$, which is a proxy for time

[3] The thermally averaged cross section $\langle\sigma v\rangle$ might itself be temperature dependent too.

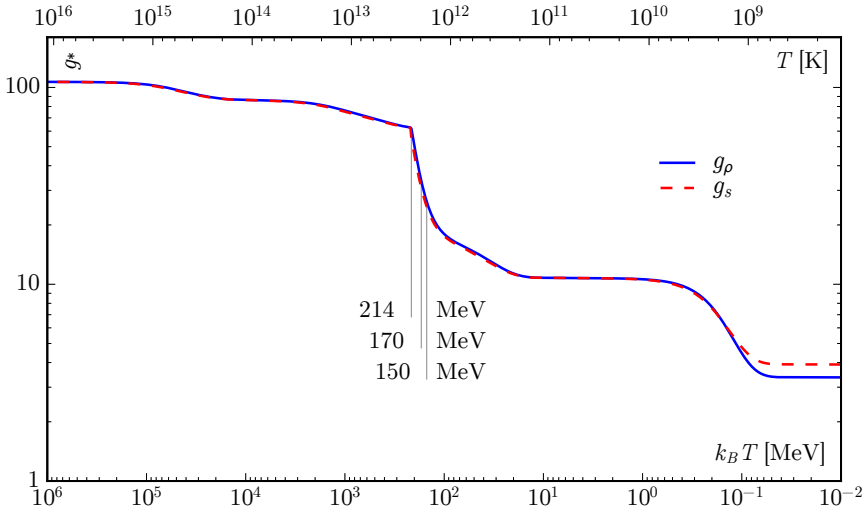

Figure 4.9. The number of degrees of freedom g_ρ and g_s contributing to the energy density and entropy density respectively as functions of temperature. They are equal down to temperatures of about $\sim 200\,\mathrm{keV}$. Image adapted from [146].

$t \sim 1/T$, and use it to replace T. Then, the relic density is estimated as

$$y_\chi^{\mathrm{fo}} \approx \sqrt{\frac{45}{8\pi^2}} \left(\frac{\sqrt{g_\rho(T_{\mathrm{fo}})}}{g_s(T_{\mathrm{fo}})} \right) \frac{z_{\mathrm{fo}}}{\langle \sigma v \rangle \, M_{\mathrm{Pl}} \, m_\chi}. \tag{4.17}$$

Looking at the definitions of g_ρ and g_s, eqs. (4.9) and (4.16), we realize that they only differ from each other when there are degrees of freedom that contribute to ρ or s while having a different temperature than the photons, which is only the case after the $e^+\,e^-$ annihilation that reheats the photons but not the neutrinos, i.e. at $T < 100\,\mathrm{keV}$, as can be seen in fig. 4.9. Also, prior to the QCD phase transition and particularly above the EW scale $T \gtrsim 100\,\mathrm{GeV}$ we may approximate $g_\rho = g_s \approx 100$ (the actual SM value is $g_\rho(T > m_t) = 106.75$). With that, we arrive at the estimate

$$y_\chi^{\mathrm{fo}} \approx 0.075 \, \frac{z_{\mathrm{fo}}}{\langle \sigma v \rangle \, M_{\mathrm{Pl}} \, m_\chi}. \tag{4.18}$$

For the freeze-out temperature, which goes into z_{fo}, we can find an estimate from the decoupling condition $\Gamma \approx H|_{T=T_{\mathrm{fo}}}$ for a given combination of $(\langle \sigma v \rangle \cdot m_\chi)$ (the approximation depends only logarithmically on $(\langle \sigma v \rangle \cdot m_\chi)$, see [147]). Typical values lie in the range $z_{\mathrm{fo}} = 15 - 35$. The relic abundance for a non-relativistic

species χ today is defined as

$$\Omega_{\rm DM} = \frac{\rho_{\rm DM}}{\rho_c} = \frac{n_{\chi,0}\, m_\chi}{\rho_c} = \frac{y_\chi^{\rm fo}\, s_0\, m_\chi}{\rho_c}, \tag{4.19}$$

where ρ_c is the critical density and the 0 index stands for values taken today. What is actually inferred from the CMB is the product $\Omega_{\rm DM}\, h^2$, where h stands for the value of the Hubble constant today in units of $100\,{\rm km\,s^{-1}\,Mpc^{-1}}$. Thus, inserting the values $\rho_c = 1.05 \times 10^{-5}\, h^2\,{\rm GeV\,cm^{-3}}$, $s_0 = 2891.2\,{\rm cm^{-3}}$, $M_{\rm Pl} = 2.4 \times 10^{18}\,{\rm GeV}$ from [96] and $y_\chi^{\rm fo}$ from eq. (4.18) we finally obtain the result

$$\Omega_{\rm DM}\, h^2 \approx 0.007\, z_{\rm fo} \left(\frac{10^{-9}\,{\rm GeV^{-2}}}{\langle \sigma v \rangle} \right), \tag{4.20}$$

which carries no explicit dependence on the DM mass and takes the correct value of $\Omega_{\rm DM}\, h^2 = 0.12$ for $z_{\rm fo} = 17$.

This approximation serves well to illustrate what is commonly known as the *WIMP miracle*, which originally made EW scale DM so appealing: if the interaction strength driving the annihilation of DM particles is of a similar size to the SM weak interaction, then the freeze-out mechanism, which is responsible for other known relic abundances, naturally produces the correct amount of DM.

This heuristic approach is very useful to get a quick estimate of the relic abundance, and particularly the relation $\Omega_{\rm DM} \sim \langle \sigma v \rangle^{-1}$, but it is just that: a very rough approximation. It leaves out some important details and it makes some effects and dependencies intransparent. The proper treatment involves solving the full Boltzmann equation, which is an integro-differential equation for the momentum distribution function of the particle in question, $f_\chi(\vec{p}, t)$, namely

$$L[f_\chi] = C[f_\chi], \tag{4.21}$$

where L is the *Liouville operator* that describes the time evolution of f_χ taking the expansion of the background into account, and C is the *collision operator* that describes all the particle interactions involved in the evolution of f_χ. In the left hand side $L[f_\chi]$ contains input from general relativity and cosmology related to the expansion of the Universe, while the right hand side $C[f_\chi]$ contains all of the particle physics input. The solution to the equation is the momentum distribution f_χ, which allows us to perform statistical physics calculations and compute the number density of χ. The complete formulation of the Boltzmann equation for a DM WIMP can be found chapter B. After some manipulations and simplifying assumptions, one arrives at

$$\frac{dn_\chi}{dt} + 3Hn_\chi = -\langle \sigma v \rangle (n_\chi^2 - n_{\chi,\rm eq}^2), \tag{4.22}$$

which after some more manipulations and introducing the relic density y_χ and the

variable $z = m/T$ can be rewritten as

$$\frac{dy_\chi}{dz} = -\frac{s\,\langle\sigma v\rangle}{z\,H}\left(y_\chi^2 - y_{\chi,\mathrm{eq}}^2\right) \tag{4.23}$$

$$\frac{dy_\chi}{dz} = -\sqrt{\frac{8\pi^2}{45}}\frac{M_{\mathrm{Pl}}\,m_\chi\,g_*^{1/2}}{z^2}\,\langle\sigma v\rangle\,\left(y_\chi^2 - y_{\chi,\mathrm{eq}}^2\right), \tag{4.24}$$

where we have defined

$$g_*^{1/2} := \frac{g_s(T)}{\sqrt{g_\rho(T)}}\cdot\left(\frac{1}{3}\frac{d\,\ln g_s(T)}{d\ln T} + 1\right). \tag{4.25}$$

Notice again that for $T > 100\,\mathrm{keV}$ we can set $g_s = g_\rho$ and in some temperature intervals they are approximately constant, so that the temperature derivative can be neglected. Concretely, we can safely set $g_*^{1/2} \approx 10.3$ for $T > 1\,\mathrm{GeV}$. Equation (4.23) can now be solved either numerically or through analytical approximations [29, 145, 147]. For the analytical approximations, one first considers the late-time/low-temperature regime, where $y_{\chi,\mathrm{eq}}$ can be neglected and eq. (4.23) becomes a homogeneous differential equation, which can then be integrated from z_{fo} to $z = \infty$ today, delivering the result

$$y_{\chi,0} = 0.75\,\frac{z_{\mathrm{fo}}}{M_{\mathrm{Pl}}\,m_\chi\,g_*^{1/2}\,\langle\sigma v\rangle}, \tag{4.26}$$

which is almost identical to eq. (4.18) except for the presence of $g_*^{1/2}$. Then, to determine z_{fo}, one examines the early-time/high-temperature regime of eq. (4.23), where the comoving density closely traces its equilibrium version. One then considers the departure of y_χ from $y_{\chi,\mathrm{eq}}$, quantified by $\Delta = (y_\chi - y_{\chi,\mathrm{eq}})/y_{\chi,\mathrm{eq}}$ and specifies z_{fo} as the temperature for which $\Delta(z_{\mathrm{fo}}) = (\sqrt{5}-11)/2 \approx 0.62$, which appears rather arbitrary, but agrees well with the numerical solution [147]. This results in

$$z_{\mathrm{fo}} + \ln(z_{\mathrm{fo}} - 1.5) - 0.5\,\ln(z_{\mathrm{fo}}) = 20.5 + \ln\left(\frac{\langle\sigma v\rangle}{10^{-26}\,\mathrm{cm^3 s^{-1}}}\right) + \ln\left(\frac{m_\chi}{\mathrm{GeV}}\right) - \ln\left(g_*^{1/2}\right),$$

which can be solved iteratively and shows that the value of z_{fo} depends only logarithmically on $\langle\sigma v\rangle$ and m_χ. Scanning over $m_\chi \in [10^{-1}..10^4]\,\mathrm{GeV}$ and inserting the necessary $\langle\sigma v\rangle$ for the observed DM relic abundance to be reached, z_{fo} takes values in the interval $[17..27]$ [4].

The final result for the relic abundance in this analytical approximation to the

[4] Steigman, Dasgupta, and Beacom emphazise in [147] that z_{fo} as computed here does not actually stand for the temperature of freeze-out, but actually for the temperature at which Y_χ starts departing from $Y_{\chi,\mathrm{eq}}$; they therefore write z_* instead of z_{fo} and show that at $z = z_*$ decoupling has not yet completely occurred because $\Gamma/H|_{z=z_*} > 1$ and annihilations still occur, depleting Y_χ until it reaches its asymptotical value of $Y_{\chi,0} = Y_{\chi,\mathrm{eq}}$ when $\Gamma/H|_{z=z_*} < 1$.

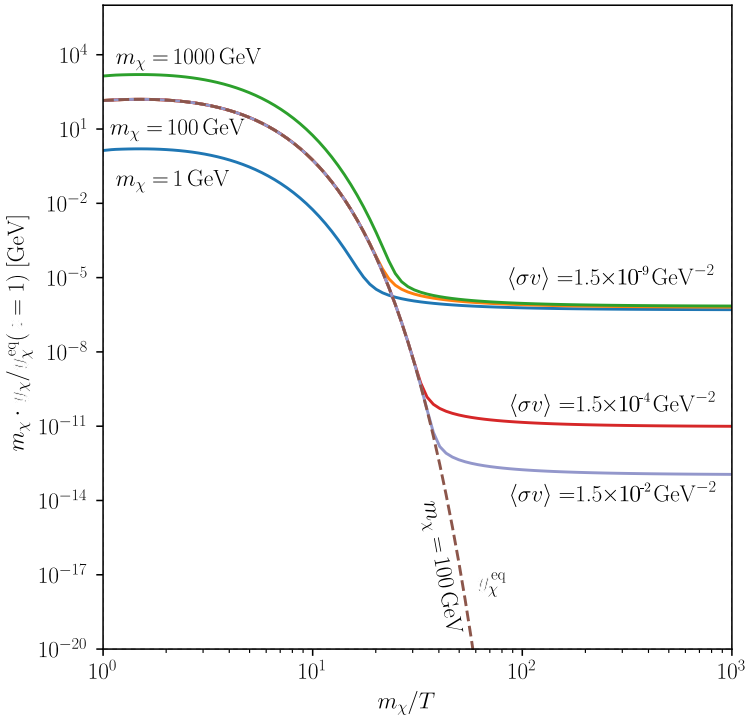

Figure 4.10. WIMP relic densities for different values of m_χ and $\langle\sigma v\rangle$. The curves are normalized by the value of $y_{\chi,\mathrm{eq}}(T = m_\chi)$ and are multiplied by m_χ, just as they appear in formula for the relic abundance, i.e. $\Omega_{\mathrm{DM}} \propto y_{\chi,0}\, m_\chi$, where m_χ cancels out and results in the non-dependence of Ω_{DM} on the WIMP mass m_χ, which we can see here clearly from the upper three curves.

solution of the Boltzmann equation is

$$\Omega_{\mathrm{DM}}\, h^2 \approx 0.084 \left(\frac{z_{\mathrm{fo}}}{g_*^{1/2}}\right) \left(\frac{10^{-9}\,\mathrm{GeV}^{-2}}{\langle\sigma v\rangle}\right). \tag{4.27}$$

The numerical solution is shown in fig. 4.10. It must be pointed out, that the Boltzmann equation derived for χ describes only the simplest WIMP scenario in a standard cosmology. The simplifying assumptions include: the WIMP χ annihilates through 2 to 2 processes $\chi\chi \leftrightarrow \bar{f}f$ into SM particles, the s-wave is the most important contribution to $\langle\sigma v\rangle$ and the cross section has no thresholds or resonances in the relevant energy range. Departures from these assumptions would necessitate a dedicated treatment, as has been studied in ref. [148].

4.4 Sterile Neutrinos as Dark Matter

Adding three RH neutrinos to the SM is a minimal and very attractive extension to the theory. Although the number of additional RH neutrinos is not strictly limited to three - one could in principle add any number of sterile neutrinos - the choice of three is natural in the sense that it reestablishes the symmetry between the lepton and quark sector, so that every LH particle has a RH partner. Since the sterile neutrinos are SM singlets, they can be endowed with a Majorana mass term and naturally generate the tiny masses of the SM neutrinos by means of the seesaw mechanism. If the lightest sterile neutrino is long lived up to cosmological time scales, it could potentially be an excellent DM candidate. This minimal extension is realized in the so called νMSM [149], where baryogenesis through leptogenesis can also be implemented, provided that the masses of the heavy sterile neutrinos are arranged in a specific pattern [150].

Here we are mostly interested in the lightest sterile neutrino as a DM candidate, which we will refer to as N_1. What requirements does N_1 have to fulfil in order to actually be a viable DM candidate? First, as mentioned above, it should be long lived; through their Yukawa coupling, sterile neutrinos can mix with active neutrinos and decay. What decay channels are open depends on the sterile neutrino mass. Since DM matter should be produced in the early Universe and continue to exist today, the lifetime of N_1 should be at least comparable to the age of the Universe in order for N_1 to be able to play the part. This will require the Yukawa coupling, or equivalently the active-sterile neutrino mixing angle, to be very small, which will place strong bounds on the parameter space of sterile neutrinos. Second, the relic abundance of N_1 must match the observations. The most precise measurement available today for the DM abundance is analysis of the CMB anisotropies by the PLANCK collaboration, $\Omega_{\rm DM}\, h^2 = 0.1200(12)$ [96]. For N_1 to make up 100% of the DM, this value must be saturated by an appropriate production mechanism at work in the early Universe. It is possible that the DM density is actually made up of multiple components and N_1 only provides a fraction of the full abundance, in which case we would find $\Omega_{N_1} < \Omega_{\rm DM}$, but in any case the N_1 abundance must not exceed the PLANCK measurement - in such cases we would rule out the production mechanism by overproduction.

In the following, we will briefly discuss the most common production mechanisms and discuss how they are constrained by astrophysical observations. We will not go into too much depth regarding the already known production mechanism, as they are not relevant to the proposition and scientific contribution of this thesis, which is a whole new and unrelated production mechanism.

4.4.1 Standard Production Mechanisms

Production by non-resonant oscillations

As we discussed in section 3.3, if sterile neutrinos are present and take part in the type I seesaw mechanism, then there is a small admixture between active

and sterile neutrinos, which leads to the production mechanism by active-sterile neutrino oscillations, first proposed by Dodelson and Widrow in 1994 [151]. In the case of three sterile states, as we are considering here, the mixing angle between $\nu_{L\alpha}$ and ν_{Ri} is

$$\theta_{\alpha i} = (m_D)_{\alpha j}\,(M_R^{-1})_{ji}, \tag{4.28}$$

and since $\theta_{\alpha i} \ll 1$ the heavy neutrinos mass eigenstates are almost totally aligned with the right handed Majorana states, i.e. $\nu_{Ri} \approx N_i$. For simplicity, in this section we will consider only one sterile neutrino N_1 with mass M_1, and ignore the other two. The sterile neutrino N_1 is here the DM candidate. Accordingly, we here denote the mixing angle between N_1 and the active neutrinos simply as θ. Because the sterile neutrinos only communicate with the SM through $\theta \ll 1$, N_1 never reaches thermal equilibrium. However, even with a vanishing initial population of sterile neutrinos, they can nevertheless be produced in the early Universe through decoherent neutrino scattering: essentially (in the quantum mechanical picture), after an active neutrino has been produced in a flavour eigenstate and begins to propagate, its mass eigenstate components evolve with their quantum mechanical phases, just like with usual neutrino oscillation, except that there is also a sterile neutrino component. By the time it is about to undergo its next scattering, its wave function is forced to collapse onto one active flavour state, or (crucially) a sterile state that evades the scattering event and begins a new propagation process. Since all of this occurs not in vacuum, but in the hot and dense plasma of the early Universe, matter and temperature effects must be taken into account, which is done by replacing the vacuum mixing angle θ by the temperature dependent mixing angle in matter $\theta_m(T)$. The rate with which sterile neutrinos can be produced by decoherent scatterings is

$$\Gamma_N \sim \Gamma_\nu\,\theta_m^2(T), \tag{4.29}$$

where the scattering rate of active neutrinos Γ_ν depends on the temperature; if decays and inverse decays involving the Higgs boson are kinematically allowed, they will dominate, whereas below the EW temperature the gauge interactions of the light neutrinos determine the rate [116], thus

$$\Gamma_\nu \sim \begin{cases} M_1^2 T/v^2, & \text{for} \quad T > T_{EW}, \\ G_F^2\,T^2 \cdot n_\nu(T) \sim G_F^2\,T^2 \cdot T^3, & \text{for} \quad T < T_{EW}. \end{cases} \tag{4.30}$$

The finite temperature potential induced by the neutrino interaction in the plasma leads to the following mixing angle in matter [152]:

$$\sin^2(2\theta_m) = \frac{(\Delta m^2/2p)^2 \sin^2(2\theta)}{(\Delta m^2/2p)^2 \sin^2(2\theta) + [(\Delta m^2/2p)\cos(2\theta) - V_T]^2}, \tag{4.31}$$

where the mass squared difference between the active and the sterile state is Δm^2 and p stands for the momentum. Furthermore, V_T stands for the finite temperature potential, which is always negative and, at the relevant temperature range, goes as $V_T = -G_{\text{eff}}\, p\, T^4$, where G_{eff} is of the order of the Fermi constant and represents the global coupling of the neutrinos to the plasma [73]. Then, the matter mixing angle can be approximated as [116]

$$\theta_m \simeq \frac{\theta}{1 + 2.4 \left(\frac{T}{200\,\text{MeV}}\right)^6 \left(\frac{1\,\text{keV}}{M_1}\right)^2}, \tag{4.32}$$

where we easily recognise that the matter-mixing angle, and thus the sterile neutrino production, is highly suppressed at $T > 100\,\text{MeV}$; indeed, inserting eq. (4.32) into eq. (4.29) and maximizing with respect to temperature, we find that peak production is achieved at

$$T_{\text{prod}}^{\text{peak}} \approx 150 \left(\frac{m}{1\,\text{keV}}\right)^{1/3} \text{MeV} \tag{4.33}$$

This temperature is in the region of the QCD phase transition, which makes the full, precise computations a lot more complex. The sterile neutrino abundance is obtained by integrating Γ_N over temperature throughout the evolution of the Universe. An analytical approximation for the resulting abundance is given by [73]

$$\Omega_{N_1} \sim 0.2 \left(\frac{\sin^2\theta}{3 \cdot 10^{-9}}\right) \left(\frac{M_1}{3\,\text{keV}}\right)^{1.8}. \tag{4.34}$$

Full computations can be found in the literature, e.g. [153]. This production mechanism, referred to as the *Dodelson-Widrow* (DW) mechanism, or also as "production by non-resonant oscillations", is straightforward and requires nothing more than the non-vanishing admixture between active and sterile neutrinos from the Yukawa term. If the Yukawa term is there, production via the DW mechanism is inevitable. Equating eq. (4.34) with the observed DM abundance, we would obtain a curve in the $(M_1,\, \sin^2\theta)$ space along which DW produced sterile neutrinos account for 100% of the DM of the Universe. However, as we will explain in the next section, X-ray (non-)observations have already ruled out this mechanism as the one responsible for producing 100% of the DM in the form of sterile neutrinos.

Production by resonant oscillations

There is an important modification that can be done to the DW mechanism. If a significant lepton asymmetry is present at the time of N_1 production, then additional matter effects must be taken into account. In short, this is done by including

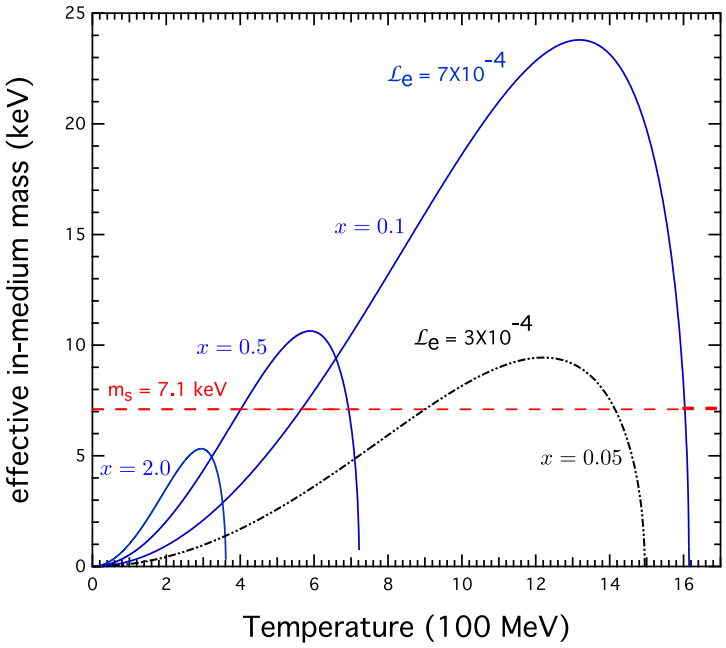

Figure 4.11. The effective in-medium neutrino mass as a function of temperature and for different values of the scaled momentum $x = p/T$ for two different values of the electron lepton number, assuming that the active-sterile transition occurs only involving the electron neutrino, namely $\mathcal{L}_e = 7 \times 10^{-4}, 3 \times 10^{-4}$. The mass of the DM neutrino is taken to be 7.1 kev, represented by the horizontal red dashed line; when it crosses the curve M_{eff} the resonance condition is fulfilled and thus the DM production is enhanced. Plot from [152].

the finite density potential V_D in the matter-mixing angle, which then reads [152]

$$\sin^2(2\theta_m) = \frac{(\Delta m^2/2p)^2 \sin^2(2\theta)}{(\Delta m^2/2p)^2 \sin^2(2\theta) + [(\Delta m^2/2p)\cos(2\theta) - V_T - V_D]^2}. \tag{4.35}$$

This now opens the possibility that the second term in the denominator vanishes, i.e.

$$0 \stackrel{!}{=} \frac{\Delta m^2}{2p}\cos(2\theta) - V_T - V_D, \tag{4.36}$$

in which case the amplitude for the active-sterile oscillations becomes maximal. This is the *Shi-Fuller* mechanism [154], which makes it possible to successfully produce sterile neutrino DM even with a much smaller vacuum mixing angle. Note that this was not possible without V_D because the finite temperature potential is always negative, $V_T < 0$. Since $\theta \ll 1$ and the mass of the sterile neutrino is much larger than the mass eigenstates mostly aligned with the active neutrinos, we can

safely approximate $\Delta m^2 \cos(2\theta) \approx M_1^2$ and thus rewrite the resonance condition as

$$M_1^2 \simeq 2p\,V_D + 2p\,V_T. \tag{4.37}$$

The density potential can be written as [152]

$$V_D = \frac{2\sqrt{2}\zeta(3)}{\pi^2}\,G_F\,\mathcal{L}_\alpha\,T^3, \tag{4.38}$$

where $\mathcal{L}_\alpha$ is a measure of the lepton number asymmetry in the flavour α. Inserting again $V_T = -G_{\text{eff}}\,p\,T^4$ we obtain the resonance condition as

$$M_{\text{eff}}^2(T) := \frac{4\sqrt{2}\,\zeta(3)}{\pi^2}\,G_F\,\mathcal{L}_\alpha\,p\,T^3 - 2G_{\text{eff}}\,p^2\,T^4 \overset{!}{\simeq} M_1^2, \tag{4.39}$$

whereby in the literature one often finds that the momentum p is replaced by the temperature-scaled momentum $x = p/T$. Thus, the effective-mass is a function of T and p (or equivalently x) and encapsulates the finite temperature and lepton asymmetry effects. When M_{eff} and M_1 cross, the resonance condition is fulfilled and the sterile neutrino production is enhanced, as can be seen in fig. 4.11. The DM neutrinos produced in this way can have a non-thermal spectrum with the bulk of the distribution shifted to lower energies, so that in this sense, the DM is colder [152].

The lepton asymmetry necessary for the resonance to successfully produce sterile neutrino DM with keV masses must be much larger than the known baryon asymmetry, namely $\eta_L \sim 10^{-6} > \eta_B \sim 10^{-10}$ [116]. Within the νMSM, it is possible to implement successful baryogenesis through leptogenesis and also generate the necessary lepton number asymmetry for the resonant production of keV sterile neutrino DM, provided that the two heavier sterile neutrinos have quasi-degenerate masses in the GeV range [155]: above the EW scale, the two heavier sterile neutrinos N_2 and N_3 generate a net lepton number through active-sterile oscillations, which is then transferred to the baryon sector by the sphalerons [156]. Below EW scale, when the sphalerons are no longer in equilibrium, N_2 and N_3 decay and thereby rebuild the lepton number asymmetry necessary for the resonant production of N_1. While this scenario seems convenient, the price to pay is the peculiar hierarchy in the Majorana mass matrix. Furthermore, X-ray constraints have also closed large regions of the parameter space where this model would work so elegantly.

Production through decays of other particles

A very different alternative is that the DM sterile neutrinos are not produced by any kind of oscillations, but are the product of the decay of some additional parent particle, for example a SM singlet scalar S. A representative realization of this scenario is discussed e.g. in Ref. [157]. The inclusion of S would allow for the

presence of a Yukawa type term between S and N_1,

$$\frac{f}{2}\,\overline{N_1{}^c}\,N_1\,S + \text{h.c.}, \tag{4.40}$$

with the coupling constant f, which opens the way for the decay $S \to N_1{}^c\,N_1$. There are many possible variations of this mechanism [152]: the parent particle can be in equilibrium or not at the era of N_1 production, there may or may not be other decay channels for S, and the parent particle S could be a vector or a fermion instead of a scalar. While many of this scenarios may be well motivated and interesting in their own right, they all go beyond the minimality of the νMSM, where the SM is extended only by three RH neutrinos.

4.4.2 Observational constraints on neutrino Dark Matter

In the following we will discuss some of the astrophysical observations that constrain the parameter space of sterile neutrino DM. Particularly for keV neutrino DM, these bounds are complementary and thus restrict the parameter space from different directions, closing in on a window of parameter space where the νMSM might survive.

The Tremaine-Gunn bound

The Tremaine-Gunn bound [158] is model independent and applies not only to sterile neutrinos but actually to any fermionic DM candidate. In short, the argument is that for fermionic DM particles with masses below a certain bound, the phase-space distribution of the DM in a galactic halo would have to violate the Pauli exclusion principle in order to explain the amount of DM observed in said galactic halo. Therefore, DM masses below said bound are forbidden.

The densest phase-space configuration in a DM halo would be realized by a self gravitating Fermi gas. Consider a spherically symmetric halo of total mass M and radius R. The maximal Fermi velocity in such a cloud is given by [159]

$$v_{\text{max}}^{\text{Fermi}} = \hbar \left(\frac{9\pi\, M}{2\, g_\chi\, m_\chi^4\, R^3} \right)^{1/3}, \tag{4.41}$$

with m_χ as the mass of a generic fermionic DM particle - in our case of sterile neutrinos, we could replace m_χ with M_1 - and g_χ stands for the number internal degrees of freedom of χ. In order for the halo not to disintegrate, $v_{\text{max}}^{\text{Fermi}}$ must be smaller than the escape velocity of the halo $v_{\text{esc}} = \sqrt{2\,G_N\,M/R}$. From this condition, after solving for m_χ, we obtain the bound

$$m_\chi \geq \left(\frac{9\pi\hbar^3}{4 g_\chi \sqrt{2\, M\, R^3\, G_N^3}} \right)^{1/4}. \tag{4.42}$$

Dwarf spheroidal galaxies (dSph) are expected to have very compact and homogeneous DM halos and therefore represent excellent environments to apply this bound, which has been done, e.g. in Ref. [159], who reported

$$m_\chi \geq 0.4\,\mathrm{keV}. \tag{4.43}$$

This formulation of the Tremaine-Gunn bound is powerful because it is almost universal: the only assumption made was that the DM halo is spherical. Beyond that, the only uncertainties come from accurately characterizing the halo with appropriate parameters M and R.

However, the bound can be strengthened by adopting additional assumptions: if we assume a particular primordial momentum distribution - in the case of thermal production, a Fermi-Dirac or a Maxwell-Boltzmann distribution depending on whether the DM was relativistic or not - then we may use *Liouville's theorem*, from which it follows that the maximum of the distribution remains unchanged throughout its evolution. Liouville's theorem applies for collisionless and dissipationless dynamics, but these are assumed to be general properties of DM, except perhaps in the case of self-interacting DM. This approach applied to sterile neutrino DM produced by the Dodelson-Widrow mechanism results in the bound [159]

$$M_1 \geq 2.79\,\mathrm{keV}\,. \tag{4.44}$$

Bounds from the Lyman-α forest

Sterile neutrinos with masses in the keV range playing the role of the DM of the Universe are usually relativistic at the time of production and become non-relativistic later in cosmological history - therefore they are often referred to as warm DM, as opposed to cold DM, which is non-relativistic already at production. Cold and warm DM impact structure formation differently: due to its relativistic velocity, warm DM has a free streaming length λ_{FS} below which it tends to impede the growth of structures. This length scale for sterile neutrinos is [116]

$$\lambda_{\mathrm{FS}} \sim 1\,\mathrm{Mpc}\left(\frac{1\,\mathrm{kev}}{M_1}\right)\left(\frac{\langle p/T\rangle}{3.15}\right), \tag{4.45}$$

where $\langle p\rangle$ is the averaged momentum of the sterile neutrinos. Thus, due to free streaming, we do not expect structures with length scales smaller than λ_{FS} to have formed if warm sterile neutrinos are the DM. The mass that would have otherwise gravitationally collapsed at those scales is

$$M_{\mathrm{FS}} \sim 3\times 10^{10}\,M_\odot\left(\frac{1\,\mathrm{kev}}{M_1}\right)^3\left(\frac{\langle p/T\rangle}{3.15}\right)^3, \tag{4.46}$$

thus we also do not expect to find cosmological structures with masses below M_{FS}. Quantitatively, warm DM suppresses the power above a certain momentum scale $k_{\mathrm{FS}} \sim \lambda_{\mathrm{FS}}^{-1}$ with respect to the power spectrum of cold DM, whereby the sup-

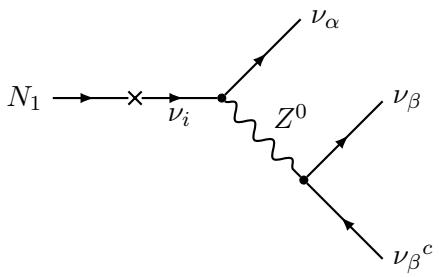

Figure 4.12. Sterile neutrino decay at three level.

pression scale k_{FS} depends on the primordial momentum distribution and the DM mass [116]. To measure the power spectrum at this small scales one measures the Lyman-α absorption line of neutral hydrogen in the intergalactic medium (IGM). While the IGM is gravitationally dominated by DM, it also contains a lot of neutral hydrogen of primordial origin. The radiation for the absorption line is provided by background quasi-stelar objects (QSO), also known as *quasars*. Since the Lyman-α line is very precisely known, spectrographic observations of the IGM allow the determination of the redshift and density of the absorbing material, from which one can then infer the power spectrum [152]. At this point it is worth emphasizing that this method constraints the free streaming length of DM, which can be translated to a constrain on the DM mass only under additional assumptions regarding the primordial DM spectrum, which is determined by the DM production mechanism. Thus, in contrast to the Tremaine-Gunn bound, this method is highly model-dependent. Depending on the assumed production mechanism and primordial spectrum, a lower bound on the mass of warm DM on the range between $10 - 20\,\mathrm{keV}$ has been computed [160, 161]. However, it must be said that Lyman-α analyses are highly sensitive to the temperature and thermal history of the IGM, which is largely unknown but can have an important effect on the results [162]. Due to this and other systematic uncertainties, Lyman-α bounds remain controversial and are therefore often not quoted in the sterile neutrino DM literature.

Constraints from X-ray searches

Sterile neutrinos as in the νMSM, with a Yukawa coupling to the SM Higgs and active neutrinos, are unavoidably unstable (unless one goes beyond the minimal extension and imposes an additional protecting symmetry). The allowed decay channels depend on the sterile neutrino mass: for masses above the EW scale, the dominant decays at three level are to the Higgs boson and a neutrino, but in this case, very different bounds apply [152]. For $M_1 < 2\,m_e$, where m_e is the electron mass, the three level channel occurs to three neutrinos, as depicted in fig. 4.12. The

decay rate for this process was calculated as [163]

$$\Gamma_{N_1\to 3\nu} = \frac{G_F^2\, m_R^5}{96\pi^3}\, \sin^2(\theta) = 6.9\times 10^{-20}\, \left(\frac{M_1}{\mathrm{keV}}\right)^5 \sin^2(\theta)\, \mathrm{s}^{-1}. \tag{4.47}$$

If the sterile neutrino is to be a viable DM candidate, then its lifetime has to be at least as large as the age of the Universe, $\tau_{N_1} = \Gamma^{-1}_{N_1\to 3\nu} \geq t_\mathrm{U} \simeq 4\times 10^{17}\,\mathrm{s}$, resulting in the following bound for the mixing angle

$$\theta^2 \leq 3.6\times 10^{-4}\, \left(\frac{10\,\mathrm{keV}}{M_1}\right)^5, \tag{4.48}$$

which is actually a rather modest bound, although it gets much stronger quickly with increasing mass. However, there is a one-loop decay channel which allows us to place a much stronger bound on θ: with charged leptons and a W boson in the loop, N_1 can decay as $N_1 \to \nu_\alpha\,\gamma$, as depicted in fig. 4.13. Since the propagators will be proportional to the inverse masses of the charged leptons in the loop, the dominant contribution is provided by electrons. The decay width for this processes has been computed to [152, 164]

$$\Gamma_{N_1\to\gamma\nu} = 5.5\times 10^{-22}\, \sin^2(2\theta)\, \left(\frac{M_1}{1\,\mathrm{keV}}\right)^5 \mathrm{s}^{-1}. \tag{4.49}$$

Comparing eq. (4.48) with eq. (4.49), we immediately see that the three level decay is ~ 100 times more frequent than the radiative decay from fig. 4.13. The reason why the radiative decay nevertheless leads to more stringent constraints is that is it is much easier to search for the photons emitted by the loop decay, than for the neutrinos produced by the three level decay. Since the active neutrino is practically massless compared to the sterile neutrino, the energy of the decay gets evenly distributed among both final particles, ν_α and γ, assuming that the decay occurs approximately at rest. For this reason this process is often referred to as a "smoking gun" for sterile neutrino DM: if we consistently detect these monochromatic photons with energy E_γ from the regions in space where we expect DM decays to occur, then that would be compelling evidence for sterile neutrino DM with $M_1 \simeq 2\,E_\gamma$.

In the last decade, many experiments have searched for this signal, which for

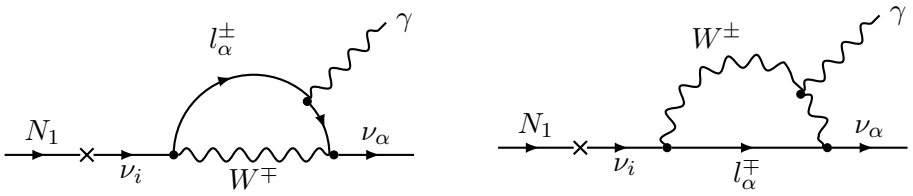

Figure 4.13. Radiative sterile neutrino decay at one loop level.

sterile neutrino masses in the keV range falls in the X-ray portion of the electromagnetic spectrum. There is a number of different types of sources from which one would expect to observe this X-ray line assuming the sterile neutrino DM hypothesis: the line should contribute to the diffuse X-ray background, since DM particles should have been decaying in small numbers everywhere in the Universe since very early times, and the line should be broad and have a continuous tail due to the redshift effect throughout the history of the Universe. However, it could be challenging to discriminate the DM contribution to the diffuse X-ray background from all other contributing sources. Instead of searching for the smeared signal in the diffuse background, one could look for it in regions of space where we expect a large overdensity in the DM distribution, such as galaxy clusters. Individual clusters would emit the same sharp line at their respective redshifts. In this case, the expected flux would be comparable to that from the X-ray background. Locally, we should also expect a measurable flux here in our own galaxy, particularly from the galactic center, where the DM density is the highest. Unfortunately, the galactic core is also the noisiest part of the galaxy, contaminating the search for the signal and making its identification more difficult. Perhaps the most promising objects to search for a signal are dwarf spheroidal galaxies (dSphs), which are low-luminosity galaxies with little amounts of gas, a very compact mass distribution dominated by DM and an almost spherical shape. A couple of dozens of dSphs around the Milky Way are known, and although dSphs are much less massive than elliptical or spiral galaxies, their proximity to us and their large signal-to-noice ratio (due to their low luminosity and comparatively less active cores) make them excellent sources to search for the DM decay line. Such X-ray searches have been performed by a multitude of telescopes, such as Suzaku, INTEGRAL, Chandra, XMM-Newton and Fermi/GBM, among others. For the most part, the null-results from these observations have lead to the constraining of the (θ^2, M_1) parameter space of sterile neutrino DM in the keV - MeV mass range, with one notable exception: a rather suspicious excess at $E_\gamma = 3.55\,\text{keV}$ has been consistently observed from multiple sources and by independent teams. The possible signal was seen in the stacked X-ray spectrum of galaxy clusters [167], in the spectrum of the Andromeda galaxy and the Perseus Cluster [168] and from the Milky Ways galactic center [169]. Interpreting this excess as a DM signal is tempting, but the data is inconclusive. The observations of the local galactic group reported in Ref. [170] could not confirm the signal. Particularly, the line has not been observed from dSphs [171], which would have been a clear indication in favour of the DM interpretation. There are also alternative explanations for the excess, e.g. the potasssium line K XVIII at 3.51 keV, but this hypothesis is inconclusive too. The true identity of the 3.55 keV line remains unclear and additional data is required to settle the matter. In Figure 4.14 we see current X-ray constraints on the sterile neutrino parameter space - the bound from Milky Way satellite counts and the BBN limit [172] apply only to sterile neutrinos produced by the Shi-Fuller [154] mechanism, as in the νMSM. Clearly, the viability of these production mechanism is under stress.

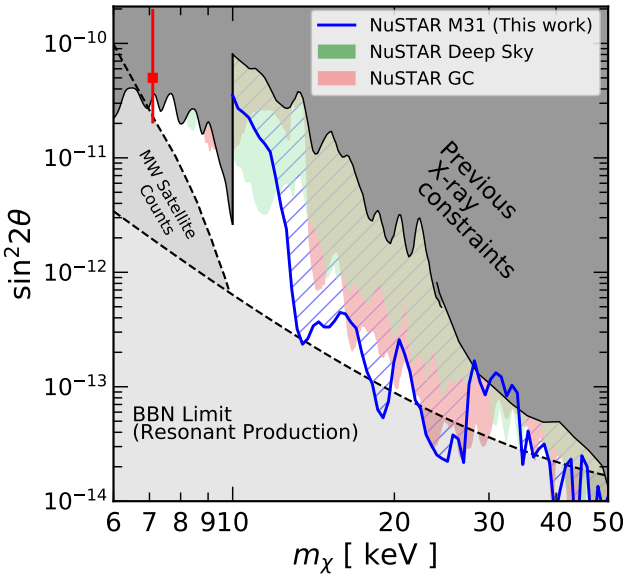

Figure 4.14. Constraints on the sterile neutrino DM parameter space presented by Ng et al. in 2019 [165]. The previous X-ray constraints includes null-observations from the Bullet Cluster and other galaxy clusters, multiple Milky Way measurements, dSphs, the diffuse X-ray background. The solid blue line traces the strongest bounds for $M_1 > 10\,\mathrm{keV}$ from stacked observations of the Andromeda M31 galaxy. The Milky Way satellite bound applies to resonantly produced sterile neutrinos and is related to the power-suppressing effect of warm dark matter at small scales. Below the BBN bound, the amount of lepton asymmetry necessary for successful DM production by resonant oscillations would be in conflict with BBN. The observed line at $E_\gamma = 3.55\,\mathrm{keV}$, suspicious of originating through the decay of a $M_1 = 7.1\,\mathrm{keV}$ sterile neutrino, is also shown in red, but it is currently excluded for non-resonant or resonant production by the Chandra observatory with data from the Milky Ways galactic center [166]. Plot from [165].

Chapter 5

A new production mechanism for sterile neutrino Dark Matter

By now we have established that sterile neutrinos are a powerful addition to the SM. They not only provide explanations to the unanswered puzzles in the neutrino sector, i.e. mass generation and oscillations. Furthermore, they restore the lepton-quark symmetry, by which every LH particle in the SM has a RH partner, and, most importantly for us, they offer an appealing DM candidate. Moreover, as in the νMSM, they could also explain the origin of the matter-antimatter asymmetry of the Universe by leptogenesis [149, 150]. Clearly, sterile neutrinos are an economic, minimal and well motivated extension of the SM, simultaneously offering elegant solutions to some of the most pressing problems of fundamental physics.

However, as discussed in section 4.4, indirect DM searches are making it ever more difficult to reconcile the two basic requirements for a DM candidate: a viable production mechanism to reproduce the observed relic abundance and an appropriately long lifetime. The most minimal and straightforward production mechanisms, namely through non-resonant [151] or resonant [154] oscillations in the early Universe are either completely ruled out or under a lot of stress from X-ray observations - see fig. 4.14. The Dodelson-Widrow mechanism requires a sizeable active-sterile mixing angle, which in turn implies a larger decay rate. The one-loop radiative decay $N_1 \to \nu_\alpha \gamma$, depicted in fig. 4.13, emits monochromatic photons at $E_\gamma = M_1/2$ which can be searched for with X-ray telescopes. The results from these searches have ruled out the Dodelson-Widrow mechanism as capable of producing 100% of the DM density in the form of sterile neutrinos. This constraints can be somewhat alleviated by the Shi-Fuller mechanism, where the oscillations that produce the sterile neutrinos occur resonantly. The resonance condition requires a large lepton asymmetry (at the level of $\Delta L > 10^{-6}$) to be present at the time of production, i.e. well below the EW temperature. With an increasing lepton number asymmetry, the production of sterile neutrinos can be successful with an ever smaller active-sterile mixing angle. However, there is a limit to this effect: first, there is a maximum amount of lepton number asymmetry that can be achieved within

the νMSM [172], and secondly, above a certain threshold, regardless of where it came from (be it the νMSM or else), the lepton asymmetry itself would have an unacceptable impact on BBN [173]. As can be seen in fig. 4.14, there remains only a small window of parameter space open, where the Shi-Fuller mechanism can successfully deliver sterile neutrino DM. Thus, alternative production mechanisms that are better compatible with the current observational constraints are highly desirable.

In section 4.3 we saw that *freeze-out*, i.e. the decoupling from thermal equilibrium of the cosmic plasma, is a reliable and natural process by which relic abundances from the early Universe can be generated, such as the CMB or the densities of the primordial chemical elements. For freeze-out to occur, the particle species in question, let's call it χ, has to be in thermal equilibrium with the cosmic plasma, which is ensured by a large enough interaction rate. More concretely, the equilibrium condition, which is that the interaction rate must be larger then the expansion rate of the Universe $\Gamma_\chi > H$, must be fulfilled. Then, as the Universe expands and cools, a temperature will be reached at which the equilibrium condition is violated, i.e. the interactions involving χ occur at a smaller rate than the expansion rate of the Universe. At that moment, the particle species χ practically stops interacting and its comoving density becomes constant thereafter - it *freezes-out*. Weakly interacting massive particles (WIMPs) are produced in a very natural manner by this mechanism. The fact that this mechanism is a natural feature of the thermodynamics of the early Universe and the coincidence known as *the WIMP miracle*,[1] are the reasons why WIMPs have been such a popular DM candidate.

Until recently, thermal freeze-out as the production mechanism for sterile neutrino DM in the minimal extension of the SM had not been considered. Addressing this issue is the main scientific contribution by the author of this thesis. The reason why this scenario had so far not been considered is that sterile neutrinos in the minimal extension of the SM could never reach thermal equilibrium in the early Universe if they are to play the part of the DM. This is because thermal equilibrium would require a sizeable neutrino Yukawa coupling, implying a large mixing angle, which would make the sterile neutrinos unstable and unacceptably short lived for a proper DM candidate.

Here, we dare to ask the question: how can we reconcile sterile neutrinos in thermal equilibrium in the early Universe with a small enough mixing angle to ensure their longevity and survival into the mature Universe. Our key realization is that, if the Yukawa coupling was actually a dynamical quantity, both requirements could be brought to peace with each other. What we need is a mechanism by which the Yukawa couplings take large values during the early stages of the Universe and then somehow become strongly suppressed at later times. Ideally, the Yukawa couplings start out in the early Universe being large enough to ensure thermal equilibrium and then, still in the radiation dominated era, suffer a drastic change and become strongly suppressed, so that the rate of the interactions due to the Yukawa couplings drops below the expansion rate of the Universe, thereby violating

[1] See section 4.3.

the equilibrium condition and effectively forcing the sterile neutrinos to freeze-out. The change in the values of the Yukawa coupling may happen abruptly or gradually, as long as the induced freeze-out generates the correct relic density. The suppression of the Yukawa couplings should be such that not only freeze-out is induced, but the mixing angle becomes small enough to comply with the longevity condition and, in the case of keV sterile neutrinos, the X-ray bounds. In principle, any mechanism which leads to the described behaviour for the Yukawa couplings could do the job.

Remarkably, this type of behaviour in the Yukawa couplings could also hold the key to solving the flavour puzzle, which we discussed in chapter 2. In many frameworks that address the flavour puzzle [13, 22], the Yukawa terms are not really fundamental but arise as part of an EFT and are therefore suppressed according to a certain pattern that is dictated by some higher symmetry or mechanism, resulting in the curious hierarchy we see in the fermion masses. What we specifically are looking for is slightly different: we want the Yukawa couplings to be present and unsuppressed with values $\sim \mathcal{O}(1)$ in the very early Universe, and only later become suppressed. Varying Yukawa couplings in this fashion have been considered before, e.g. by Servant and her colleagues in the context of EW baryogenesis [174–176]. While there might be many possible ways to implement such varying Yukawa couplings, for concreteness we will here build an implementation via the Froggatt-Nielsen (FN) mechanism (the FN mechanism was introduced in section 2.1), inspired by the work of Baldes, Konstandin, and Servant in Ref. [176]. The key idea is simple: we consider the SM extended by three sterile neutrinos and embedded in a FN model. Then, the bare Yukawa couplings are $\mathcal{O}(1)$ and the effective Yukawa couplings are multiplied by powers of the FN suppression factor $\lambda = \langle\Theta\rangle/\Lambda_{\mathrm{FN}}$, which is the ratio of the flavon vev to the flavour scale. In contrast to what is usually done, we will assume that the vev of the flavon is initially $\langle\Theta\rangle \approx \Lambda_{\mathrm{FN}}$, implying that the FN suppression factor is initially $\mathcal{O}(1)$, i.e. the effective Yukawa couplings are unsuppressed. Particularly, the sterile neutrinos would then have couplings as strong as the top quark and thus be in thermal equilibrium. We then need the assistance of an additional scalar field coupled to the flavon (it could be the SM Higgs or some other new scalar) which also acquires a vev by spontaneous symmetry breaking (SSB). This is the crucial part: as the additional scalar field relaxes to its true minimum in field space, it drags the vev of the flavon along with it until they both reach the their coordinates for the true minimum in the full scalar-field space. At the end of this phase transition (PT) the vev of the flavon has a value $\langle\Theta\rangle = \epsilon\,\Lambda_{\mathrm{FN}}$ with $\epsilon < 1$. Thus, it is this additional PT that enforces the FN suppression. We will show that, depending on the FN charges, the suppression could be drastic enough to induce the freeze-out of the sterile neutrinos and ensure their stability on cosmological time scales.

In this Chapter we will introduce the mechanism sketched above and perform a proof-of-principle calculation on a toy model for sterile neutrino dark matter, showing that the mechanism can successfully generate the observed DM relic abundance by the induced freeze-out and achieve the long-time stability of the sterile neutrinos. We then formulate a complete FN model for the lepton sector, where the neutrino

masses and oscillations are brought about by the type-I seesaw mechanism, DM is produced by the PT-induced freeze-out and the mass hierarchy in the lepton sector is explained by the FN mechanism.

This chapter is based on Refs. [55, 177] and closely follows the material presented therein. The author of this thesis is also the main author of Ref. [55] and the single author of Ref. [177].

5.1 Proof of Principle on a simplified toy model

Here we first attempt to use a very simple toy model to investigate the main features of the framework we are proposing. Thereby we closely follow Ref. [55] by the author of this thesis. The goal is to show that sterile neutrinos with a Yukawa coupling to the SM can be produced through freeze-out, i.e. decoupling from thermal equilibrium in the early Universe, and at the same time be stable in cosmological time scales so that they may play the role of the DM of the Universe. To achieve this goal we seek to promote the neutrino Yukawa coupling to a dynamical quantity that has different values before and after a particular phase transition. At this stage we focus only on the feasibility of DM production and stability, and do not concern ourselves with the generation of light neutrino masses - we leave that for the next section. The toy model we use consists of the SM extended by:

1. one RH Majorana neutrino N that couples through a Yukawa term only to the first generation lepton doublet,

2. the FN flavon Θ and the $U(1)_{\mathrm{FN}}$ flavour symmetry which is broken by the vev of the flavon, and

3. and additional SM singlet scalar field, Σ, equipped with an additional global symmetry $\mathcal{G}_\Sigma$, which undergoes SSB and is responsible for the PT that drives the change in the Yukawa coupling.

The Flavon, the sterile neutrino and the SM fermions are all charged under the $U(1)_{\mathrm{FN}}$ flavour symmetry with charges as given in table 5.1, while the additional scalar field Σ is the only field charged under the global $\mathcal{G}_\Sigma$ symmetry. At this point, we do not need to further specify $\mathcal{G}_\Sigma$ - it could, for example, be a U(1) or a Z_2 symmetry. Also, within this toy model we will restrict ourselves to the case of very heavy sterile neutrinos, well above the EW scale. This restriction is arbitrary and serves only for concreteness and simplicity. In the next section we consider the interesting case of keV sterile neutrinos. Prior to the breaking of the flavour symmetry, the Lagrangian is $U(1)_{\mathrm{FN}}$ invariant, and since the flavon has a flavour charge $q_\Theta = -1$, the Yukawa and Majorana terms have to be multiplied by powers of the flavon according to the flavour charges of the fermions. Aside from the kinetic terms and the scalar potential (which we will discuss in a moment), the

Table 5.1. FN charges in our simplified model.

Field	$\bar{L}$	e_R	N	Θ
$U(1)_{\mathrm{FN}}$ Charge	q_L	q_R	q_N	-1

new terms in the Lagrangian are

$$Y_e \left(\frac{\Theta}{\Lambda_{\mathrm{FN}}}\right)^{q_L+q_R} \bar{L}\, H\, e_R + Y_\nu \left(\frac{\Theta}{\Lambda_{\mathrm{FN}}}\right)^{q_L+q_N} \bar{L}\, \widetilde{H}\, N + \frac{1}{2} M_R \left(\frac{\Theta}{\Lambda_{\mathrm{FN}}}\right)^{2q_N} \overline{N^c} N, \tag{5.1}$$

with L as the lepton doublet of the first generation and e_R as the RH electron. Again, in this toy model we are only considering a single-generation set up, and thus the Yukawa couplings and the Majorana mass are scalars here.

When the flavon acquires a vev, thereby spontaneously breaking the $U(1)_{\mathrm{FN}}$ symmetry, the Yukawa couplings and the Majorana mass get scaled by powers of the FN factor $\lambda = \langle\Theta\rangle/\Lambda_{\mathrm{FN}}$, which is usually $\lambda < 1$. However, in contrast to this, we now demand that at temperatures below the flavour scale and above the Σ-PT, the flavon vev takes the value $\langle\Theta\rangle = \Lambda_{\mathrm{FN}}$, such that $\lambda = 1$ and consequently the Yukawa couplings and the Majorana mass are unsuppressed at this energy scale. Then, as the Universe keeps cooling and reaches the critical temperature $T_c \sim \Lambda_\Sigma$ at which the Σ-PT takes place, the Σ field acquires a vev. Here, we demand that as the vev of Σ transitions from zero to its finite value, it drags the flavon vev with it, as shown in fig. 5.1. This situation, where the vev of the flavon changes from $\sim \mathcal{O}(1)$ to a much smaller value due to a PT, has been described previously by Baldes, Konstandin, and Servant [176]. Other authors have considered the impact of phase transitions on the production of sterile neutrinos, see e.g. Refs. [178–183], but our of PT-induced freeze-out, is different to those previous works.

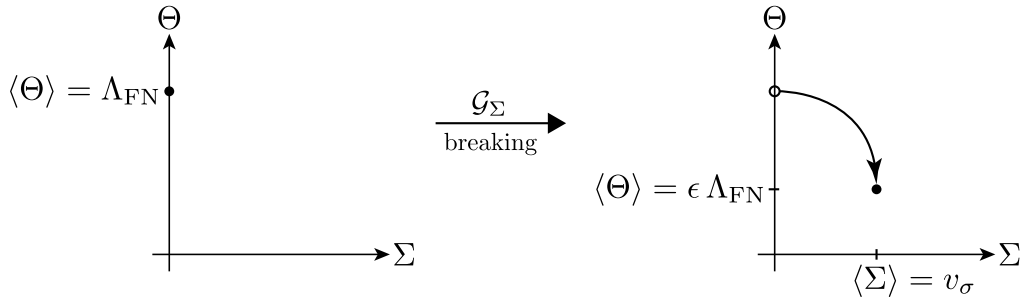

Figure 5.1. Coordinates of the minimum of the scalar potential in field space. When the vev of the Σ field makes the transition $\langle\Sigma\rangle : 0 \to v_\sigma$, it drags the flavon with it.

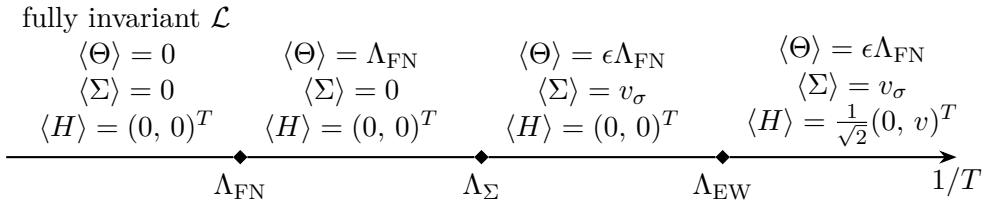

Figure 5.2. Energy scales in the toy model, with the scalar vevs in the corresponding energy ranges. The vevs are the coordinates in the full scalar field-space where the potential finds its minimum.

Figure 5.2 shows the energy scales and the values that the scalar vevs take in the different phases. Assuming that the Σ-PT occurs in the way described above, we can reinterpret the FN factor λ as a function of the vev of Σ, i.e.

$$\lambda(\langle\Sigma\rangle) = \begin{cases} 1, & \text{for} \quad \langle\Sigma\rangle = 0 \\ \epsilon, & \text{for} \quad \langle\Sigma\rangle = v_\sigma. \end{cases} \tag{5.2}$$

The specific trajectory in field space taken by Σ during the PT does not concern us. What matters to us is only the fact that λ takes different values before and after the PT.

But what conditions have to be met in order for the PT to occur in this manner? Here we assume that the scales are hierarchical as $\Lambda_{\rm FN} > \Lambda_\Sigma \gg \Lambda_{\rm EW}$ and the couplings between the Higgs and the other two scalars are tiny, such that their dynamics can be considered decoupled. Then we can write the scalar potential for Θ and Σ and disregard the Higgs,

$$V(\Theta,\,\Sigma) = \mu_\theta^2\,\Theta^\dagger\Theta + \lambda_\theta\,(\Theta^\dagger\Theta)^2 + \mu_\sigma^2\,\Sigma^\dagger\Sigma + \lambda_\sigma\,(\Sigma^\dagger\Sigma)^2 + \lambda_{\theta\sigma}\,(\Theta^\dagger\Theta)(\Sigma^\dagger\Sigma). \tag{5.3}$$

As was shown by the author of this thesis in [55] and is reviewed in section A.2, the conditions that the parameters of this potential have to fulfill in order for the PT to occur are

$$\lambda_{\theta\sigma} < 2\,\lambda_\sigma \left(\frac{v_\sigma}{\Lambda_{\rm FN}}\right)^2, \tag{5.4}$$

$$\lambda_\theta < \lambda_\sigma \left(\frac{v_\sigma}{\Lambda_{\rm FN}}\right)^4, \tag{5.5}$$

which imply that the mixing between Θ and Σ is small, and

$$m_\Theta^2 < 2\lambda_\sigma\, v_\sigma^2\, \epsilon^2 \left(\frac{v_\sigma}{\Lambda_{\rm FN}}\right)^2. \tag{5.6}$$

Thus, if eqs. (5.4) to (5.6) hold, then the Σ-PT does indeed cause the shift in the flavon vev as sketched in fig. 5.1. Since we can roughly approximate $v_\sigma \sim \Lambda_\Sigma$, and

$\Lambda_\Sigma < \Lambda_{\rm FN}$, we can set

$$\delta := \left(\frac{v_\sigma}{\Lambda_{\rm FN}}\right) \sim \left(\frac{\Lambda_\Sigma}{\Lambda_{\rm FN}}\right) < 1, \tag{5.7}$$

and together with eq. (5.6) we can place an approximate lower bound for the temperature of the Σ-PT that depends on the flavon mass,

$$m_\theta\, \epsilon^{-1}\, \delta^{-1} < \Lambda_\Sigma \sim T_c. \tag{5.8}$$

Now that we know that, under the conditions stated above, the flavon vev shifts as $\langle\Theta\rangle : \Lambda_{\rm FN} \to \epsilon\, \Lambda_{\rm FN}$ we consider the Yukawa coupling and the Majorana mass as effectively varying quantities during the PT. We can thus now write

$$Y_{\rm eff} = Y_\nu\ [\lambda(\langle\Sigma\rangle)]^{q_L+q_N} = \begin{cases} Y_\nu, & \text{for} \quad T > T_c \\ Y_\nu\, \epsilon^{\,q_L+q_N}, & \text{for} \quad T < T_c \end{cases}, \tag{5.9}$$

$$M_{\rm eff} = M_R\ [\lambda(\langle\Sigma\rangle)]^{2q_N} = \begin{cases} \widetilde{M} := M_R, & \text{for} \quad T > T_c \\ M := M_R\, \epsilon^{\,2q_N}, & \text{for} \quad T < T_c \end{cases}. \tag{5.10}$$

Here we define $\widetilde{M}$ as the early, unsuppressed value of the Majorana mass, i.e. before the Σ-PT shifts the vev of the flavon; we could also refer to them as the initial values, while without the tilde, M stands for the suppressed value, taken after the Σ-PT, which could also be referred to as its late or final value.

The next step is to select FN charges for our toy model. To find suitable choices we consider the desired effect on the electron mass, the neutrino Yukawa coupling and the Majorana mass.

The electron mass: since within the FN framework the bare electron Yukawa coupling will be $\mathcal{O}(1)$, the value of the electron mass requires that

$$m_e = Y_e\, \frac{v}{\sqrt{2}}\, \epsilon^{q_L+q_R} \approx 5 \times 10^{-4}\,\text{GeV} \quad \Rightarrow \quad q_L + q_R \approx \frac{-5}{\log_{10}(\epsilon)}. \tag{5.11}$$

The Majorana mass: since we are considering DM neutrinos heavier than the Higgs, the sterile neutrino mass after the PT, i.e. the suppressed mass, should satisfy

$$\epsilon^{\,2q_N}\, M_R \gtrsim 2 \cdot 10^2\,\text{GeV} \tag{5.12}$$

$$\Rightarrow \quad q_N \lesssim \frac{\log_{10}(2 \cdot 10^2) - \log_{10}\left(\frac{M_R}{\text{GeV}}\right)}{2\log_{10}(\epsilon)}. \tag{5.13}$$

The longevity of Dark Matter: we demand that our sterile neutrinos be stable on cosmological time scales. Because we are considering sterile neutrinos heavier

than the Higgs, they will decay primarily as $N \to h\,\nu_L$. Thus, the inverse rate of this decay must be larger than the age of the universe, i.e.

$$\Gamma^{-1}_{N\to h\nu} > t_0 \approx 7 \cdot 10^{41}\,\mathrm{GeV}^{-1}. \tag{5.14}$$

Inserting eq. (5.9) we get the condition

$$\frac{(Y_\nu\,\epsilon^{\,q_L+q_N})^2 M_R\,\epsilon^{\,2q_N}}{16\pi} < \frac{1}{7}\cdot 10^{-41}\,\mathrm{GeV} \tag{5.15}$$

$$\Rightarrow \quad q_L + 2q_N > \frac{\log_{10}\left(\frac{16\pi}{7}\times 10^{-41}(Y_\nu)^{-2}(M_R/\mathrm{GeV})^{-1}\right)}{2\,\log_{10}(\epsilon)}. \tag{5.16}$$

These conditions eqs. (5.11), (5.13) and (5.16) depend on the parameters ϵ, Y_ν and M_R. In the spirit of the FN framework, the bare neutrino Yukawa coupling should be $Y_\nu \sim \mathcal{O}(1)$, and the FN suppression factor should be $\epsilon < 1$; for concreteness, we set them to

$$Y_\nu = 0.1\,, \qquad \epsilon = 0.01\,, \tag{5.17}$$

and for the bare Majorana mass we consider $10^4\,\mathrm{GeV} \leq M_R \leq 10^{16}\,\mathrm{GeV}$, since the Majorana scale could be as high as the GUT scale [46]. Although this is a rather arbitrary choice, it serves the simplicity we are seeking with this toy model, and again, we are only seeking a proof of principle at this point. In the next section we will duly consider the keV mass range. For a plausible FN model we prefer that the flavour charges take possibly small integer values. Therefore, we search for appealing choices for the flavour charges by solving the problem

$$\underset{q_L,q_R,q_N\,\in\,\mathbb{Z}}{\text{minimize}}\,(|q_L| + |q_R| + |q_N|) \tag{5.18}$$

under the conditions defined by eqs. (5.11), (5.13) and (5.16) and with the parameters from eq. (5.17). We find that the flavour charges comply with the simpler relations

$$q_L + q_R = 2\,, \qquad q_L + q_N = 11\,, \qquad q_N = \begin{cases} 0, & M_R \in \left[10^4,\,10^8\right)\,\mathrm{GeV} \\ 1, & M_R \in \left[10^8,\,10^{12}\right)\,\mathrm{GeV} \\ 2, & M_R \in \left[10^{12},\,10^{16}\right)\,\mathrm{GeV} \end{cases}. \tag{5.19}$$

Thus, we see that depending on the mass range in which M_R lies, we can have three different sets of flavour charges. In the following, we will discuss the case for $M_R \in \left[10^4,\,10^8\right)$ GeV; the case where M_R lies in any of the other two intervals was discussed by the author of this thesis in Ref. [55] and is qualitatively very similar to the scenario presented here.

With the flavour charges chosen above the cosmological stability of the sterile neutrino DM is ensured thanks to the dynamical suppression of the neutrino Yukawa coupling implemented in our framework. We now proceed to compute the

relic abundance produced by the induced freeze-out of the sterile neutrinos. To summarize, the model parameters we are working with are

$$\epsilon = 0.01\,, \qquad Y_\nu = 0.1\,, \qquad M_R \in \left[10^4,\, 10^8\right]\ \text{GeV}\,, \tag{5.20}$$

$$q_N = 0\,, \qquad q_L = 11\,, \qquad q_R = -9\,. \tag{5.21}$$

To obtain the sterile neutrino relic abundance we will solve the Boltzmann equation, which we encountered already in section 4.3. In the standard WIMP scenario, DM annihilations are the main processes driving freeze-out. In contrast to that, for sterile neutrinos with a bare Yukawa coupling $Y_\nu \sim \mathcal{O}(1)$ to the SM, the interactions responsible for maintaining (chemical-) thermal equilibrium are decays, inverse decays

$$N \rightleftharpoons H\, L \tag{5.22}$$

and Higgs- or lepton-mediated scatterings involving quarks and gauge bosons A, such as

$$N\, L \rightleftharpoons Q_L\, q_R\,, \qquad N\, L \rightleftharpoons H\, A\,, \qquad N\, H \rightleftharpoons L\, A, \tag{5.23}$$

all of which change the number of sterile neutrinos by one, i.e. $\Delta N = 1$. These processes have been throughly studied in the context of leptogenesis [184–186]. When we discussed the Boltzmann equation for WIMPs in section 4.3, we introduced the thermalized cross section for WIMP annihilations $\langle\sigma v\rangle$, and, as is customary in the WIMP DM literature, we expressed the Boltzmann equation using this quantity. For the processes in eqs. (5.22) and (5.23), with which we are concerned here, the Boltzmann equation is usually written slightly differently, using the thermal interaction rate γ^{eq} instead of $\langle\sigma v\rangle$ (see chapter B). The Boltzmann equation then reads [186]

$$z\, H\, \frac{dy_N}{dz} = \left(\frac{\gamma_{\text{D}}^{\text{eq}} + \gamma_{\text{S}}^{\text{eq}}}{n_N^{\text{eq}}}\right) \left(y_N^{\text{eq}} - y_N\right), \tag{5.24}$$

where $\gamma_{\text{D,S}}^{\text{eq}}$ stands for the rate of decays or scatterings respectively,[2] and we have disregarded the derivative of the number of entropic degrees of freedom in the plasma with respect to temperature, i.e. $d\,\ln g_s(T)/d\ln T = 0$. Recall the definition of z, namely $z = M/T$. While scatterings with the sterile neutrinos as the mediator are very important for leptogenesis [184], they are irrelevant for us because they do not change the number of sterile neutrinos.

Since the computation we are attempting takes place in the very early Universe, at energies above Λ_{EW}, particles have thermal masses but no physical masses. Thus, for the rates $\gamma_{\text{D}}^{\text{eq}}$ and $\gamma_{\text{S}}^{\text{eq}}$ we use the expressions derived in Ref. [186], which include the thermal corrections and the running of couplings. Both rates, unaffected by the

[2] The relation between the scattering rate and the thermalized cross section is $\gamma_{xy\to ab}^{\text{eq}} = \langle\sigma v\rangle_{xy\to ab} \cdot n_x^{\text{eq}}\, n_y^{\text{eq}}$.

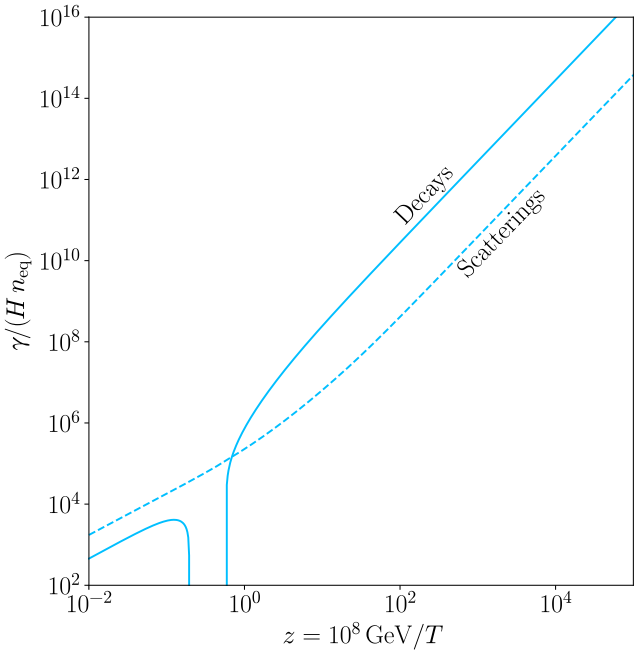

Figure 5.3. The decay and scattering rate of sterile neutrinos, normalized by the equilibrium density and Hubble parameter, for an early mass at the upper end of the range in consideration, $M_R = 10^8\,\mathrm{GeV}$, and without the effect of the suppression of the Yukawa couplings or the Majorana mass. For other values of M_R the curves would look qualitatively the same but would be vertically shifted. Clearly, for $z = 1$ the decay rate dominated over the scattering by ~ 2 orders of magnitude - in the non-relativistic regime. For $z < 1$, i.e. when the sterile neutrinos are relativistic, the scatterings actually overcome the decays. The gap in the decay rate around $10^{-1} < z < 10^0$ is due to the fact that in that temperature interval the thermal masses of the Higgs, leptons and sterile neutrinos kinematically forbid all two-body decays, i.e. $m_H(T) - m_L(T) < M_R < m_H(T) + m_L(T)$.

dynamical FN suppression and normalized by $H\, n_N^{\rm eq}$ are shown in fig. 5.3, where one can clearly see that the decays and inverse decays dominate the dynamics of the sterile neutrinos for $z > 1$, i.e. when they are non-relativistic, while the $2 \leftrightharpoons 2$ scatterings take precedence in the relativistic regime. The curious gap in the decay rate occurs because at those temperatures the thermal masses of the participating particles kinematically forbid all two-body decays. Note that $\gamma^{\rm eq}/H$ actually grows as the temperature decreases, which means that instead of evolving towards freeze-out, the unaided sterile neutrinos with $\mathcal{O}(1)$ bare Yukawa couplings tend to interact ever more strongly with the thermal bath. This make the necessity of the drastic suppression of the Yukawa coupling clear, which, as we will shortly see, can be

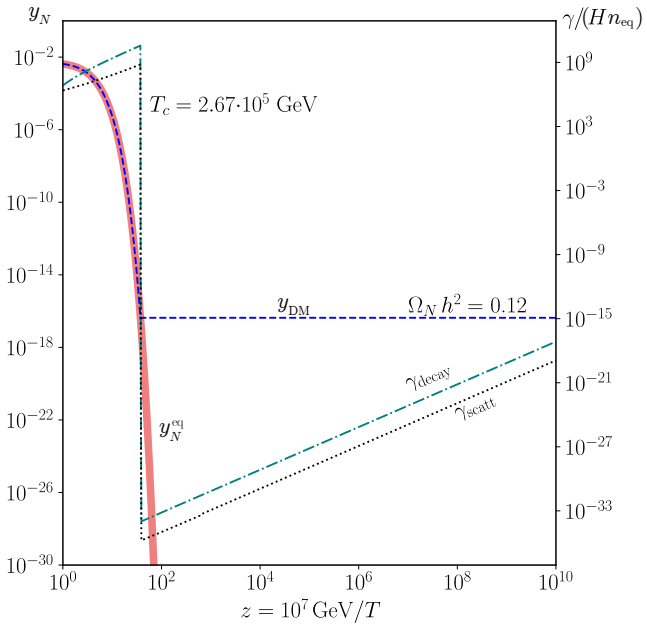

Figure 5.4. The solution to the Boltzmann equation $y_{\rm DM}(z)$ with the varying Yukawa coupling implemented for $M_R = 10^7\,\text{GeV}$ is plotted as the blue dashed line. The temperature of the Σ-PT was chosen such that the full DM relic abundance is reproduced. The decay and scattering rates (normalized by $H\,n_N^{\rm eq}$) are plotted of the right axis and show the dramatic effect of the sudden suppression of the Yukawa coupling.

achieved by the mechanism proposed in this work.

Now we implement the change in the effective neutrino Yukawa coupling. The effect is caused by the shift in the flavon vev, which occurs due to the Σ field dragging the flavon along as it transitions to its vev. Since we are not interested in the particular dynamics of the PT itself, but simply on the different values taken by the Yukawa coupling before and after the PT, we choose to parameterize it as

$$Y_{\rm eff}(z) = \frac{1}{2}\left[(Y_\nu - Y_\nu^s)\,\tanh\left(\left(1-\frac{z}{z_c}\right)\frac{1}{\tau}\right) + Y_\nu + Y_\nu^s\right], \tag{5.25}$$

which is in fact a smoothed step function going from Y_ν for $z < z_c$ to Y_ν^s for $z_c < z$. Thus, z_c is a proxy for the temperature T_c of the Σ-PT and τ is a parameter that measures its duration. The superscript s in Y_ν^s stands for *suppressed* and it is given by $Y_\nu^s = \epsilon^{q_L+q_N} Y_\nu$. For our computations, we set $\tau = 0.001$, Y_ν and Y_ν^s are fixed by eqs. (5.9) and (5.20), and finally, z_c is taken as a free parameter. Since we chose to assign zero flavour charge to the sterile neutrinos $q_N = 0$, the Majorana mass suffers no suppression. Had we decided otherwise, we would need to parameterize the effective Majorana mass too.

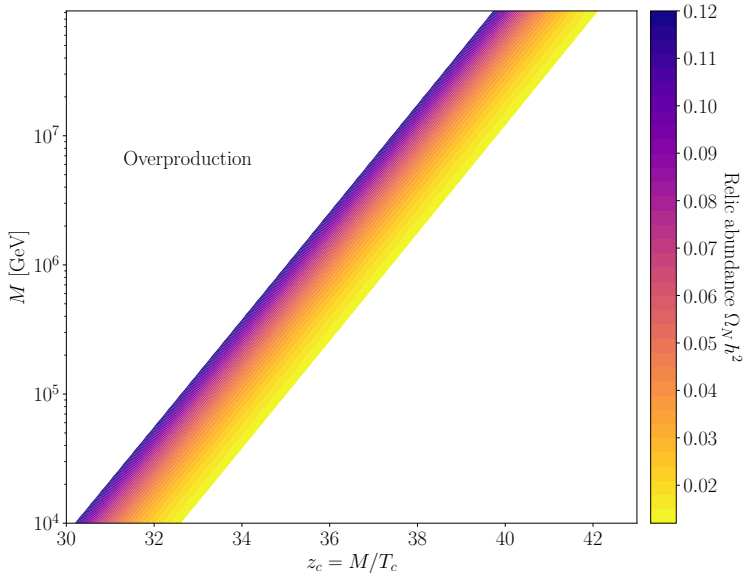

Figure 5.5. Within the colored stripe, the framework proposed in this thesis successfully up to 100% of the DM of the Universe through the induced freeze-out of the sterile neutrinos in our toy model. The effectively varying Yukawa coupling gets strongly suppressed during a PT and forced the sterile neutrinos to decouple.

The result of the Boltzmann equation for our toy model with a DM neutrino mass of $M_R = 10^7$ GeV is shown in fig. 5.4 as the blue dashed line. The relic density y_N starts out tracing its equilibrium value $y_N^{\rm eq}$, represented here by the thick red line, until the PT occurs. The temperature of the Σ-PT is chosen so that the sterile neutrino relic abundance matches the observed DM abundance. In this example, the value is $z_c = 37.45$, implying $T_c = 2.67 \times 10^5$ GeV. The Σ-PT instantaneously decouples y_N from $y_N^{\rm eq}$. The dashed-dotted and dotted lines show the decay- and scattering rates (normalized by $(H\, n_{\rm eq})$) on the right axis; they display the drastic suppression effect through the effective Yukawa coupling, which enters the rates with the second power, due to the change in the flavon vev. After the induced freeze-out, the rates are so small that the DM neutrinos are completely decoupled from the rest of the bath and their relic density stays constant.

Next we solve the Boltzmann equation and compute the sterile neutrino relic abundance for the complete mass range under consideration, i.e. $M_R \in [10^4,\, 10^8]$ GeV. The relic abundance is given by

$$\Omega_N\, h^2 = \frac{s_0\, M_R\, y_N^{\rm fo}(z_c)}{\rho_{\rm c}}\, h^2, \tag{5.26}$$

with the entropy density today $s_0 = 2891.2\,\mathrm{cm}^{-3}$ and the critical density $\rho_c = 1.05 \times 10^{-5}\,h^2\,\mathrm{GeV\,cm}^{-3}$. As discussed above, the sterile neutrino relic density y_N^{fo} is fixed by the Σ-PT and thus depends mainly on T_c or equivalently z_c. Thus, the parameters over which we perform the scan are M_R and z_c. The result of the scan is shown in fig. 5.5, where we see that throughout the whole mass range it is always possible to generate a contribution of up to 100% to the DM abundance of the Universe from sterile neutrinos produced by the mechanism presented here. Even though the considered mass range spans 4 orders of magnitude, the critical temperature for the Σ-PT is always a fraction of the DM mass, between $T_c \approx M_R/40$ and $M_R/30$ - the relic abundance depends only logarithmically on z_c. As the author of this thesis showed in [55], the situation is very similar to the case where one chooses a non-zero flavour charge for the sterile neutrinos $q_N \neq 0$, and a larger initial Majorana mass, as suggested in eq. (5.19). In those scenarios, the parameter scan looks qualitatively the same with the exception that the mass of the sterile neutrinos also become suppressed by the changing vev of the flavon during the Σ-PT. For example, with $M_R = 10^{10}\,\mathrm{GeV}$ and $q_N = 1$, the mass of the DM neutrinos after the PT would be $M_R^s = 10^6\,\mathrm{GeV}$.

This finalizes our discussion of this toy model. We have shown that, in principle, it is possible for sterile neutrinos to be strongly coupled to the SM thermal bath in the early Universe by $\mathcal{O}(1)$ Yukawa couplings, and if these Yukawa couplings become strongly suppressed at some point in time, the sterile neutrinos can be forced to drop out of thermal equilibrium and have their comoving density fixed at its last equilibrium value. The key conceptual element is the varying Yukawa coupling, which we implemented by embedding our toy model in a FN framework, in which the Yukawa terms arise as effective Operators that contain powers of the flavon vev. The actual change in the Yukawa couplings is then induced by an additional PT which alters the vev of the flavon.

We emphasise that the concept proposed here is more general than the concrete realization that was investigated in this section: there might be many other possible ways to implement varying Yukawa couplings, and any of them can in principle induce the freeze-out of an initially thermalized species.

5.2 keV Sterile Neutrino Dark Matter by thermal freeze-out

In the previous section, we showed that the concept of varying effective Yukawa couplings in the early Universe is indeed capable of providing a mechanism for sterile neutrino DM genesis from thermal freeze-out. This mechanism does not rely on the (resonant or otherwise) oscillations between active and sterile neutrino states, nor does it involve the decays from heavier parent particles. The notion of varying Yukawa couplings is reminiscent of a possible solution to the flavour puzzle, discussed in chapter 2. Indeed, the FN mechanism [20], which we have adapted to implement the Varying Yukawa couplings, is a popular way to address the flavour puzzle. In this section, we attempt to construct a more realistic model, including all three lepton generations, and aim to achieve the following goals:

1. successful production of keV sterile neutrino DM through the induced freeze-out from the varying Yukawa couplings,

2. while simultaneously generating the masses of the active neutrinos by the type-I seesaw mechanism and recovering the PMNS mixing matrix,

3. and also generating the mass hierarchy in the lepton sector by the means of the FN framework.

The set-up that we use for this implementation starts with the SM extension by three RH neutrinos N_i, which we then embed in a FN model by adding the flavon Θ and assigning flavour charges to the flavon and all fermions. While in the previous section we introduced an additional BSM scalar whose PT was responsible for driving the shift in the flavon vev, we now let the SM Higgs take up this role. Thus, before the electroweak phase transition (EWPT), we will set the flavon vev equal to the flavour scale $\langle\Theta\rangle = \Lambda_{\rm FN}$, such that the effective Yukawa couplings are unsuppressed. Then, during the EWPT when the scalar potential relaxes to its true minimum and the Higgs assumes its non-zero vev, the flavon vev gets dragged along and ends up with a slightly smaller value than before, $\langle\Theta\rangle = \epsilon\,\Lambda_{\rm FN}$. Since the effective Yukawa couplings are essentially $\mathcal{O}(1)$ coefficients multiplied by powers of the flavon vev, they can become exponentially suppressed, even if the change in the flavon vev was moderate. Although the sterile neutrinos were initially tightly coupled to the thermal plasma by their $\mathcal{O}(1)$ Yukawa couplings, the new value of the Yukawa couplings after the EWPT might be suppressed strongly enough to drive the rate of their interactions below the expansion rate of the Universe, thereby inducing the freeze-out of the comoving neutrino density and creating a sterile neutrino relic abundance. Consequently, it is the EWPT that induces the sterile neutrino DM freeze-out and fixes its relic abundance. Furthermore, the sterile neutrinos might even become stable on cosmological time scales provided that the suppression is drastic enough, and thus avoid the constraints from indirect DM searches.

This section is based on and closely follows Ref. [177], of which the author of this thesis is the single author. Here we first address the issue of DM genesis and investigate the parameters necessary to generate a 100% contribution from keV sterile neutrinos to $\Omega_{\rm DM}$ by the mechanism proposed here, i.e. induced freeze-out during the EWPT. Secondly, we investigate what FN parameters and coefficients are needed to correctly generate the lepton flavour hierarchy, the light neutrino masses and the PMNS matrix starting from a specific Majorana mass matrix as a benchmark point. And finally, we variate the Majorana mass matrix to scan the sterile neutrino parameter space where our model successfully accomplices all set goals.

5.2.1 Dark Matter genesis from varying Yukawa couplings

In the previous section 5.1 we showed that change in the Yukawa coupling driven by the shift in the flavon vev will force initially thermalized sterile neutrinos to freeze-out provided the suppression of the Yukawa coupling is drastic enough. We extend the SM by three RH neutrinos $N_i = (N_1, N_2, N_3)$ and the flavon sector, assigning flavour charges to the flavon and all fermions as given in table 5.2.

The relevant part of the Lagrangian is

$$\begin{aligned} -\mathcal{L}_{\rm eff} \supset\; & \bar{L}_i\, Y^E_{ij}\, H\, E_{Rj} \left(\frac{\langle\Theta\rangle}{\Lambda_{\rm FN}}\right)^{q_{\bar{L}i}+q_{Rj}} + \bar{L}_i\, Y^\nu_{ij}\, \tilde{H}\, N_j \left(\frac{\langle\Theta\rangle}{\Lambda_{\rm FN}}\right)^{q_{\bar{L}i}+q_{Nj}} \\ & + \frac{1}{2}\overline{N^c_i}\,(M_N)_{ij}\, N_j \left(\frac{\langle\Theta\rangle}{\Lambda_{\rm FN}}\right)^{q_{Ni}+q_{Nj}} + \text{h.c.} \end{aligned} \tag{5.27}$$

With the FN factor $\lambda = \langle\Theta\rangle/\Lambda_{\rm FN}$ we can define the effective Yukawa and Majorana mass matrices,

$$(Y^\nu_{\rm eff})_{ij} = (Y^\nu)_{ij}\,[\lambda]^{q_{\bar{L}_i}+q_{N_j}}, \qquad (M_{\rm eff})_{jk} = (M_N)_{jk}\,[\lambda]^{q_{N_j}+q_{N_k}}. \tag{5.28}$$

The key idea in our framework is that, initially, the vev of the flavon is $\langle\Theta\rangle = \Lambda_{\rm FN}$ such that the FN factor is $\lambda = 1$ and thus both the Yukawa and Majorana mass matrices are equal to the bare matrices Y^E, Y^ν and M_N in eq. (5.27). Particularly, since the entries in the bare Yukawa matrices are all $\mathcal{O}(1)$, so too would the effective Yukawa matrices be. Crucially, this allows the sterile neutrinos be strongly coupled to the thermal bath and therefore in equilibrium, because their Yukawa interactions

Table 5.2. FN charges for the lepton doublets L_i, charged singlets E_{R_j}, sterile neutrinos N_k, the flavon Θ and the Higgs H, respectively.

Field	L_i	E_{R_j}	N_k	Θ	H
$U(1)_{\rm FN}$ Charge	q_{L_i}	q_{R_j}	q_{N_k}	-1	0

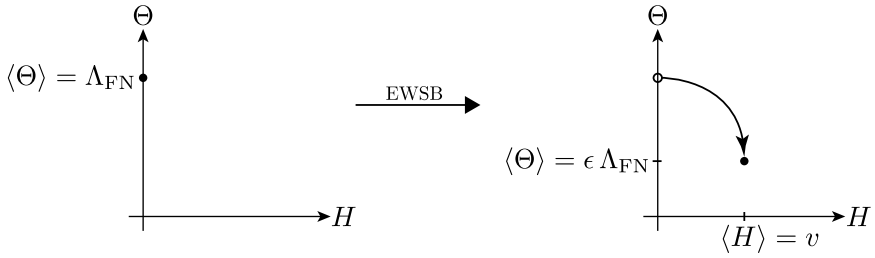

Figure 5.6. Position of the minimum of the scalar potential in field space. During the EWPT the Higgs transitions to the true vacuum and the flavon gets dragged along. Although the Higgs is a doublet and only its neutral component takes a non-zero vev, here and in eq. (5.29) it is depicted in one dimension for simplicity.

would be as strong as those of the top-quark in the SM. Similarly, assuming that the entries in the bare Majorana mass matrix M_N do not display any type of special structure (hierarchy, anarchy, etc.), all entries are characterized by the Majorana scale Λ_M (which is UV-unconstrained), and so we can write $M_N \sim \Lambda_M$. However, as the Universe expands and cools, at some point the EWPT kicks in and the Higgs field acquires its non-vanishing vev. Since the potential contains both scalars, $V = V(H, \Theta)$, it is reasonable to expect that the new minimum will be found at a completely new point in field space, i.e. the coordinates of the vacuum in field space shift during the EWPT as

$$(\langle H\rangle, \langle\Theta\rangle) = (0, \Lambda_{\rm FN}) \to (v, \epsilon\,\Lambda_{\rm FN}), \tag{5.29}$$

with $\epsilon < 1$, as depicted in fig. 5.6.

The three-level scalar potential for this scenario is

$$V(H, \Theta) = \mu_H^2\, H^\dagger H + \lambda_H\,(H^\dagger H)^2 + \mu_\Theta^2\,\Theta^\dagger\Theta + \lambda_\Theta\,(\Theta^\dagger\Theta)^2 + \lambda_{H\,\Theta}(\Theta^\dagger\Theta)(H^\dagger H),$$

and is equivalent to the potential from eq. (5.3) discussed in the previous section. As mentioned around eq. (5.3), and discussed in Refs. [55, 176], it is possible for this potential to behave in the manner described in fig. 5.6, i.e. the simultaneous shift in the vevs of both scalars, given the equivalents of eqs. (5.4) and (5.5). The finite temperature and quantum corrections to this potential, with the dynamics here required, were discussed by Baldes, Konstandin, and Servant in Ref. [187] in the context of varying Yukawa couplings to achieve EW Baryogenesis.

From now on, we take the shift in the flavon vev as defined in eq. (5.29) and depicted in fig. 5.6 for granted. As a consequence of the shift in the flavon vev, the FN factor λ is a function of $\langle\Theta\rangle$. The precise trajectory in field space along which the flavon transitions from $\Lambda_{\rm FN}$ to $\epsilon\,\Lambda_{\rm FN}$ is not important to us; what matters is only that it has different values before and after the EWPT, which occurs at

$T = T_c = T_{\mathrm{EW}}$,

$$\lambda(\langle\Theta\rangle) = \begin{cases} 1, & \text{for} \quad T > T_{\mathrm{EW}} \\ \epsilon, & \text{for} \quad T < T_{\mathrm{EW}}. \end{cases} \tag{5.30}$$

With this we can now rewrite the effective Yukawa and Majorana mass matrix,

$$\begin{aligned} (Y^{\nu}_{\mathrm{eff}})_{ij} &= (Y^{\nu})_{ij}\, [\lambda]^{q_{\bar{L}_i} + q_{N_j}} \\ &= \begin{cases} (Y^{\nu})_{ij}, & \text{for} \quad T > T_{\mathrm{EW}} \\ (Y^{\nu})_{ij}\, \epsilon^{q_{\bar{L}_i} + q_{N_j}}, & \text{for} \quad T < T_{\mathrm{EW}} \end{cases}, \end{aligned} \tag{5.31}$$

$$\begin{aligned} (M_{\mathrm{eff}})_{jk} &= (M_N)_{jk}\, [\lambda]^{q_{N_j} + q_{N_k}} \\ &= \begin{cases} (\widetilde{M})_{jk} = (M_N)_{jk}, & \text{for} \quad T > T_{\mathrm{EW}} \\ (M)_{jk} = (M_N)_{jk}\, \epsilon^{q_{N_j} + q_{N_k}}, & \text{for} \quad T < T_{\mathrm{EW}} \end{cases}, \end{aligned} \tag{5.32}$$

and equivalently for Y^{E}_{eff}. In the case of the Majorana mass matrix, we introduce additional notation in eq. (5.32), which will be useful shortly: the matrix $(\widetilde{M})_{jk}$ stands for the unsuppressed Majorana mass matrix, to which we may also refer to as the *early* Majorana mass matrix, because it is valid at times *earlier* than the EWPT (note that early Majorana mass matrix $\widetilde{M}$ and the bare Majorana mass matrix M_N are identical due to the fact that $\lambda = 1$ at early times). Similarly, the matrix $(M)_{jk}$ stands for the suppressed Majorana mass matrix, to which we may also refer to as the *late* Majorana mass matrix, because it holds for times *later* than the EWPT, when the suppression by the *late* flavon vev is imposed. Thus, here we use the words *early* and *late* to reference the epochs before and after the EWPT respectively.

As discussed in section 3.3, within the seesaw approximation the eigenvalues of the Majorana mass matrix are the masses of the heavy neutrino states, which are mostly composed of the RH neutrinos. In our scenario however, the masses of the sterile neutrinos are different before and after the EWPT due to the FN suppression by the change in the flavon vev, which is induced during the EWPT itself. Thus, we distinguish between the early and late Majorana mass eigenvalues:

$$\mathbb{EV}\left[\,\widetilde{M}\,\right] = \left(\widetilde{M}_1,\, \widetilde{M}_2,\, \widetilde{M}_3\right), \qquad \mathbb{EV}\left[\,M\,\right] = (M_1,\, M_2,\, M_3)\,. \tag{5.33}$$

We set the lightest sterile neutrino N_1 to play the role of the DM particle; its mass prior to the EWPT is $\widetilde{M}_1$. After the EWPT the individual entries in the Yukawa matrix and in the Majorana mass matrix are rescaled by powers of the FN factor λ, and consequently the eigenvalues of the matrices are redefined. The new mass eigenvalue corresponding to the DM neutrino is M_1, which we could also call *the DM mass*. This distinction between the early and late masses of the DM neutrino N_1 is important because both enter the relic abundance equation, as we

now discuss. Provided that the flavour charges of the lepton doublets and sterile neutrinos are chosen appropriately, this mechanism forces the DM sterile neutrinos to freeze-out. In the next section we will make sure that the flavour charges are indeed appropriately chosen. For now, assuming that the Yukawa suppression is drastic enough to keep the DM neutrinos stable on cosmological time scales, we can readily compute the relic abundance of the DM neutrinos,

$$\Omega_{\rm DM}\, h^2 = \frac{s_0\, y_{\rm fo}\, M_1}{\rho_{\rm c}/h^2}, \tag{5.34}$$

with the entropy density today s_0, the critical density $\rho_{\rm c}$ and $y_{\rm fo}$ as the frozen-out relic density of N_1. Note that N_1 was certainly non-relativistic before freeze-out, i.e. before the EWPT, because its mass $\widetilde{M}_1$ is determined by Majorana scale Λ_M which is certainly above $\Lambda_{\rm EW} \sim T_{\rm EW}$. Thus, for a non-relativistic DM neutrino initially in thermal equilibrium, we can write

$$y_{\rm fo} = y_{N_1}^{\rm eq}(T_{\rm EW}, \widetilde{M}_1) = \frac{45}{(2\pi^5)^{3/2} g_s} \left(\frac{\widetilde{M}_1}{T_{\rm EW}}\right)^{3/2} e^{-\widetilde{M}_1/T_{\rm EW}}, \tag{5.35}$$

with the entropic number of degrees of freedom g_s as defined in eq. (4.16). Although in eq. (5.34) the DM mass M_1 appears explicitly, the early mass $\widetilde{M}_1$ enters the equation through $y_{\rm fo}$. Therefore, the DM relic abundance produced through our mechanism depends on the three variables $\widetilde{M}_1$, M_1 and $T_{\rm EW}$. Inserting the values from Ref. [11] for $\Omega_{\rm DM}\, h^2$, s_0 and $\rho_{\rm c}$, we plot the relic abundance eq. (5.34) as a function of these three parameters in fig. 5.7. On the left panel of fig. 5.7 each line stands for a different value of $T_{\rm EW}$, which is the temperature at which the freeze-out of the DM sterile neutrinos is induced. Each point along a line stands for a combination of early and late DM masses which, at the given freeze-out temperature, generates the full DM abundance as observed by Planck [96]. For example, with a DM mass of $M_1 = 7.1\,\text{keV}$, as suggested by some of the observations discussed in section 4.4.2, and a critical temperature for the EWPT of $T_{\rm EW} = 150\,\text{GeV}$, the early unsuppressed mass should be $\widetilde{M}_1 \approx 1\,\text{TeV}$ in order for N_1 to make up 100% of the DM of the Universe. On the right panel of fig. 5.7, each line shows the relic abundance produced at a freeze-out temperature of $T_{\rm EW} = 150\,\text{GeV}$. For early and late mass combinations along the upper line, for example, a contribution of only 1% to the DM abundance is produced. Until now we have ignored the two heavier sterile neutrinos N_2 and N_3, which we now briefly consider. If their late masses also lie in the keV range, i.e. $M_{2,3} \gtrsim M_1$ but their early masses lie above $3\,\text{TeV}$ and $T_{\rm EW} = 150\,\text{GeV}$, then their contribution to $\Omega_{\rm DM} h^2$ will be negligible, while N_1 with $M_1 = 7.1\,\text{keV}$ and $\widetilde{M}_1 \approx 1\,\text{TeV}$ would make up all of the DM. It is easy to see why the contribution from the two heavier neutrinos is negligible in this case: when N_1 freezes-out at $T_{\rm EW} = 150\,\text{GeV}$ with the correct comoving density y_{N_1}, the densities of $N_{2,3}$ are Boltzmann suppressed as $\exp(-\widetilde{M}_{2,3}/T_{\rm EW})$ by their larger masses.

Thus, we conclude from this discussion that, for reasonable temperatures of

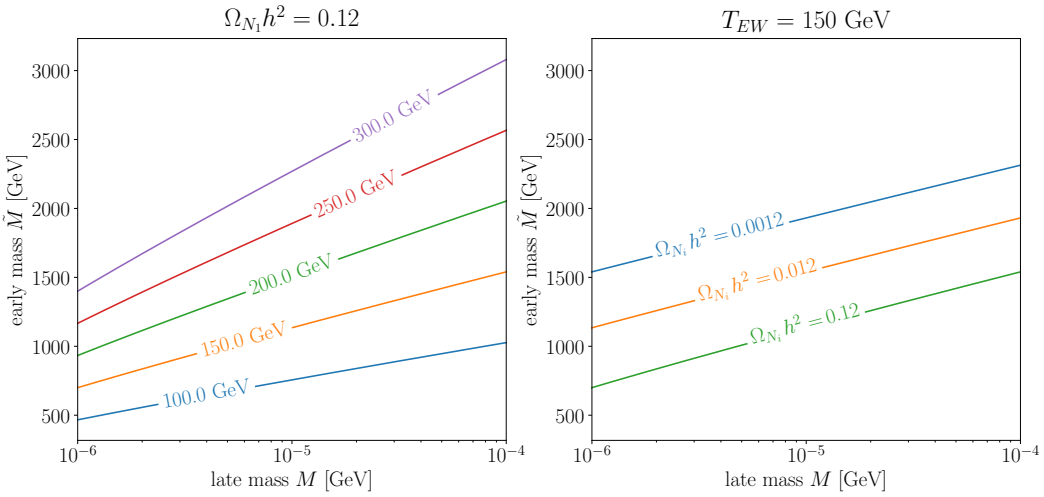

Figure 5.7. *Left panel:* lines of full DM abundance for multiple freeze-out temperatures. Points along a line identify pairs of early and late mass $(\widetilde{M}, M)$ for which a sterile neutrino decoupling at the given temperature of that line has a relic abundance compatible with 100% of the observed DM abundance. *Right panel:* For a freeze-out temperature of $T_{\mathrm{EW}} = 150\,\mathrm{GeV}$, the lines trace combinations of $(\widetilde{M}, M)$ whose relic density contribute 100%, 10% and 1% to the observed DM abundance. The contribution to $\Omega_{\mathrm{DM}}h^2$ from sterile neutrinos with late masses in the range displayed and early masses above 3 TeV is negligible.

the EWPT, we can correctly produce sterile neutrino DM with keV masses if the unsuppressed mass lies in the TeV range, and the unsuppressed masses of the heavier sterile neutrinos lie at least slightly above.

We point out that, although we are assuming that the vev of the flavon gets dragged along by the vev of the Higgs during the EWPT, or in other words, the vevs of both scalars change their values simultaneously, this is actually not strictly mandatory for the viability of the DM production mechanism proposed in this thesis. The vev of the flavon could make the transition $\langle\Theta\rangle : \Lambda_{\mathrm{FN}} \to \epsilon\,\Lambda_{\mathrm{FN}}$ before or after the EWPT; what is crucial is only that the shift occurs. And the temperature at which said shift occurs, whatever it may be, is the freeze-out temperature. Such two-stepped PT, in which two scalars evolve their vevs sequentially as opposed to simultaneously, have been discussed e.g. in Ref. [188]. The assumption that the shift in the flavon vev occurs with the EWPT simply fixes the freeze-out temperature to the temperature of the EWPT itself, i.e. $T_{\mathrm{fo}} = T_{\mathrm{EW}}$.

5.2.2 Choosing appropriate Froggatt-Nielsen Charges

This section closely resembles section 4 of Ref. [177] by the author of this thesis. We attempt to formulate a specific FN effective model which simultaneously addresses

the following issues:

(i) Generate the light neutrino masses and explain the oscillation phenomena by the type-I seesaw mechanism with three RH neutrinos,

(ii) Offer an explanation to the flavour puzzle by generating the mass hierarchy in the lepton sector through the FN mechanism.

(iii) provide a viable DM candidate, the lightest sterile neutrino N_1, which is kept safely stable on cosmological time scales by the dynamic suppression of the neutrino Yukawa coupling. The correct N_1 relic abundance is generated by the dynamic suppression of the Yukawa coupling, which, as discussed in the previous section, induces the decoupling of N_1 from the thermal bath during the EWPT.

To clearly demonstrate that such models exist, we set out to specify the FN charges and $\mathcal{O}(1)$ coefficients that satisfy the requirements stated above. For the first requirement our model should reproduce the neutrino data, i.e. the mass squared differences Δm^2_{sol} and Δm^2_{atm} as well as the PMNS matrix. Similarly, for the second requirement we need to reproduce the masses of the charged leptons. And finally, for the long-time longevity of the DM sterile neutrino, we must make sure that the FN suppressed Yukawa coupling translates into an active-sterile mixing angle that is small enough to be compatible with the results from the X-ray searches.

For the FN factor we define

$$\epsilon = 0.1\,, \qquad \text{and thus} \qquad \lambda = \frac{\langle\Theta\rangle}{\Lambda_{\text{FN}}} = \begin{cases} 1 & : \quad \text{before EWPT} \\ \epsilon = 0.1 & : \quad \text{after EWPT} \end{cases}. \tag{5.36}$$

After the EWPT, the relevant part of the Lagrangian contains the mass terms for the fermions and reads

$$-\mathcal{L}_m = \overline{E_{L\alpha}}\,(m_E)_{\alpha\beta}\,E_{R\,\beta} + \overline{\nu_{L\alpha}}\,(m_D)_{\alpha i}\,\nu_{Ri} + \frac{1}{2}\,\overline{N_i^c}\,(M)_{ij}\,N_j, \tag{5.37}$$

with the entries of the mass matrices scaled by the FN factor as

$$\begin{aligned} (m_E)_{\alpha\beta} &= v\,\epsilon^{q_{\bar{L}\alpha}}\,Y^E_{\alpha\beta}\,\epsilon^{q_{R_\beta}}\,, \\ (m_D)_{\alpha i} &= v\,\epsilon^{q_{\bar{L}\alpha}}\,Y^\nu_{\alpha i}\,\epsilon^{q_{N_i}}\,, \\ (M)_{ij} &= \epsilon^{q_{N_i}}\,(M_N)_{ij}\,\epsilon^{q_{N_i}}\,, \end{aligned} \tag{5.38}$$

where the exponent q_f stands for the FN charge of the fermion f as named in table 5.2. It is convenient to define diagonal matrices whose elements are the FN suppression factors of the lepton families, i.e.

$$Q_{\bar{L}} = \text{diag}(\epsilon^{q_{\bar{L}_e}}, \epsilon^{q_{\bar{L}_\mu}}, \epsilon^{q_{\bar{L}_\tau}}), \qquad Q_N = \text{diag}(\epsilon^{q_{N_1}}, \epsilon^{q_{N_2}}, \epsilon^{q_{N_3}}), \tag{5.39}$$

and the matrix for the flavour charges of the charged lepton singlets Q_E defined analogously. Also, assuming that the bare Majorana mass matrix has no special hierarchy (which is the spirit of the FN mechanism), we can extract the Majorana scale Λ_M from M_N and write $M_N = \Lambda_M Y^N$, where Y^N is a symmetric coefficient matrix with $\mathcal{O}(1)$ entries. Then, the mass matrices can be written in the matrix notation

$$m_E = v\, Q_{\bar{L}}\, Y^E\, Q_E, \quad m_D = v\, Q_{\bar{L}}\, Y^\nu\, Q_N, \quad M = \Lambda_M\, Q_N\, Y^N\, Q_N. \tag{5.40}$$

In contrast to the situation in the νMSM [149, 150] and elsewhere, we here cannot start in a basis in which m_E and M are already diagonal, because each entry in these matrices gets its own individual FN suppression factor, and only after rescaling each entry we may diagonalize the matrices. This fact is important for the following computations.

To find appropriate values for the flavour charges we start with the matrices from eq. (5.40) under the assumption that Y^N, Y^ν, $Y^E \sim \mathcal{O}(1)$ and place conditions on the eigenvalues: for the eigenvalues of the mass matrix of the charged leptons m_E, the eigenvalues are known and thus the condition is to recover them. For the Majorana mass matrix M, we use the results from fig. 5.7 to set the scale of the eigenvalues before and after the FN suppression. And for the neutrino Dirac mass matrix m_D, we use the constraints on the mixing angle from the X-ray searches to *reverse-engineer* a condition on the entries of m_D.

The Majorana mass matrix

To estimate the Majorana scale and the necessary flavour charges of the sterile neutrinos q_{N_i} we recall the results from the previous section presented in fig. 5.7, where we saw that for DM neutrinos with keV masses, the unsuppressed Majorana matrix should be $\sim 10^3\,\mathrm{GeV}$. First, it is worth noting that the masses associated with the sterile neutrinos are the eigenvalues of the Majorana mass matrix, which is not a priori diagonal within the FN framework. The early mass eigenvalues sit on the diagonalized version of $\widetilde{M}$, and the latter is identical to the bare Majorana mass matrix $M_N = Y^N \Lambda_M$. The diagonalization is performed by an orthogonal matrix $\widetilde{U}$ such that

$$\widetilde{M}^d = \widetilde{U}^T\, M_N\, \widetilde{U} = \widetilde{U}^T\, \Lambda_M\, Y^N\, \widetilde{U}. \tag{5.41}$$

Thus, demanding that $\widetilde{M}^d \sim 10^3\,\mathrm{GeV}$ and with $\widetilde{U} \sim \mathcal{O}(0.1)$ and $Y^N \sim \mathcal{O}(1)$, we arrive at the Majorana scale

$$\Lambda_M = 10^4\,\mathrm{GeV}. \tag{5.42}$$

Similarly, the late mass eigenvalues for the sterile neutrinos after the EWPT are obtained with the orthogonal matrix U,

$$M^d = U^T\, Q_N(\Lambda_M\, Y^N)\, Q_N\, U, \tag{5.43}$$

from which the requirement that the eigenvalues lie in the keV region, $M^d \sim \mathcal{O}(\text{keV})$ implies that $\epsilon^{q_{N_i}+q_{N_j}} \sim 10^{-9}$. Resulting from this estimation, two options for the flavour charges of the sterile neutrinos stand out, namely

$$Q_N = \begin{pmatrix} \epsilon^4 & & \\ & \epsilon^4 & \\ & & \epsilon^4 \end{pmatrix} \quad \text{as option A, and} \quad Q_N = \begin{pmatrix} \epsilon^5 & & \\ & \epsilon^4 & \\ & & \epsilon^4 \end{pmatrix} \quad \text{as option B.} \tag{5.44}$$

Option A is special, because it implies that all three sterile neutrinos have the same flavour charge, $q_{N_i} = 4$ for $i = 1, 2, 3$, and Q_N is proportional to the identity matrix $\mathbf{1}$, so we can write $Q_N = \epsilon^4\mathbf{1}$. As a result, the early- and late Majorana mass matrices are also proportional to each other, $M = \epsilon^8\,\widetilde{M} = \epsilon^8\Lambda_M\, Y^N$, and thus both matrices are diagonalized by the same orthogonal matrix, $\widetilde{U} = U$. This is not the case for option B.

The partial result from these considerations is that we have fixed the value of the Majorana scale $\Lambda_M = 10^4\,\text{GeV}$, and the flavour charges for the sterile neutrinos as in eq. (5.44) such that the DM production can be successful as described in the previous section section 5.2.1.

The neutrino Dirac mass matrix

Our next task is to identify suitable choices for the flavour charges of the lepton doublets, which enter the neutrino Dirac mass matrix m_D as defined in eq. (5.40). The conditions we have on m_D are that the neutrino mass squared differences and the PMNS matrix are correctly recovered. Furthermore, m_D also enters the active-sterile mixing angle which is constrained by the X-ray searches discussed in section 4.4.2.

Of course, there are many possible choices for the lepton doublet flavour charges, and we could spend quite some time investigating some of them via trial-and-error. Luckily, the so-called *Casas-Ibarra-parameterization* [189] offers a more systematic approach. In short, it gives us a parameterization of m_D in terms of the mass eigenvalues of the light and heavy neutrinos, the PMNS matrix, and one arbitrary orthogonal matrix carrying free parameters. By construction, the neutrino Dirac mass matrix m_D built by this parameterization automatically delivers the mass eigenvalues and the PMNS matrix fed into it as input. Evidently, this promises to be very useful for our purposes. However, the Casas-Ibarra-parameterization, as it was originally derived and is usually presented, assumes that the Majorana mass matrix and the charged lepton mass matrix can be represented in a basis in which they are both diagonal. But, since we are building a FN model, we may

not make this assumption and must instead rederive the parameterization for the more general case of non-diagonal M_N and m_E. The derivation is presented in section A.1. The result is

$$m_D = i\, V^\star \sqrt{m_\nu^d}\, R\, \widetilde{U} \sqrt{\widetilde{M}^d}\, \widetilde{U}^T\, Q_N, \tag{5.45}$$

where m_ν^d is the diagonal matrix carrying the mass eigenvalues of the light neutrinos, $\widetilde{M}^d$ and $\widetilde{U}$ are defined in eq. (5.41), Q_N can be chosen as one of the two matrices in eq. (5.44) and R is the arbitrary orthogonal matrix carrying the free parameters. The freedom in the free parameters within R reflects that fact that there exist many possible choices for the entries of the bare neutrino Yukawa matrix Y^ν leading to the same eigenvalues in m_ν^d. Furthermore, V is the matrix that diagonalizes the light neutrino Majorana mass matrix, i.e. $m_\nu^d = V^\dagger m_\nu V$ as defined in eq. (3.34). In the SM, because one can take the charged lepton mass matrix to be diagonal, V is actually just the PMNS matrix. For us, however, because we are building a FN model, m_E has to be diagonalized by a biunitary transformation, i.e. $m_E^d = W_L^\dagger\, m_E\, W_R$, where W_L and W_R are unitary matrices. The PMNS matrix is then given by $V_{\text{PMNS}} = W_L^\dagger\, V$.

Recall from eq. (5.40) that $m_D = v\, Q_{\bar{L}}\, Y^\nu\, Q_N$, which we can insert in eq. (5.45) to eliminate Q_N, so that the flavour charges of the lepton doublets are the only ones left in the equation,

$$Q_{\bar{L}}\, Y^\nu = \frac{i}{v}\, V^\star \sqrt{m_\nu^d}\, R\, \widetilde{U} \sqrt{\widetilde{M}^d}\, \widetilde{U}^T. \tag{5.46}$$

The precise scale of the light neutrino masses is, as of today, still unknown; although the KATRIN experiment has placed an upper bound of $m_\nu < 0.8\,\text{eV}$[3] at 90% C.L. [190]. Thus, a conservative estimate for the size of the entries in the diagonalized light neutrino mass matrix is $m_\nu^d \sim \mathcal{O}(0.1\,\text{eV}) \simeq \mathcal{O}(10^{-10}\,\text{GeV})$, and for the early masses of the sterile neutrinos we may estimate $\widetilde{U} \sqrt{\widetilde{M}^d}\, \widetilde{U}^T \sim (\mathcal{O}(10^4\,\text{GeV}))^{1/2}$. This, together with $Y^\nu \sim \mathcal{O}(1)$, and $R, V, \sim \mathcal{O}(0.1)$, gives us an estimate of the scale of the necessary FN suppression, resulting in the following possible (not unique) choice for the flavour charges of the lepton doublets,

$$Q_{\bar{L}} = \begin{pmatrix} \epsilon^7 & & \\ & \epsilon^7 & \\ & & \epsilon^7 \end{pmatrix}, \tag{5.47}$$

i.e. the flavour charges of the lepton doublets can be chosen as

$$q_{\bar{L}} = \{q_{\bar{L}_e},\, q_{\bar{L}_\mu},\, q_{\bar{L}_\tau}\} = \{7,\, 7,\, 7\}. \tag{5.48}$$

Consequently, the mass hierarchy in the lepton sector must be generated by different

[3] The bound is placed on the observable defined in [190] as $m_\nu^2 = \sum_i |(V_{\text{PMNS}})_{ei}|^2 m_i^2$, which in the literature is often denoted as m_β^2.

flavour charges for the charged lepton singlets. Empirically, we find that a good choice which is able to correctly reproduce the charged lepton mass eigenvalues with $Y^E \sim \mathcal{O}(1)$ is given by

$$q_R = \{q_{R_e}, q_{R_\mu}, q_{R_\tau}\} = \{-3, -4, -4\}. \tag{5.49}$$

To summarize, we have fixed the Majorana scale and all the flavour charges by demanding that the mass eigenvalues are correctly generated from $\mathcal{O}(1)$ bare Yukawa couplings and coefficients: the known masses of the charged leptons, the light neutrino mass scale, and the early and late masses of the sterile neutrinos lie in the right ranges such that the DM production via the varying effective Yukawa coupling during the EWPT can successfully occur, as shown in fig. 5.7. The obtained results can be summarized as

$$\begin{aligned} \Lambda_M &= 10^4\,\text{GeV}\,, & q_N &= \begin{cases} \{4,\,4,\,4\}: & \text{option A} \\ \{5,\,4,\,4\}: & \text{option B} \end{cases}\,, \\ q_{\bar{L}} &= \{7,\,7,\,7\}\,, & q_R &= \{-3,\,-4,\,-4\}\,. \end{aligned} \tag{5.50}$$

The longevity of the Dark Matter sterile neutrino

Now, although the mass scales of the sterile neutrinos before and after the EWPT have been implemented correctly for DM genesis by the parameters in eq. (5.50), we still have to investigate their compatibility with the constraints from indirect DM searches. The X-ray searches described in section 4.4.2 have placed an upper bound on the mixing angle of the lightest sterile neutrino with the active neutrino sector, which is approximately [152]

$$\sin^2(2\theta_1) \approx 2\,(\theta_1)^2 \lesssim 2 \times 10^{-5} \left(\frac{\text{keV}}{M_1}\right)^5, \tag{5.51}$$

where the mixing angle is question is defined as

$$(\theta_1)^2 = \sum_{\alpha=e,\mu,\tau} \theta_{\alpha,1}^2 = \sum_{\alpha=e,\mu,\tau} \frac{|(m_D)_{\alpha 1}|^2}{(M_1)^2}. \tag{5.52}$$

Notice that the sum can be written as an element of a matrix, namely

$$\sum_\alpha |(m_D)_{\alpha 1}|^2 = \sum_\alpha (m_D)^*_{\alpha 1} (m_D)_{\alpha 1} = \sum_\alpha (m_D^\dagger)_{1\alpha}\,(m_D)_{\alpha 1} = \left(m_D^\dagger\, m_D\right)_{11}. \tag{5.53}$$

Thus, inserting our Casas-Ibarra parameterization, eq. (5.45), we arrive at

$$\begin{aligned}(\theta_1)^2 &= \frac{\left(m_D^\dagger\, m_D\right)_{11}}{(M_1)^2} \\ &= \frac{1}{(M_1)^2}\left(Q_N\,\widetilde{U}\,\sqrt{\widetilde{M}^d}\,\widetilde{U}^T\,R^\dagger\,m_\nu^d\,R\,\widetilde{U}\,\sqrt{\widetilde{M}^d}\,\widetilde{U}^T\,Q_N\right)_{11},\end{aligned} \tag{5.54}$$

where the matrix V has conveniently cancelled out.

To investigate whether our model is capable of producing a lightest sterile neutrino compatible with eq. (5.51), we must get more concrete and specify the input that enters eq. (5.54) and compute $(\theta_1)^2$. For clarity, we discuss each ingredient of eq. (5.54) separately in the following:

- The matrix m_ν^d contains the mass eigenvalues of the light neutrinos. As stated above, the absolute scale of the neutrino masses is still unknown - only an upper bound from the KATRIN experiment, namely $< 0.8\,\text{eV}$ at 90% C.L. [190], can be given. However, we know from oscillation data that [191]

$$\begin{aligned}\Delta m_{21}^2 &= m_2^2 - m_1^2 = 7.5\times10^{-5}\,\text{eV}^2, \\ |\Delta m_{31}^2| &= |m_3^2 - m_1^2| = 2.5\times10^{-3}\,\text{eV}^2.\end{aligned} \tag{5.55}$$

  In accordance with this, for a specific benchmark point, we now set

$$m_1 = 0\,\text{eV}, \qquad m_2 = 8.7\times10^{-3}\,\text{eV}, \qquad m_3 = 5\times10^{-2}\,\text{eV}, \tag{5.56}$$

  so that $m_\nu^d = \text{diag}(m_1, m_2, m_3)$ is considered fixed and can be inserted into eq. (5.54).

- For the matrices $\widetilde{M}$ and $\widetilde{U}$, it turns out to be very convenient to choose the FN charges from Option A in eq. (5.50). This is because, as mentioned around eq. (5.44), in Option A all sterile neutrinos have the same flavour charge, so that the respective FN suppression matrix is proportional to the unit matrix, $Q_N = \epsilon^4\,\mathbf{1}$. As a consequence, the early and late Majorana mass matrices are also proportional to each other, $M = \epsilon^8\,\widetilde{M}$, and both matrices are diagonalized by the same basis transformation, i.e. $U = \widetilde{U}$. This means that the diagonalized matrices will also be related to each other as $M^d = \epsilon^8\,\widetilde{M}^d$. Therefore, by choosing the late mass eigenvalues M_1, M_2, M_3, the early, i.e. unsuppressed mass eigenvalues are automatically fixed too. A natural choice for a benchmark point is to set the DM mass to match the suspicious X-ray line mentioned in section 4.4.2 at $E_\gamma = 3.55\,\text{keV}$, i.e. $M_1 = 7.1\,\text{keV}$ and make the other two sterile neutrinos slightly heavier, e.g. $M_2 = 20\,\text{keV}$ and $M_3 = 30\,\text{keV}$ - this is an arbitrary but plausible choice. Thus the

diagonalized Majorana mass matrices would be

$$M^d = \mathrm{diag}(7.1,\, 20,\, 30)\,\mathrm{keV} \tag{5.57}$$

$$\widetilde{M}^d = \mathrm{diag}(0.71,\, 2,\, 3)\,\mathrm{TeV}. \tag{5.58}$$

Looking at the left panel of fig. 5.7 we recognize that a sterile neutrino with early mass $\widetilde{M}_1 = 710\,\mathrm{GeV}$ and $M_1 = 7.1\,\mathrm{keV}$ will be produced with the correct relic abundance to account for 100% of the DM of the Universe if it freezes-out at a temperature of $T_{\mathrm{EW}} \approx 100\,\mathrm{GeV}$. Similarly, the masses of the two heavier neutrinos imply that their densities were already be vastly depleted at the moment of freeze-out due to the Boltzmann suppression of their higher masses, so that they do not add to the DM density.

Next, we must specify a matrix $\widetilde{U}$, whose defining property is that it diagonalizes $\widetilde{M}$, i.e.

$$\widetilde{M}^d = \widetilde{U}^T\, \widetilde{M}\, \widetilde{U}. \tag{5.59}$$

Recall that the early Majorana mass matrix is identical to the bare Majorana mass matrix, thus $\widetilde{M} = \Lambda_M\, Y^N$. In principle, there exist infinitely many matrices $\widetilde{M}$ with the eigenvalues as chosen in eq. (5.58). We can pick a specific one by generating a random orthogonal matrix $\widetilde{U}$ such that the diagonalization delivers the right eigenvalues and the coefficient matrix is close to order unity, i.e. $Y^N \sim \mathcal{O}(1)$.

With this, the matrices $\widetilde{M}$ and $\widetilde{U}$ as well as M_1 are fixed and can be inserted into eq. (5.54).

- The last ingredient of eq. (5.54) is the orthogonal matrix R, which is arbitrary and encodes the freedom to choose the $\mathcal{O}(1)$ individual entries of the bare Yukawa coupling matrix Y^ν. One straightforward choice for R would be the unit matrix, $R = \mathbf{1}$; however, inserting this, along with the other results for the benchmark point described above, lead to $(\theta_1)^2 \sim 10^{-6}$, which violates the X-ray bound eq. (5.51). Thus, we must search for specific choices of R which minimize $(\theta_1)^2$ and check if they are compatible with the X-ray bound. This is the next step in our discussion.

The orthogonal matrix R of free parameters

Being a 3×3 orthogonal matrix, R has 3 free parameters and can straightforwardly be parameterized as three consecutive rotations about three perpendicular axes. For example, for the three orthogonal directions defined by the standard basis in 3D space, and with the three rotation angles α, β, γ, we may write R as

$$R := R(\alpha,\, \beta,\, \gamma) = R_3(\gamma)\, R_2(\beta)\, R_1(\alpha). \tag{5.60}$$

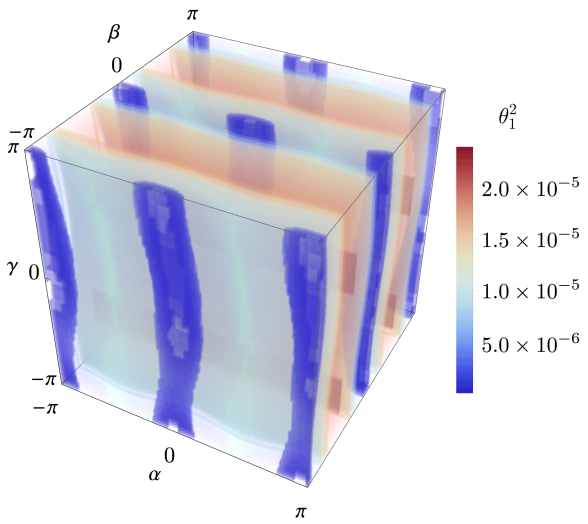

Figure 5.8. The mixing angle squared between the lightest sterile neutrino N_1 with all active neutrinos, $(\theta_1)^2$, defined in eq. (5.54) with input from eqs. (5.56) to (5.58) and the arbitrary orthogonal matrix R. Here, $(\theta_1)^2$ is sampled as a function of the three angles (α, β, γ) that parameterize R as three consecutive orthogonal rotations, as defined in eq. (5.60). The smallest values for the mixing angle $(\theta_1)^2$ can be expected in the dark blue regions of the (α, β, γ)-cube. These regions seem to form three bands around $\alpha = -\pi, 0, \pi$ and $\beta = -\pi, 0, \pi$.

In principle, we could simply insert this parameterization of R into eq. (5.54), together with the other ingredients specified above, and minimize $(\theta_1)^2$ with respect to the three free parameters (α, β, γ) to see if the global minimum satisfies the X-ray bound eq. (5.51). Unfortunately, given the simple parameterization eq. (5.60), the optimization problem is a complex system of highly non-linear equations, which makes the computation difficult and inefficient. A more practical approach is to numerically search for local minima. However, that requires us to define a region in the (α, β, γ)-space, in the vicinity of which the local minimum might be searched for. To identify such regions, we sample values of $(\theta_1)^2$ in the (α, β, γ)-space, which is cube with an edge length equal to 2π. The result of the sampling is displayed in fig. 5.8 and shows the regions of the (α, β, γ)-cube where $(\theta_1)^2$ becomes interestingly small in dark blue color. These regions of interest, where $(\theta_1)^2$ might be compatible with the X-ray bound, appear to form continuous bands in the (α, β, γ)-cube around $\alpha = -\pi, 0, \pi$ and $\beta = -\pi, 0, \pi$, and seem to be fairly independent of γ.

For a closer examination, we consider the plane $\gamma = 0$ and treat it as a representative sub-space of the (α, β, γ)-cube. The resulting plot, shown in the left panel of fig. 5.9, shows $(\theta_1)^2$ as a scalar function in the (α, β) plane. As expected, we identify

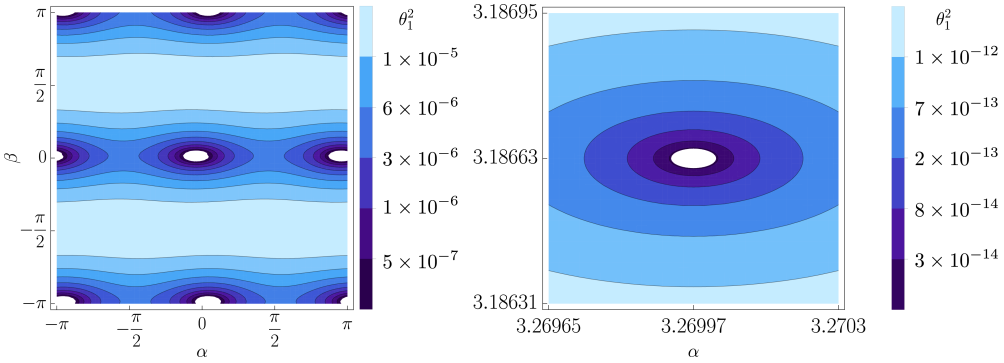

Figure 5.9. *Left panel*: contour lines for the mixing angle of the lightest sterile neutrino N_1 with all active neutrinos, i.e. $(\theta_1)^2$ as defined in eq. (5.54). Using the Casas-Ibarra parameterization for the Dirac mass matrix, $(\theta_1)^2$ can be given as a function of an arbitrary orthogonal matrix R, which is parametrised by a general rotation in three dimensions, as shown in fig. 5.8. In order for our DM sterile neutrino N_1 to be compatible with the X-Ray bounds from eq. (5.51), we are searching for the matrices R for which $(\theta_1)^2$ is the smallest. This plot shows the cut of the cube in fig. 5.8 at $\gamma = 0$. We find four regions of interest in the (α, β) plane where $(\theta_1)^2$ becomes interestingly small and potentially compatible with the X-ray constarins.
Right panel: Zoom into the local minimum near $(\alpha, \beta) = (\pi, \pi)$ and confirm that $(\theta_1)^2$ does indeed become small enough for the DM sterile neutrinos to be safe from the X-Ray bound given by eq. (5.51), which, for $M_1 = 7.1\,\text{keV}$ demands that $\theta_1^2 \lesssim 4.2 \times 10^{-10}$.

four[4] regions of interest where the value of $(\theta_1)^2$ becomes very small, indeed beyond the scope of the color bar, which is why the regions appear white. On the left panel of fig. 5.9 we zoom into the region of interest near $(\alpha, \beta) = (\pi, \pi)$ and confirm that $(\theta_1)^2$ does indeed turn much smaller. Inserting the mass of our DM sterile neutrino $M_1 = 7.1\,\text{keV}$ into eq. (5.51), the find that, for this mass, we X-ray bound demands that $(\theta_1)^2 \lesssim 4.2 \times 10^{-10}$, which is indeed fulfilled for every point in the right panel of fig. 5.9. In fact, The minimum of $(\theta_1)^2$ in the vicinity of $(\alpha, \beta, \gamma) = (\pi, \pi, 0)$ is numerically determined to be located at $(\alpha, \beta, \gamma) = (3.26997, 3.18663, 0)$ and takes the value $(\theta_1)^2_{\text{min}} = 1.59 \times 10^{-20}$, which is well safe from the X-ray constraints.

It is worth emphasizing that this specific region in the (α, β, γ)-space of R matrices is not unique. Similar minima can be found in the vicinity of $(\alpha, \beta) = (0, \pi)$, $(\pi, 0)$ and $(0, 0)$, with any value of γ, and in each case reaching the same order of magnitude $(\theta_1)^2_{\text{min}} \sim 10^{-21}$. This demonstrates that there are infinitely many possible choices for R, or equivalently for the entries in the bare Yukawa matrix Y^ν, for which the lightest sterile neutrino N_1 has such a small mixing angle

[4] there are four, not nine regions of interest, since the regions on the edges should not be counted twice because of the periodicity of the (α, β, γ)-space.

with the active neutrinos that it evades the current X-ray constraints. We also point out that, although we used a randomly generated orthogonal matrix for $\widetilde{U}$ (as explained below eq. (5.59)) to compute fig. 5.8, we checked that the results discussed here are qualitatively unaltered by using other randomly generated matrices $\widetilde{U}$. In other words, using different $\widetilde{U}$ might lead to fig. 5.8 looking slightly different. However, that is irrelevant; what matters is only whether or not matrices R exist, such that the X-Ray bound is respected, and we confirmed that the answer yes in all cases.

The case of unequal flavour charges for the sterile neutrinos

Now we turn to briefly discuss Option B in eq. (5.50), where the flavour charges for the sterile neutrinos are

$$q_N = \{5,\, 4,\, 4\}\,, \quad \text{and thus} \quad Q_N = \text{diag}\big(\epsilon^5,\, \epsilon^4,\, \epsilon^4\big)\,. \tag{5.61}$$

For convenience, we here restate the definition of the early ($\widetilde{M}$) and late (M) Majorana mass matrices,

$$\widetilde{M} = \Lambda_M\, Y^N, \qquad M = Q_N\, \Lambda_M\, Y^N\, Q_N = Q_N\, \widetilde{M}\, Q_N. \tag{5.62}$$

In contrast to the situation with Option A, here Q_N is not proportional to the identity matrix, which means that the early and late Majorana mass matrices are also not proportional to each other. Therefore, their eigenbasis is not the same, meaning that they are diagonalized by different orthogonal transformation matrices $\widetilde{U} \neq U$.

When using Option A from eq. (5.50), we were able to choose the late Majorana mass eigenvalues and, because of the direct proportionality between them, the early Majorana mass eigenvalues were then also automatically fixed. This differs from the situation we have now with Option B; choosing one set of eigenvalues allows us no statement on the other, because early and late mass eigenvalues belong to matrices with different eigenbasis. Still, in order to compute $(\theta_1)^2$ from eq. (5.54) we need to input the eigenvalues of the two matrices, which are not proportional to each other but still related by eq. (5.62). We proceed in the following manner. We choose to keep the same late mass eigenvalues as previously, i.e. $M^d = \text{diag}(7.1,\, 20,\, 30)$ keV. There exist infinitely many non-diagonal matrices with the elements in M^d as its eigenvalues. We find one specific such matrix M by using a randomly generated orthogonal transformation matrix U to rotate M^d away from the representation in its eigensysten,

$$M = U\, M^d\, U^T. \tag{5.63}$$

Once we have a specific M, we can easily compute $\widetilde{M}$ by

$$\widetilde{M} = Q_N^{-1}\, M\, Q_N^{-1}, \tag{5.64}$$

and can then also compute its eigenvalues, which are the elements sitting in $\widetilde{M}^d$, and its normalized eigenvectors, which make up the columns of $\widetilde{U}$. Thus, similarly to what we did previously with Option A, we have fixed all ingredients of eq. (5.54) by generating only one random orthogonal matrix, namely U.

However, there is still one issue to consider: as discussed in section 5.2.1 and particularly in fig. 5.7, the successful production of keV DM in our model requires that the early Majorana mass eigenvalues lie within a certain range in the low TeV scale. Specifically, for a DM mass of $M_1 = 7.1\,\text{keV}$, and an EWPT-induced freeze-out at a reasonable temperature, say $T_{EW} \in [100,\, 300]\,\text{GeV}$, we must demand that $\widetilde{M}_1 \in [700,\, 2000]\,\text{GeV}$ and $M_{2,3} \gtrsim 3000\,\text{GeV}$. Whether or not this is realized depends on the randomly generated orthogonal transformation matrix U. Thus, we computed the eigenvalues of $\widetilde{M}$ for 100 000 different randomly generated orthogonal matrices U and confirmed that, in $\sim 70\%$ of the instances, the resulting eigenvalues did lie in the desired region, thereby demonstrating that the production of keV DM sterile neutrinos is feasible, which was our goal. Note that these considerations were not necessary in the case of using Option A for the flavour charges of the sterile neutrinos, because in that case we could fix the early mass eigenvalues $\widetilde{M}^d$ by our choice of late mass eigenvalues M^d.

As a concrete and representative example, consider a realization where, after choosing $M^d = \text{diag}(7.1,\, 20,\, 30)\,\text{keV}$, the randomly generated matrix U leads to the following early Majorana mass eigenvalues

$$\widetilde{M}^d = \text{diag}(1.19,\, 2.86,\, 124.94)\,\text{TeV}. \tag{5.65}$$

Thus, the lightest sterile neutrino initially has a mass of $\widetilde{M}_1 = 1.19\,\text{TeV}$, and, after the EWPT occurs causing the dynamic suppression of the Yukawa couplings and Majorana masses, the lightest sterile neutrino ends up with a mass $M_1 = 7.1\,\text{keV}$. If the EWPT occurs at $T_{\text{EW}} \approx 165\,\text{GeV}$, then the lightest sterile neutrino is forced to decouple from the thermal bath due to the sudden and drastic suppression of the Yukawa coupling, and its relic density freezes-out matching the observed DM abundance, as is shown in fig. 5.10. Having confirmed that successful DM production is still feasible even after choosing the flavour charges of the sterile neutrinos as in Option B of eq. (5.50), we can again redo the computation for $(\theta_1)^2$ by inserting all ingredients into eq. (5.54) to check that the sterile neutrinos are still compatible with the X-ray bounds. The result of this repeated analysis is qualitatively very similar to figs. 5.8 and 5.9, displaying four bands of local minima in the (α, β, γ)-space of the matrix R, namely in the vicinity of $(\alpha,\, \beta,\, \gamma) = \{(0, 0, \gamma),\, (0, \pi, \gamma),\, (\pi, 0, \gamma),\, (\pi, \pi, \gamma)\}$ for $\gamma \in [-\pi, \pi]$. Also, the value of the numerically determined minimum in these regions of interest is again $(\theta_1)^2_{\text{min}} \sim 10^{-21}$, thus making the lightest sterile neutrinos compatible with the current X-ray constraints and safely long lived to play the role of DM of the Universe.

This shows that, for the benchmark point discussed here, which is defined by the model parameters in eq. (5.50) and late mass eigenvalues $M^d = \text{diag}(7.1,\, 20,\, 30)\,\text{keV}$,

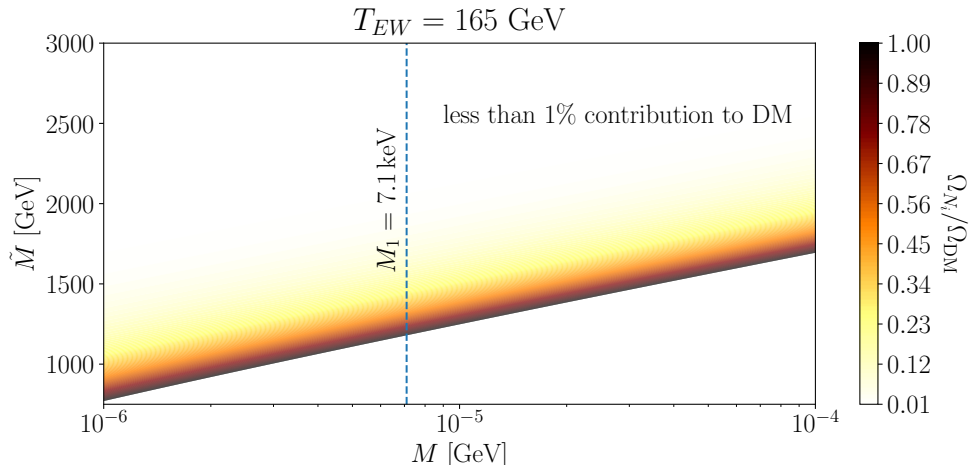

Figure 5.10. The color scale shows the contribution to the DM abundance from sterile neutrinos early masses $\widetilde{M}$ in the $\mathcal{O}(1)$ TeV range and late masses M in the keV range. The change from early to late masses is driven by the dynamical suppression of the effective Majorana mass matrix caused by a shift in the flavon vev during the EWPT, which also drives a dramatic suppression of the effective Yukawa couplings. Here, the EWPT is assumed to occur at $T_{EW} = 165\,\text{GeV}$. The flavour charges of the sterile neutrinos are chosen as $q_N = \{5, 4, 4\}$. The dashed vertical line shows the position of our DM neutrino with a mass $M_1 = 7.1\,\text{keV}$. With an early mass eigenvalue of $\widetilde{M}_1 \approx 1.2\,\text{TeV}$ the lightest sterile neutrino N_1 accounts for 100% of the DM relic abundance. The other two sterile neutrinos with late masses $M_2 = 20\,\text{keV}$ and $M_3 = 30\,\text{keV}$ and early masses $\widetilde{M}_{2,3} \gtrsim 2.5\,\text{TeV}$ contribute practically nothing to the DM abundance, because their equilibrium density has already been completely depleted by their Boltzmann suppression at the moment of the EWPT.

the DM production mechanism proposed in this thesis and first published in Refs. [55, 177], is able to correctly generate the observed DM abundance and reproduce the known light neutrino parameters while also alleviating the flavour puzzle in the lepton sector. For a concrete example showing the entries in the Yukawa and Majorana matrices, see section A.3.

Beyond the 7.1 keV mass benchmark point

Up until this point we have studied a scenario where the sterile neutrino DM has a very specific mass, namely $M_1 = 7.1\,\text{keV}$. As mentioned in section 4.4.2, this specific mass is well motivated because a curious X-ray signal has been observed [152], which can be interpreted as a hint for a decaying sterile neutrino DM with precisely this mass. However, that interpretation is still controversial and contested

(see the end of section 4.4.2).

Thus, we now address the possibility of DM sterile neutrinos with masses $M_1 \neq 7.1\,\text{keV}$ within the framework presented in this chapter. For convenience, we again choose Option A for the flavour charges of the sterile neutrinos, i.e. $q_N = \{4, 4, 4\}$, so that the diagonalized late and early Majorana mass matrices are proportional to each other and related as $M^d = \epsilon^8\,\widetilde{M}^d$. We start by considering again the same late mass eigenvalues that we have been studying so far, namely $M^d = \text{diag}(7.1, 20, 30)$ keV with the corresponding late mass eigenvalues $\widetilde{M}^d = \text{diag}(0.71, 2, 3)$ TeV. Our strategy is to sweep through the M_1 mass axis, for which we introduce a dimensionless parameter s and use it to define the mass matrix $M^d(s)$ as

$$M^d(s) = s \cdot M^d = s \cdot \begin{pmatrix} 7.1 & & \\ & 20 & \\ & & 30 \end{pmatrix} \text{keV}, \quad \text{with} \quad s \in \mathbb{R}. \tag{5.66}$$

Thus, the dimensionless parameter s linearly rescales the late sterile neutrino mass eigenvalues. Consequently, the early mass eigenvalues in $\widetilde{M}^d$ get rescaled accordingly, $\widetilde{M}^d(s) = s \cdot \widetilde{M}^d$. Thus, by varying the dimensionless parameter s we can homogeneously rescale both $\widetilde{M}^d$ and M^d and sweep through the mass axis. The eigenbasis matrices $U = \widetilde{U}$ are left unaltered by this rescaling. The question left to answer is: how does $(\theta_1)^2$ behave with this rescaling? Since $(\theta_1)^2$, as defined in eq. (5.54), is proportional to two powers of $\sqrt{\widetilde{M}^d}$ while being inversely proportional to $(M_1)^2$, we conclude that the mixing angle scales as

$$(\theta_1)^2 \propto s^{-1}. \tag{5.67}$$

Thus, in the $\left(M_1,\, (\theta_1)^2\right)$ parameter space, we may start of from the point previously calculated as $\left(M_1 = 7.1\,\text{keV},\, (\theta_1)^2 \approx 10^{-21}\right)$ and extrapolate using the scaling with the parameter s. The result of this exercise is shown in fig. 5.11. We checked that the results of the extrapolation shown in fig. 5.11 are indeed correct by explicitly computing $(\theta_1)^2$ for multiple mass eigenvalues along the extrapolation lines.

Remember that when building our FN model, we assumed that the lightest active neutrino is massless, see eq. (5.56). Now, we drop this assumption and recompute the mixing angle between N_1 and the active neutrino states $(\theta_1)^2$ for tiny yet non-vanishing masses for the lightest active neutrino state, i.e. $m_1 \neq 0$. We find that finite values of m_1 have an important impact on $(\theta_1)^2$; indeed the capability of the lightest sterile neutrino to have tiny enough mixing angle θ_1 as to evade the current X-ray constraints is dependent on the mass of the lightest active neutrino being itself as tiny as possible. This is depicted in fig. 5.11 by the black lines, where each line is marked by the value of m_1 to which it corresponds. The area above each line is the region in parameter space where the mechanism proposed here provides a viable DM candidate, which is stable on cosmological time scales and evades the X-Ray constraints, while also reproducing the PMNS parameters and the known

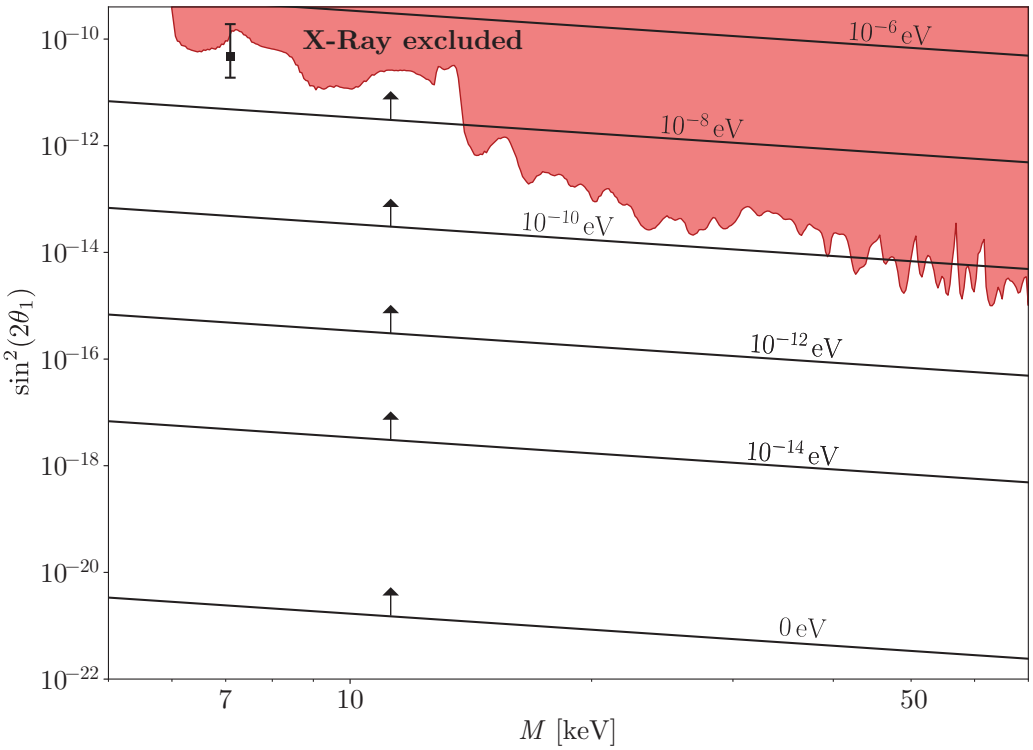

Figure 5.11. The red shaded area in the the plot is excluded by the X-Ray NuSTAR GC survey [192]. We empirically find that the minimal mixing angle which can be reached within our model depends on the mass of the lightest active neutrino m_1. Thus, each line stands for m_1 as marked over it. The parameter space above each line is the region where the mechanism proposed here is able to produce sterile neutrino DM while recovering the PMNS parameters and the known mass squared differences of the active neutrinos.

mass squared differences of the active neutrinos. Furthermore, for a late DM mass $M_1 = 50\,\text{keV}$, the corresponding early mass is approximately $\widetilde{M}_1 = 5\,\text{TeV}$. For this combination of masses, successful DM production according to eq. (5.34) is achieved at a freeze-out temperature $T_{EW} \approx 550\,\text{GeV}$, which is not unreasonable.

This finalizes our discussion of the mechanism proposed in this thesis. In the next chapter, we summarize the present discussion, and offer some concluding remarks and state possible directions for further research.

Chapter 6

Summary and Conclusions

In this thesis the author proposes a new production mechanism for sterile neutrino dark matter in the early Universe. In contrast to the common approaches found in the literature, the presented mechanism relies neither on the oscillations between active and sterile neutrinos, nor on the decay of heavier parent particles to produce the sterile neutrinos. Instead, the mechanism is inspired by the so-called *freeze-out* mechanism, typical for WIMP dark matter. Freeze-out is a very natural process to generate relic abundances and follows immediately from the thermodynamics of an expanding Universe. In essence, the high temperature of the early Universe allows for frequent interactions among the particles present, which thereby form a kind of cosmic fluid in thermal equilibrium. As the Universe expands and cools, the rates with which some of these interactions occur might fall below the expansion rate of the Universe, causing the particle species which communicated with the rest of the plasma only through said interactions to decouple from thermal equilibrium. For minimally coupled right handed Majorana neutrinos as dark matter candidates, i.e. those that couple to the SM only through the Yukawa term in the Lagrangian and have no further interactions with the SM, production by freeze-out has not been considered before. The reason for this is that such right handed neutrinos, cannot reach thermal equilibrium in the early Universe (which is a basic requirement for freeze-out) and simultaneously be stable on cosmological time scales. This conflict arises because the neutrino Yukawa coupling would need to be rather sizeable for the sterile neutrinos to thermalize, but is also required to be very small in order to prevent the sterile neutrinos from decaying too quickly, leaving us with no dark matter. The production mechanism proposed in this thesis attempts to tackle this conflict. The core idea behind our mechanism is simple and can be distilled as follows: If the neutrino Yukawa coupling is allowed to vary during some period in the early cosmological history, going from large values at early times to much smaller values at later times, then the sterile neutrinos could reach thermal equilibrium during the early stage, and then be forced to freeze-out and stay quasi-stable due to the change in their Yukawa couplings.

A production mechanism for sterile neutrino dark matter is desirable for the

following reasons. Adding three right handed Majorana neutrinos to the SM is an elegant and minimal yet very powerful extension to the theory, often referred to as νMSM [149, 150, 153]. Within the νMSM, the relic abundance of the sterile neutrino dark matter is produced by the *Dodelson-Widrow-* or the *Shi-Fuller* mechanisms [151, 154]. However, these are already either ruled-out or under a lot of pressure from the indirect dark matter searches, as discussed in section 4.4.2. Therefore, a new production mechanism for sterile neutrino dark matter, that still adheres to the minimality of the νMSM, i.e. does not introduce new exotic neutrino interactions, is in demand. Furthermore, the notion of varying Yukawa couplings, which is the basis for the mechanism we propose, is reminiscent of a possible solution to the flavour puzzle, which could add to the appeal of the νMSM and our mechanism.

Although there might exist many possible ways to implement varying Yukawa couplings, we here have chosen to do so by embedding the νMSM in a Froggatt-Nielsen model (introduced in section 2.1). The sterile neutrinos still only couple through their Yukawa coupling and have no additional interactions beyond the νMSM. The key feature of the Froggatt-Nielsen mechanism, is that the flavon and all fermions are charged under a global symmetry $U(1)_{\mathrm{FN}}$. Therefore, the Yukawa and Majorana terms are modified to include powers of the flavon according to the charges of the fermions, so that the Yukawa terms are $U(1)_{\mathrm{FN}}$ invariant. The effect is basically the rescaling of the Yukawa couplings and Majorana masses by the Froggatt-Nielsen factor λ, which is the ratio of the flavon vev to the flavour scale Λ_{FN}. Our mechanism assumes that the Froggatt-Nielsen factor is initially $\lambda = 1$, meaning that initially all effective Yukawa couplings are still unsuppressed and $\sim \mathcal{O}(1)$, thus allowing the sterile neutrinos to thermalize. Now comes the key point: during a phase transition, e.g. the electroweak phase transition, the scalar potential of the theory relaxes into a new true vacuum, whose coordinates in field space are different to those of the false vacuum also in the flavon dimension. In other words, the flavon vev changes during the phase transition, so that so that afterwards the Froggatt-Nielsen factor becomes $\lambda < 1$, thus effectively enforcing the suppression of the Yukawa couplings and Majorana masses. In this sense, it is the phase transition that induces the variation of the Yukawa couplings.

In this thesis, we have discussed the feasibility of a change in the flavon vev during a phase transition, which as also been discussed e.g. in Refs. [176, 187, 193]. Then, taking the electroweak phase transition as the one responsible for the desired change in the flavon vev, we have shown that it is possible to formulate Froggatt-Nielsen models with the following features:

1. Prior to the electroweak phase transition, the lightest sterile neutrino is in thermal equilibrium. As soon as the phase transition occurs, the effective Yukawa couplings become strongly suppressed by the change in the flavon vev. Consequently, the lightest sterile neutrino is forced to freeze-out. For reasonable temperatures of the electroweak phase transition, the frozen-out relic density of the lightest sterile neutrino can match the observed dark matter abundance. Thus, successful dark matter genesis is achieved.

2. By the synergy of the seesaw and Froggatt-Nielsen mechanisms, the SM light neutrino masses (or more precisely, the mass squared differences) and the parameters of the PMNS matrix are recovered.

3. The bare Yukawa couplings of the lepton sector are all close to $\mathcal{O}(1)$ and the observed hierarchy is generated by the Froggatt-Nielsen mechanism. Thus, the flavour puzzle in the lepton sector is alleviated.

As discussed in section 5.2, the successful production of keV dark matter sterile neutrinos relies on the masses of the sterile neutrinos before the electroweak phase transition to be $\mathcal{O}(1-5\,\mathrm{TeV})$, and the necessary longevity of the dark matter sterile neutrinos to evade the X-ray constrains can be realized if lightest active neutrino mass eigenstate is massless or at least lighter than $\sim 10^{-8}\,\mathrm{eV}$.

In sum, the mechanism proposed in this thesis represents a simple and appealing way to generate sterile neutrino DM and active neutrino masses, while also addressing the flavour puzzle. Our mechanism can be seen as complementary to the νMSM, as it reopens regions of the parameters space that are already ruled out for the standard production mechanisms.

While these results are interesting and encouraging in their own right, there are still many aspects of the mechanism proposed here that require further research. First of all, the Froggatt-Nielsen embedding studied here is certainly not the only possible way to implement varying Yukawa couplings. Other realizations, e.g. within 5-dimensional Randall-Sundrum models [193, 194] or involving the concept of partial compositeness [175], might also be possible and could perhaps display interesting phenomenological features. Secondly, since in our framework the Majorana masses are also affected by the change in the vev of the flavon, dedicated research into the impact of this issue on the momentum distribution of the sterile neutrino dark matter is important and necessary to uncover possible issues regarding structure formation. Also, while in the νMSM the matter-antimatter asymmetry of the Universe is addressed by leptogenesis, other studies have suggested that Yukawa couplings varying during the electroweak phase transition could enable electroweak baryogenesis, e.g. [174]. Therefore, the issue of the matter-antimatter asymmetry within the framework proposed here should also be further investigated. And finally, of course, a UV-complete theory that displays the Yukawa behaviour here described would indeed be very welcomed.

We conclude these overenthusiastic final remarks with a sobering statement: although it is fascinating to imagine a Swiss knife type of solution to the problems in fundamental physics - one that addresses multiple of the open questions at once - we must perhaps brace ourselves for the possibility that such a theory lies beyond our imagination.

To close the loop, remember *Hamlet*: "... there are more things in heaven and earth, [...] than are dreamt of in your philosophy..."

Appendices

Appendix A

Additional Material

A.1 Deriving the Casas-Ibarra parameterization for Froggatt-Nielsen models

Within a FN mechanism, the effective Dirac and Majorana mass matrices are given by (see eq. (5.40)

$$m_D = v\, Q_{\bar{L}}\, Y^{\nu}\, Q_N, \qquad M = Q_N\, \Lambda_M\, Y^N\, Q_N. \tag{A.1}$$

The Q matrices carrying the FN suppression factors are diagonal. The seesaw mechanism gives us the Majorana mass matrix for the light neutrinos m_ν as

$$\begin{aligned} m_\nu =& - m_D\, M^{-1}\, m_D^T \\ =& - v\, Q_{\bar{L}}\, Y^{\nu}\, Q_N\, {Q_N}^{-1}\, \left(\Lambda_M\, Y^N\right)^{-1}\, {Q_N}^{-1}\, Q_N Y_\nu^T\, Q_{\bar{L}}\, v \\ =& - v\, Q_{\bar{L}}\, Y^{\nu}\, \left(\Lambda_M\, Y^N\right)^{-1}\, Y_\nu^T\, Q_{\bar{L}}\, v \\ =& - \tilde{m}_D\, \tilde{M}^{-1}\, \tilde{m}_D^T, \end{aligned} \tag{A.2}$$

where we have conveniently defined

$$\tilde{m}_D = v\, Q_{\bar{L}}\, Y^{\nu}, \qquad \tilde{M} = \Lambda_M\, Y^N. \tag{A.3}$$

With an orthogonal matrix $\tilde{U}$, $\tilde{M}$ is diagonalized by $\tilde{M} = \tilde{U}\, \tilde{M}^d\, \tilde{U}^T$ and $\tilde{M}^d$ is diagonal, then we may write

$$\tilde{M}^{-1} = \tilde{U}\, \sqrt{\tilde{M}^d}^{-1}\, \sqrt{\tilde{M}^d}^{-1}\, \tilde{U}^T. \tag{A.4}$$

Similarly, m_ν is diagonalized as $m_\nu^d = V^T\, m_\nu\, V$, with an orthogonal matrix V. Then, we have

$$m_\nu^d = i^2\, V^T \tilde{m}_D\, \tilde{U}\, \sqrt{\tilde{M}^d}^{-1}\, \sqrt{\tilde{M}^d}^{-1}\, \tilde{U}^T\, \tilde{m}_D^T\, V. \tag{A.5}$$

Multiplying this equation from the left and from the right with $\sqrt{m_\nu^d}^{-1}$ we obtain

$$\begin{aligned}\mathbf{1} &= i\,\sqrt{m_\nu^d}^{-1}\,V^T\tilde{m}_D\,\tilde{U}\,\sqrt{\tilde{M}^d}^{-1}\,\sqrt{\tilde{M}^d}^{-1}\,\tilde{U}^T\,\tilde{m}_D^T\,V\,\sqrt{m_\nu^d}^{-1}\,i \\ &= \left(-i\,\sqrt{m_\nu^d}^{-1}\,V^T\tilde{m}_D\,\tilde{U}\,\sqrt{\tilde{M}^d}^{-1}\right)\left(-i\,\sqrt{m_\nu^d}^{-1}\,V^T\tilde{m}_D\,\tilde{U}\,\sqrt{\tilde{M}^d}^{-1}\right)^T, \end{aligned} \tag{A.6}$$

Thus, we conclude that the expression in the parenthesis must be an orthogonal matrix, which we name R. Isolating $\tilde{m}_D$ from R, we are left with

$$\tilde{m}_D = i\,V^\star\,\sqrt{m_\nu^d}\,R\,\sqrt{\tilde{M}^d}\,\tilde{U}^T, \tag{A.7}$$

and finally, recalling the definition of $\tilde{m}_D$, we multiply from the right with Q_N to obtain

$$m_D = i\,V^\star\,\sqrt{m_\nu^d}\,R\,\sqrt{\tilde{M}^d}\,\tilde{U}^T, Q_N. \tag{A.8}$$

A.2 The scalar potential

The conditions under which the vev of a scalar field Θ can be modified during a phase transition are examined. The computations are taken identically from Ref. [55] by the author of this thesis.

Consider the potential of two scalar fields, Θ and Σ, along with the energy scales Λ_{FN} and Λ_Σ at which the scalar fields assume their respective vevs. The potential can be written as

$$V(\Theta,\,\Sigma) = \mu_\theta^2\,\Theta^\dagger\Theta + \lambda_\theta\,(\Theta^\dagger\Theta)^2 + \mu_\sigma^2\,\Sigma^\dagger\Sigma + \lambda_\sigma\,(\Sigma^\dagger\Sigma)^2 + \lambda_{\theta\sigma}\,(\Theta^\dagger\Theta)(\Sigma^\dagger\Sigma). \tag{A.9}$$

Without loss of generality, we assume that both fields acquire their vev's only along their real components and substitute

$$\Theta \longrightarrow \frac{1}{\sqrt{2}}\,\theta, \qquad\qquad \Sigma \longrightarrow \frac{1}{\sqrt{2}}\,\sigma, \tag{A.10}$$

leading to

$$V(\theta,\sigma) = \frac{\mu_\theta^2}{2}\,\theta^2 + \frac{\lambda_\theta}{4}\,\theta^4 + \frac{\mu_\sigma^2}{2}\,\sigma^2 + \frac{\lambda_\sigma}{4}\,\sigma^4 + \frac{\lambda_{\theta\sigma}}{4}\,\theta^2\sigma^2. \tag{A.11}$$

The minimum of the potential is given by the zeros of the field space gradient:

$$\nabla_{\theta,\sigma}V = \begin{pmatrix}\theta\,(\mu_\theta^2 + \lambda_\theta\,\theta^2 + \frac{\lambda_{\theta\sigma}}{2}\,\sigma^2)\\ \sigma\,(\mu_\sigma^2 + \lambda_\sigma\,\sigma^2 + \frac{\lambda_{\theta\sigma}}{2}\,\theta^2)\end{pmatrix}\Bigg|_{(v_\theta,v_\sigma)} \overset{!}{=} \begin{pmatrix}0\\0\end{pmatrix}. \tag{A.12}$$

We recognise the following cases:

(i) **Before the $U(1)_\Sigma$ phase transition:** At temperatures $\Lambda_\Sigma < T < \Lambda_{\text{FN}}$ we

demand

$$v_\theta = \Lambda_{\rm FN}, \qquad \text{and} \qquad v_\sigma = 0. \tag{A.13}$$

Thus, the first component of $\nabla_{\theta,\sigma} V = 0$ implies

$$\mu_\theta^2 = -\lambda_\theta \, \Lambda_{\rm FN}^2. \tag{A.14}$$

(ii) **After $U(1)_\Sigma$ symmetry breaking:**
At temperatures $T < \Lambda_\Sigma$ we demand

$$v_\theta = \epsilon \, \Lambda_{\rm FN}, \qquad \text{and} \qquad v_\sigma \neq 0, \tag{A.15}$$

with $0 < \epsilon < 1$. Thus, the first component of $\nabla_{\theta,\sigma} V = 0$ implies

$$\mu_\theta^2 + \lambda_\theta \, \epsilon^2 \, \Lambda_{\rm FN}^2 + \frac{\lambda_{\theta\sigma}}{2} \, v_\sigma^2 = 0. \tag{A.16}$$

With Eq. (A.14) this is equivalent to

$$\underbrace{\left(1 - \epsilon^2\right)}_{\sim 1} \left(\frac{\Lambda_{\rm FN}}{v_\sigma}\right)^2 = \frac{\lambda_{\theta\sigma}}{2 \, \lambda_\theta} \qquad \Rightarrow \qquad \left(\frac{\Lambda_{\rm FN}}{v_\sigma}\right)^2 \approx \frac{\lambda_{\theta\sigma}}{2 \, \lambda_\theta}. \tag{A.17}$$

Next we compute the mass parameters:

$$m_{\theta\theta}^2 = \partial_\theta^2 V = \mu_\theta^2 + 3\lambda_\theta v_\theta^2 + \frac{1}{2}\lambda_{\theta\sigma} v_\sigma^2, \tag{A.18}$$

$$m_{\sigma\sigma}^2 = \partial_\sigma^2 V = \mu_\sigma^2 + 3\lambda_\sigma v_\sigma^2 + \frac{1}{2}\lambda_{\theta\sigma} v_\theta^2, \tag{A.19}$$

$$m_{\theta\sigma}^2 = \partial_\theta \partial_\sigma V = \lambda_{\theta\sigma} v_\sigma v_\theta. \tag{A.20}$$

The mass matrix is

$$M = \begin{pmatrix} m_{\theta\theta}^2 & m_{\theta\sigma}^2 \\ m_{\theta\sigma}^2 & m_{\sigma\sigma}^2 \end{pmatrix} \tag{A.21}$$

and its corresponding mass eigenvalues are

$$m_\sigma^2 = \lambda_\sigma v_\sigma^2 + \lambda_\theta v_\theta^2 + \sqrt{(\lambda_\sigma v_\sigma^2 - \lambda_\theta v_\theta^2)^2 + (\lambda_{\theta\sigma} v_\theta v_\sigma)^2}, \tag{A.22}$$

$$m_\theta^2 = \lambda_\sigma v_\sigma^2 + \lambda_\theta v_\theta^2 - \sqrt{(\lambda_\sigma v_\sigma^2 - \lambda_\theta v_\theta^2)^2 + (\lambda_{\theta\sigma} v_\theta v_\sigma)^2}. \tag{A.23}$$

The mixing angle between θ and σ is given by

$$\tan(2\alpha) = \frac{\lambda_{\theta\sigma} v_\theta v_\sigma}{\lambda_\sigma v_\sigma^2 - \lambda_\theta v_\theta^2} = \frac{\lambda_{\theta\sigma} v_\sigma \, \epsilon \, \Lambda_{\rm FN}}{\lambda_\sigma v_\sigma^2 - \lambda_\theta \, \epsilon^2 \, \Lambda_{\rm FN}^2}. \tag{A.24}$$

As we will see in a moment, in our scenario, the mixing angle is automatically very small, implying

$$\lambda_{\theta\sigma} v_\theta v_\sigma \ll |\lambda_\sigma v_\sigma^2 - \lambda_\theta v_\theta^2|, \tag{A.25}$$

which means that the mass eigenvalues can be approximated by

$$m_\sigma^2 = 2\,\lambda_\sigma v_\sigma^2, \tag{A.26}$$
$$m_\theta^2 = 2\,\lambda_\theta v_\theta^2. \tag{A.27}$$

Now, for the stationary point $(\theta,\,\sigma) = (v_\theta,\,v_\sigma) = (\epsilon\,\Lambda_{\mathrm{FN}},\,v_\sigma)$ to be indeed a minimum of the potential, the determinant of the mass matrix must be positive definite:

$$\det(M) = \det \begin{pmatrix} \partial_\theta^2 V & \partial_\sigma \partial_\theta V \\ \partial_\sigma \partial_\theta V & \partial_\sigma^2 V \end{pmatrix} \Bigg|_{(v_\theta, v_\sigma)} > 0, \tag{A.28}$$

which results in

$$4\,\lambda_\sigma \lambda_\theta > \lambda_{\theta\sigma}^2. \tag{A.29}$$

From this relation and with Eq. (A.17), we derive constraints on the coupling constants

$$\lambda_{\theta\sigma} < 2\,\lambda_\sigma \left(\frac{v_\sigma}{\Lambda_{\mathrm{FN}}}\right)^2, \tag{A.30}$$
$$\lambda_\theta < \lambda_\sigma \left(\frac{v_\sigma}{\Lambda_{\mathrm{FN}}}\right)^4. \tag{A.31}$$

These constraints consistently imply the smallness of the mixing angle. Finally, we obtain a bound on the mass of the flavon by combining Eqs. (A.27) and (A.31),

$$m_\theta^2 < 2\lambda_\sigma\, v_\sigma^2\, \epsilon^2 \left(\frac{v_\sigma}{\Lambda_{\mathrm{FN}}}\right)^2. \tag{A.32}$$

From this analysis we have learned that, if eqs. (A.30) to (A.32) hold, then the $U(1)_\Sigma$ phase transition can cause a shift in the value of the flavon vev.

A.3 A benchmark point for keV dark matter, neutrino masses and lepton flavour

A specific benchmark point for a Froggatt-Nielsen model as discussed in chapter 5 is presented. This appendix is taken identically from Ref. [177] by the author of this thesis.

We start with the following mass eigenvalues for the SM leptons:

$$m_E^d = \mathrm{diag}(0.511 \times 10^{-3},\, 0.105,\, 1.776)\,\mathrm{GeV}, \tag{A.33}$$
$$m_\nu^d = \mathrm{diag}(0,\, 8.7 \times 10^{-3},\, 5 \times 10^{-2})\,\mathrm{eV}, \tag{A.34}$$

and for the mass of the sterile neutrinos before the EWPT we choose

$$\tilde{M}^d = \mathrm{diag}(710,\, 2000,\, 3000)\,\mathrm{GeV}. \tag{A.35}$$

The FN charges for the charged singlets, the doublets, and the sterile neutrinos are taken to be

$$q_E = \{-3,\, -4,\, -4\}, \qquad q_L = \{7,\, 7,\, 7\}, \qquad q_N = \{4,\, 4,\, 4\}. \tag{A.36}$$

respectively. The bare Majorana mass matrix is given by $\tilde{M} = \Lambda_M\, Y^N$, where we set $\Lambda_M = 10^4\,\mathrm{GeV}$, and is related to its diagonal version by the orthogonal matrix $\tilde{U}$, which we set to

$$\tilde{U} = \begin{pmatrix} -0.200 & -0.696 & -0.690 \\ 0.868 & 0.209 & -0.460 \\ -0.465 & 0.687 & -0.559 \end{pmatrix}, \quad \text{leading to} \quad Y^N = \begin{pmatrix} 0.242 & 0.054 & 0.027 \\ 0.054 & 0.125 & 0.077 \\ 0.027 & 0.077 & 0.203 \end{pmatrix} \tag{A.37}$$

After the EWPT, the suppressed mass eigenvalues of the sterile neutrinos are

$$M^d = \mathrm{diag}(7.1,\, 20,\, 30)\,\mathrm{keV}. \tag{A.38}$$

Since in this case all sterile neutrinos have the same FN charge, the eigenbasis of the matrices $\tilde{M}$ and M are the same. The randomly generated unitary matrix W_L, used to diagonalize the charged lepton mass matrix by $m_E^d = W_L^\dagger\, m_E\, W_R$ and compute the matrix $V = W_L\, V_{\mathrm{PMNS}}$ used in eq. (5.45) is given by

$$W_L = \begin{pmatrix} -0.598 + i\,0.289 & -0.508 - i\,0.023 & -0.548 + i\,0.009 \\ -0.377 + i\,0.531 & 0.558 + i\,0.123 & 0.161 - i\,0.474 \\ -0.364 - i\,0.057 & 0.485 - i\,0.424 & -0.054 + i\,0.668 \end{pmatrix}. \tag{A.39}$$

Finally, the Yukawa matrices for the neutrinos and charged singlets are

$$|Y^\nu| = \begin{pmatrix} 0.030 & 7.381 & 1.031 \\ 0.029 & 4.681 & 4.068 \\ 0.025 & 3.308 & 4.142 \end{pmatrix}, \qquad |Y^E| = \begin{pmatrix} 3.14 & 2.59 & 2.98 \\ 1.89 & 2.21 & 2.86 \\ 5.57 & 3.28 & 3.53 \end{pmatrix}. \tag{A.40}$$

Although there still is some hierarchy in the columns of Y^ν, it is remarkably less severe. The mixing angle for the DM neutrino with all active neutrinos is $\theta_1^2 = 2.86 \times 10^{-10}$ which is below the bound of $\theta_{1\,\mathrm{bound}}^2 = 4.16 \times 10^{-10}$ at a DM mass $M_1 = 7.1\,\mathrm{keV}$.

Appendix B

The Boltzmann equation

The integrated form of the Boltzmann equation for cold relics is derived. The treatment here presented follows that by Kolb and Turner [29] and Gondolo and Gelmini [145]. Our aim here is not to derive a very general expression, but to make the relevant assumptions and simplifications more transparent.

Let the particle momentum distribution of a particle species χ be denoted by $f_\chi(t, \vec{p})$. Then, the Boltzmann equation is

$$L[f_\chi] = C[f_\chi], \tag{B.1}$$

where L is the Liouville operator which describes the change in time of f_χ and C is the collision operator. On the cosmological background, the left hand side of eq. (B.1) is given by

$$L[f_\chi] = E\,\frac{\partial f_\chi}{\partial t} - \frac{\dot{a}}{a}\,|\vec{p}|^2\,\frac{\partial f_\chi}{\partial E}. \tag{B.2}$$

Integrating over p_χ

$$\frac{\partial}{\partial t}\int \frac{d^3p_\chi g_\chi}{(2\pi)^3}\,f_\chi - H\int \frac{d^3p_\chi g_\chi}{(2\pi)^3}\,\frac{|\vec{p}|^2}{E}\,\frac{\partial f_\chi}{\partial E} = \int \frac{d^3p_\chi g_\chi}{(2\pi)^3}\,\frac{C[f_\chi]}{E} \tag{B.3}$$

$$\dot{n}_\chi + 3Hn_\chi = \int \frac{d^3p_\chi g_\chi}{(2\pi)^3}\,\frac{C[f_\chi]}{E}, \tag{B.4}$$

having used partial integration. In general, for processes $\chi + a + b + \cdots \leftrightharpoons i + j + \ldots$,

and with f_i for the momentum distribution of the species i, we have

$$\begin{aligned}
\dot{n}_\chi + 3Hn_\chi &= \int \frac{d^3p_\chi g_\chi}{(2\pi)^3}\frac{C[f_\chi]}{E} \\
&= -\int d\pi_\chi d\pi_a d\pi_b \dots d\pi_i d\pi_j \dots \\
&\quad (2\pi)^4\delta^{(4)}(p_\chi + p_a + p_b + \dots - p_i - p_j - \dots) \\
&\times \sum_{\text{spins}} \Big[\; |\mathcal{M}|^2_{\chi+a+b+\dots\to i+j+\dots} f_\chi\, f_a\, f_b \dots (1 \pm f_i)(1 \pm f_j)\dots \\
&- \; |\mathcal{M}|^2_{i+j+\dots\to\chi+a+b+\dots} f_i\, f_j \dots (1 \pm f_\chi)(1 \pm f_a)\dots \Big],
\end{aligned} \tag{B.5}$$

with $d\pi_i := g_i d^3p_i/[(2\pi)^3 2E_i]$ and $\mathcal{M}$ for the matrix elements of the relevant process. Also, the signs $\pm$ apply accordingly for bosons or fermions. Next, one assumes that all species except χ are kept in equilibrium. For concreteness, consider processes of the form $\chi + \psi \leftrightharpoons a + b$. Then, one may write

$$\begin{aligned}
\int \frac{d^3p_\chi g_\chi}{(2\pi)^3}\frac{C[f_\chi]}{E} = -\int d\pi_\chi d\pi_\psi d\pi_a d\pi_b (2\pi)^4\delta^{(4)}(p_\chi + p_\psi - p_a - p_b) \\
\times \sum_{\text{spins}} \Big[|\mathcal{M}|^2_{\chi+\psi\to a+b}\, f_\chi\, f_\psi (1 \pm f_a)(1 \pm f_b) \\
- |\mathcal{M}|^2_{a+b\to\chi+\psi}\, f_a\, f_b (1 \pm f_\chi)(1 \pm f_\psi) \Big].
\end{aligned} \tag{B.6}$$

The following simplifying assumptions can then be made:

- χ is non-relativistic and the distribution functions of other species are small, i.e. $(1 \pm f_i) \approx 1$.

- CP or T invariance holds, such that

$$|\mathcal{M}|^2 := |\mathcal{M}|^2_{\chi+\psi\to a+b} = |\mathcal{M}|^2_{a+b\to\chi+\psi}. \tag{B.7}$$

- Since all species other than χ and ψ stay in equilibrium and the δ-function enforces energy conservation, one may substitute

$$f_a f_b = f_a^{\text{eq}} f_b^{\text{eq}} = e^{-(E_1+E_2)/T} = e^{-(E_\chi+E_\psi)/T} = f_\chi^{\text{eq}} f_\psi^{\text{eq}}. \tag{B.8}$$

- χ maintains kinetic equilibrium. Therefore,

$$\frac{f_\chi f_\psi}{n_\chi n_\psi} = \frac{f_\chi^{\text{eq}} f_\psi^{\text{eq}}}{n_\chi^{\text{eq}} n_\psi^{\text{eq}}}. \tag{B.9}$$

With these assumptions, the Boltzmann equation may be rewritten as

$$\dot{n}_\chi + 3Hn_\chi = \int \frac{d^3p_\chi g_\chi}{(2\pi)^3}\,\frac{C[f_\chi]}{E}$$

$$\begin{aligned}
&= -\int d\pi_\chi d\pi_\psi d\pi_a d\pi_b (2\pi)^4\delta^{(4)}(p_\chi + p_\psi - p_1 - p_2)\sum_{\text{spins}}|\mathcal{M}|^2\Big[f_\chi\, f_\psi - f_a\, f_b\Big]\\
&= -\int d\pi_\chi d\pi_\psi d\pi_a d\pi_b (2\pi)^4\delta^{(4)}(\dots)\sum_{\text{spins}}|\mathcal{M}|^2 f_\chi^{\text{eq}}\, f_\psi^{\text{eq}}\left(\frac{n_\chi\, n_\psi}{n_\chi^{\text{eq}}\, n_\psi^{\text{eq}}} - 1\right)\\
&= -\int d\pi_\chi d\pi_\psi d\pi_a d\pi_b (2\pi)^4\delta^{(4)}(\dots)\sum_{\text{spins}}|\mathcal{M}|^2\,\frac{f_\chi^{\text{eq}} f_\psi^{\text{eq}}}{n_\chi^{\text{eq}}\, n_\psi^{\text{eq}}}\left(n_\chi\, n_\psi - n_\chi^{\text{eq}}\, n_\psi^{\text{eq}}\right)\\
&= -\left\{\int d\pi_\chi d\pi_\psi\left[\int d\pi_a d\pi_b (2\pi)^4\delta^{(4)}(\dots)\sum_{\text{spins}}|\mathcal{M}|^2\right]\frac{f_\chi^{\text{eq}} f_\psi^{\text{eq}}}{n_\chi^{\text{eq}}\, n_\psi^{\text{eq}}}\right\}\left(n_\chi\, n_\psi - n_\chi^{\text{eq}}\, n_\psi^{\text{eq}}\right)\\
&= -\left\{\int d\pi_\chi d\pi_\psi\,[4\,F\,\sigma]\,\frac{f_\chi^{\text{eq}} f_\psi^{\text{eq}}}{n_\chi^{\text{eq}}\, n_\psi^{\text{eq}}}\right\}\left(n_\chi\, n_\psi - n_\chi^{\text{eq}}\, n_\psi^{\text{eq}}\right), \qquad \text{(B.10)}
\end{aligned}$$

where we have defined $F = [(p_\chi \cdot p_\psi)^2 - m_\chi^2 m_\psi^2]^{1/2}$. The expression in the curly braces in the last line is the thermal cross section $\langle\sigma v\rangle$. Thus, one finally arrives at the familiar expression

$$\dot{n}_\chi + 3Hn_\chi = -\langle\sigma v_{\text{mol}}\rangle\left(n_\chi\, n_\psi - n_\chi^{\text{eq}}\, n_\psi^{\text{eq}}\right). \qquad \text{(B.11)}$$

For the case where self-annihilations are the driving interactions, simply set $\psi = \bar{\chi}$.

Alternatively, one can use the thermal rate γ^{eq} instead of the thermal cross section. The former is defined as

$$\gamma^{\text{eq}}_{\chi+\psi\leftrightharpoons a+b} = \int d\pi_\chi d\pi_\psi\left[\int d\pi_a d\pi_b (2\pi)^4\delta^{(4)}(\dots)\sum_{\text{spins}}|\mathcal{M}|^2\right] f_\chi^{\text{eq}}\, f_\psi^{\text{eq}}, \qquad \text{(B.12)}$$

where the matrix elements $\mathcal{M}$ are meant as those for the process under consideration, i.e. $\chi + \psi \leftrightharpoons a + b$. In this case, the Boltzmann equation in its final form is

$$\dot{n}_\chi + 3Hn_\chi = -\gamma^{\text{eq}}_{\chi+\psi\leftrightharpoons a+b}\left(\frac{n_\chi\, n_\psi}{n_\chi^{\text{eq}}\, n_\psi^{\text{eq}}} - 1\right). \qquad \text{(B.13)}$$

We notice that if ψ also stays in thermal equilibrium, then n_ψ can be cancelled.

Disclaimer

The material presented in this dissertation is based on independent, peer-reviewed and published research performed by the author at the Max-Planck Institut für Kernphysik in Heidelberg, Germany.

Chapters 1 to 4 can be considered as a review of the topics on which the scientific contribution by the author builds upon. Said contributions are contained in Chapter 5, whereby section 5.1 is based on Ref. [1], of which the author of this dissertation is the main contributor and his supervisors are listed as coauthors. Further, Section 5.2 is based on Ref. [2], of which the author of this dissertation is the sole contributor and author.

Beyond the cited publications, the author has engaged in unpublished, exploratory studies regarding

- the running of the top-quark Yukawa coupling, with Moritz Platscher;
- new observational constraints on primordial black hole dark matter, with Cristina Benso, Oliver Scholer and Jakob Stegman;
- late production of dark matter, with Christian Döring and Stefan Vogl;
- seeded cosmological phase transitions, with Christian Döring and Stefan Vogl.

List of publications by Carlos F. Jaramillo G.

[1] Carlos Jaramillo, Manfred Lindner, and Werner Rodejohann. "Seesaw neutrino dark matter by freeze-out". In: *JCAP* 04 (2021), p. 023. DOI: 10.1088/1475-7516/2021/04/023. arXiv: 2004.12904 [hep-ph].

[2] Carlos Jaramillo. "Reviving keV sterile Neutrino Dark Matter". In: *JCAP* 10 (Oct. 2022), p. 093. DOI: 10.1088/1475-7516/2022/10/093. arXiv: 2207.11269 [hep-ph].

Acknowledgments

First and foremost, I am happy to thank my supervisor, Prof. Dr. Dr. h.c. Manfred Lindner, who welcomed me into his research group already during the final stages of my undergraduate studies and thereby paved the way for my scientific career and development. I am deeply and sincerely grateful for his unwavering support and trust throughout my doctoral studies. Under his mentorship, I enjoyed the liberty and encouragement to develop and pursue my own original ideas, which I consider a true privilege. I also thank PD Dr. Werner Rodejohann, whose guidance and expertise were of invaluable importance, particularly during the early stages of my work.

Working at the Max-Planck-Institute for Nuclear Physics has been a wonderful experience, especially because of the proximity and close contact with so many talented and inspiring scientists, young and senior, who were always happy to engage in discussions and share their knowledge. I also thank Anja Berneiser and Britta Schwarz, who with their hard work behind the scenes enable the smooth functioning of the group and contribute greatly to its success.

I am thankful to Prof. Dr. Tilman Plehn, for agreeing to take the time to read and review this thesis as well as to the members of my doctoral committee Prof. Dr. Matthias Bartelmann and PD Dr. Teresa Marrodán Undagoitia.

To my friends and colleagues, who not only supported me by proof-reading my work, but who have been with me through ups and downs, I am most grateful: Andrei Angelescu, Cristina Benso, Salvador Centelles Chulia, Frederik Depta, Christian Döring, Johannes Herms, Sudip Jana, Jonas Rezacek, Thomas Rink, Manibrata Sen, Andreas Trautner and many more.

To my fellow PhD students and to my friends who are no longer members of the insitute, particularly Ingolf Bischer, Thomas Hugle and Moritz Platscher: Thank you for being part of this fabulous journey.

To my mom, brother and my late dad: thank you for everything, I love you.

And finally, there is someone who I can no longer thank, but who will always be in my heart... *Julia*. You walked by my side since my very first semester in Karlsruhe. If I achieved anything in the last 12 years, it has been thanks to you, thanks to your support and your love. I will forever miss you.

List of Abbreviations

BAU baryon asymmetry of the Universe

BAO baryon acoustic oscillations

BSM beyond the Standard Model

BBN big bang nucleosynthesis

BH black hole

CMB cosmic microwave background

CνB cosmic neutrino background

CC charged current

DM dark matter

DOF degree of freedom

dSph dwarf spheroidal galaxy

EFT effective field theory

EWSB electroweak symmetry breaking

EW electroweak

EWPT electroweak phase transition

FN Froggatt-Nielsen

GW gravitational wavesx

GUT grand unified theory

LHC large hadron collider

LH left-handed

MACHO Massive Compact Halo Object

IGM intergalactic medium

NC neutral current

νMSM neutrino Minimal Standard Model

QFT quantum field theory

QSO quasi-stelar objects

PBH primordial black holes

PT phase transition

RH right-handed

SM Standar Model of particle physics

SSB spontaneous symmetry breaking

SDSS Sloan digital sky survey

SUSY supersymmetry

ULDM ultra light dark matter

UHECR ultra high energy cosmic rays

vev vacuum expectation value

WIMP weakly interacting massive particle

Bibliography

[1] Serguei Chatrchyan et al. "Observation of a New Boson at a Mass of 125 GeV with the CMS Experiment at the LHC". In: *Phys. Lett. B* 716 (2012), pp. 30–61. DOI: 10.1016/j.physletb.2012.08.021. arXiv: 1207.7235 [hep-ex].

[2] Georges Aad et al. "Observation of a new particle in the search for the Standard Model Higgs boson with the ATLAS detector at the LHC". In: *Phys. Lett. B* 716 (2012), pp. 1–29. DOI: 10.1016/j.physletb.2012.08.020. arXiv: 1207.7214 [hep-ex].

[3] Oliver Fischer et al. "Unveiling hidden physics at the LHC". In: *Eur. Phys. J. C* 82.8 (2022), p. 665. DOI: 10.1140/epjc/s10052-022-10541-4. arXiv: 2109.06065 [hep-ph].

[4] S. Bilenky. "Neutrino oscillations: From a historical perspective to the present status". In: *Nucl. Phys. B* 908 (2016), pp. 2–13. DOI: 10.1016/j.nuclphysb.2016.01.025. arXiv: 1602.00170 [hep-ph].

[5] NobelPrize.org - Nobel Prize Outreach AB 2023. *The Nobel Prize in Physics 2015*. June 2023. URL: https://www.nobelprize.org/prizes/physics/2015/summary/.

[6] F. Zwicky. "Die Rotverschiebung von extragalaktischen Nebeln". In: *Helvetica Physica Acta* 6 (1933), pp. 110–127.

[7] Gianfranco Bertone and Dan Hooper. "History of dark matter". In: *Rev. Mod. Phys.* 90.4 (2018), p. 045002. DOI: 10.1103/RevModPhys.90.045002. arXiv: 1605.04909 [astro-ph.CO].

[8] Matthew D. Schwartz. *Quantum Field Theory and the Standard Model*. Cambridge University Press, Mar. 2014. ISBN: 978-1-107-03473-0, 978-1-107-03473-0.

[9] Nicola Cabibbo. "Unitary Symmetry and Leptonic Decays". In: *Phys. Rev. Lett.* 10 (1963), pp. 531–533. DOI: 10.1103/PhysRevLett.10.531.

[10] Makoto Kobayashi and Toshihide Maskawa. "CP Violation in the Renormalizable Theory of Weak Interaction". In: *Prog. Theor. Phys.* 49 (1973), pp. 652–657. DOI: 10.1143/PTP.49.652.

[11] P.A. Zyla et al. “Review of Particle Physics”. In: *PTEP* 2020.8 (2020). and 2021 update, p. 083C01. DOI: 10.1093/ptep/ptaa104.

[12] J. J. Gomez-Cadenas et al. “The Search for neutrinoless double beta decay”. In: *Riv. Nuovo Cim.* 35.2 (2012), pp. 29–98. DOI: 10.1393/ncr/i2012-10074-9. arXiv: 1109.5515 [hep-ex].

[13] Y. Nir. “Flavour Physics and CP Violation”. In: *7th CERNLatin-American School of High-Energy Physics*. 2015, pp. 123–156. DOI: 10.5170/CERN-2015-001.123. arXiv: 1605.00433 [hep-ph].

[14] Stuart Raby. “Introduction to theories of fermion masses”. In: Jan. 1995. arXiv: hep-ph/9501349.

[15] Zurab Berezhiani. “Fermion masses and mixing in SUSY GUT”. In: *ICTP Summer School in High-energy Physics and Cosmology*. Dec. 1995. arXiv: hep-ph/9602325.

[16] Graham G. Ross. “Models of fermion masses”. In: *Theoretical Advanced Study Institute in Elementary Particle Physics (TASI 2000): Flavor Physics for the Millennium*. June 2000, pp. 775–824.

[17] Prateek Agrawal and Kiel Howe. “A Flavorful Factoring of the Strong CP Problem”. In: *JHEP* 12 (2018), p. 035. DOI: 10.1007/JHEP12(2018)035. arXiv: 1712.05803 [hep-ph].

[18] David B. Kaplan. “Flavor at SSC energies: A New mechanism for dynamically generated fermion masses”. In: *Nucl. Phys. B* 365 (1991), pp. 259–278. DOI: 10.1016/S0550-3213(05)80021-5.

[19] Stephan J. Huber and Qaisar Shafi. “Fermion masses, mixings and proton decay in a Randall-Sundrum model”. In: *Phys. Lett. B* 498 (2001), pp. 256–262. DOI: 10.1016/S0370-2693(00)01399-X. arXiv: hep-ph/0010195.

[20] C. D. Froggatt and Holger Bech Nielsen. “Hierarchy of Quark Masses, Cabibbo Angles and CP Violation”. In: *Nucl. Phys.* B147 (1979), pp. 277–298.

[21] Lorenzo Calibbi et al. “The Messenger Sector of SUSY Flavour Models and Radiative Breaking of Flavour Universality”. In: *JHEP* 06 (2012), p. 018. DOI: 10.1007/JHEP06(2012)018. arXiv: 1203.1489 [hep-ph].

[22] K. S. Babu. “TASI Lectures on Flavor Physics”. In: *Theoretical Advanced Study Institute in Elementary Particle Physics: The Dawn of the LHC Era*. 2010, pp. 49–123. DOI: 10.1142/9789812838360_0002. arXiv: 0910.2948 [hep-ph].

[23] Miriam Leurer, Yosef Nir, and Nathan Seiberg. “Mass matrix models”. In: *Nucl. Phys. B* 398 (1993), pp. 319–342. DOI: 10.1016/0550-3213(93)90112-3. arXiv: hep-ph/9212278.

[24] Martin Bauer, Torben Schell, and Tilman Plehn. “Hunting the Flavon”. In: *Phys. Rev. D* 94.5 (2016), p. 056003. DOI: 10.1103/PhysRevD.94.056003. arXiv: 1603.06950 [hep-ph].

[25] G. K. Leontaris and G. G. Ross. "Yukawa couplings and fermion mass structure in F-theory GUTs". In: *JHEP* 02 (2011), p. 108. DOI: 10.1007/JHEP02(2011)108. arXiv: 1009.6000 [hep-th].

[26] Emilian Dudas and Eran Palti. "Froggatt-Nielsen models from E(8) in F-theory GUTs". In: *JHEP* 01 (2010), p. 127. DOI: 10.1007/JHEP01(2010)127. arXiv: 0912.0853 [hep-th].

[27] Wolfgang Pauli. *Aufsaetze und Vortraege ueber Physik und Erkenntnistheorie*. Vieweg Teubner Verlag, 1961. DOI: 10.1007/978-3-663-07092-4.

[28] C. L. Cowan et al. "Detection of the Free Neutrino: a Confirmation". In: *Science* 124.3212 (July 1956), pp. 103–104. DOI: 10.1126/science.124.3212.103.

[29] Edward W. Kolb and Michael S. Turner. "The Early Universe". In: *Front. Phys.* 69 (1990), pp. 1–547.

[30] Frank Close. *Particle Physics: A Very Short Introduction*. Oxford University Press, May 2004. ISBN: 9780192804341. DOI: 10.1093/actrade/9780192804341.001.0001. URL: https://doi.org/10.1093/actrade/9780192804341.001.0001.

[31] Y. Fukuda et al. "Evidence for Oscillation of Atmospheric Neutrinos". In: *Physical Review Letters* 81.8 (Aug. 1998), pp. 1562–1567. DOI: 10.1103/physrevlett.81.1562. URL: https://doi.org/10.1103%2Fphysrevlett.81.1562.

[32] SNO Collaboration. "Direct Evidence for Neutrino Flavor Transformation from Neutral-Current Interactions in the Sudbury Neutrino Observatory". In: *Phys. Rev. Lett. 89: 011301, 2002* (Apr. 21, 2002). DOI: 10.1103/PhysRevLett.89.011301. arXiv: http://arxiv.org/abs/nucl-ex/0204008v2 [nucl-ex].

[33] B. Pontecorvo. "Mesonium and anti-mesonium". In: *Sov. Phys. JETP* 6 (1957), p. 429.

[34] B. Pontecorvo. "Inverse beta processes and nonconservation of lepton charge". In: *Zh. Eksp. Teor. Fiz.* 34 (1957), p. 247.

[35] Ziro Maki, Masami Nakagawa, and Shoichi Sakata. "Remarks on the unified model of elementary particles". In: *Prog. Theor. Phys.* 28 (1962), pp. 870–880. DOI: 10.1143/PTP.28.870.

[36] B. Pontecorvo. "Neutrino Experiments and the Problem of Conservation of Leptonic Charge". In: *Zh. Eksp. Teor. Fiz.* 53 (1967), pp. 1717–1725.

[37] Kai Zuber. *Neutrino Physics, Second Edition*. Taylor and Francis, Aug. 2011. DOI: 10.1201/b11065.

[38] P. F. de Salas et al. "2020 global reassessment of the neutrino oscillation picture". In: *JHEP* 02 (2021), p. 071. DOI: 10.1007/JHEP02(2021)071. arXiv: 2006.11237 [hep-ph].

[39] Ivan Esteban et al. "The fate of hints: updated global analysis of three-flavor neutrino oscillations". In: *JHEP* 09 (2020), p. 178. DOI: 10.1007/JHEP09(2020)178. arXiv: 2007.14792 [hep-ph].

[40] M. Aker et al. "Direct neutrino-mass measurement with sub-electronvolt sensitivity". In: *Nature Phys.* 18.2 (2022), pp. 160–166. DOI: 10.1038/s41567-021-01463-1. arXiv: 2105.08533 [hep-ex].

[41] Evgeny Kh. Akhmedov and Alexei Yu. Smirnov. "Paradoxes of neutrino oscillations". In: *Phys. Atom. Nucl.* 72 (2009), pp. 1363–1381. DOI: 10.1134/S1063778809080122. arXiv: 0905.1903 [hep-ph].

[42] Evgeny Kh. Akhmedov and Joachim Kopp. "Neutrino Oscillations: Quantum Mechanics vs. Quantum Field Theory". In: *JHEP* 04 (2010). [Erratum: JHEP 10, 052 (2013)], p. 008. DOI: 10.1007/JHEP04(2010)008. arXiv: 1001.4815 [hep-ph].

[43] Evgeny Akhmedov. "Quantum mechanics aspects and subtleties of neutrino oscillations". In: *International Conference on History of the Neutrino: 1930-2018*. Jan. 2019. arXiv: 1901.05232 [hep-ph].

[44] L. Wolfenstein. "Neutrino Oscillations in Matter". In: *Phys. Rev.* D17 (1978). [,294(1977)], pp. 2369–2374. DOI: 10.1103/PhysRevD.17.2369.

[45] S. P. Mikheyev and A. Yu. Smirnov. "Resonance Amplification of Oscillations in Matter and Spectroscopy of Solar Neutrinos". In: *Sov. J. Nucl. Phys.* 42 (1985). [,305(1986)], pp. 913–917.

[46] E. Kh. Akhmedov. "Neutrino physics". In: (Jan. 25, 2000). arXiv: http://arxiv.org/abs/hep-ph/0001264v2 [hep-ph].

[47] A. Yu. Smirnov. "The MSW effect and matter effects in neutrino oscillations". In: *Phys. Scripta T* 121 (2005). Ed. by L. Bergström et al., pp. 57–64. DOI: 10.1088/0031-8949/2005/T121/008. arXiv: hep-ph/0412391.

[48] Shinya Kanemura and Kei Yagyu. "Radiative corrections to electroweak parameters in the Higgs triplet model and implication with the recent Higgs boson searches". In: *Phys. Rev. D* 85 (2012), p. 115009. DOI: 10.1103/PhysRevD.85.115009. arXiv: 1201.6287 [hep-ph].

[49] Sanjoy Mandal et al. "Toward deconstructing the simplest seesaw mechanism". In: *Phys. Rev. D* 105.9 (2022), p. 095020. DOI: 10.1103/PhysRevD.105.095020. arXiv: 2203.06362 [hep-ph].

[50] Steven Weinberg. "Baryon and Lepton Nonconserving Processes". In: *Phys. Rev. Lett.* 43 (1979), pp. 1566–1570. DOI: 10.1103/PhysRevLett.43.1566.

[51] Peter Minkowski. "$\mu \to e\gamma$ at a Rate of One Out of 10^9 Muon Decays?" In: *Phys. Lett.* B67 (1977), pp. 421–428.

[52] Rabindra N. Mohapatra and Goran Senjanovic. "Neutrino Masses and Mixings in Gauge Models with Spontaneous Parity Violation". In: *Phys. Rev.* D23 (1981), p. 165.

[53] Tsutomu Yanagida. "Horizontal Symmetry and Masses of Neutrinos". In: *Prog. Theor. Phys.* 64 (1980), p. 1103.

[54] Murray Gell-Mann, Pierre Ramond, and Richard Slansky. "Complex Spinors and Unified Theories". In: *Conf. Proc.* C790927 (1979), pp. 315–321. arXiv: 1306.4669 [hep-th].

[55] Carlos Jaramillo, Manfred Lindner, and Werner Rodejohann. "Seesaw neutrino dark matter by freeze-out". In: *JCAP* 04 (2021), p. 023. DOI: 10.1088/1475-7516/2021/04/023. arXiv: 2004.12904 [hep-ph].

[56] M. Magg and C. Wetterich. "Neutrino Mass Problem and Gauge Hierarchy". In: *Phys. Lett. B* 94 (1980), pp. 61–64. DOI: 10.1016/0370-2693(80)90825-4.

[57] J. Schechter and J. W. F. Valle. "Neutrino Masses in SU(2) x U(1) Theories". In: *Phys. Rev. D* 22 (1980), p. 2227. DOI: 10.1103/PhysRevD.22.2227.

[58] C. Wetterich. "Neutrino Masses and the Scale of B-L Violation". In: *Nucl. Phys. B* 187 (1981), pp. 343–375. DOI: 10.1016/0550-3213(81)90279-0.

[59] J. Bernabeu et al. "Lepton Flavor Nonconservation at High-Energies in a Superstring Inspired Standard Model". In: *Phys. Lett. B* 187 (1987), pp. 303–308. DOI: 10.1016/0370-2693(87)91100-2.

[60] Robert Foot et al. "Seesaw Neutrino Masses Induced by a Triplet of Leptons". In: *Z. Phys. C* 44 (1989), p. 441. DOI: 10.1007/BF01415558.

[61] Ernest Ma. "Verifiable radiative seesaw mechanism of neutrino mass and dark matter". In: *Phys. Rev. D* 73 (2006), p. 077301. DOI: 10.1103/PhysRevD.73.077301. arXiv: hep-ph/0601225.

[62] K. S. Babu. "Model of 'Calculable' Majorana Neutrino Masses". In: *Phys. Lett. B* 203 (1988), pp. 132–136. DOI: 10.1016/0370-2693(88)91584-5.

[63] A. Zee. "Quantum Numbers of Majorana Neutrino Masses". In: *Nucl. Phys. B* 264 (1986), pp. 99–110. DOI: 10.1016/0550-3213(86)90475-X.

[64] A. Zee. "Charged Scalar Field and Quantum Number Violations". In: *Phys. Lett. B* 161 (1985), pp. 141–145. DOI: 10.1016/0370-2693(85)90625-2.

[65] Yi Cai et al. "From the trees to the forest: a review of radiative neutrino mass models". In: *Front. in Phys.* 5 (2017), p. 63. DOI: 10.3389/fphy.2017.00063. arXiv: 1706.08524 [hep-ph].

[66] F. Zwicky. "On the Masses of Nebulae and of Clusters of Nebulae". In: *Astrophys. J.* 86 (1937), pp. 217–246. DOI: 10.1086/143864.

[67] Sinclair Smith. "The Mass of the Virgo Cluster". In: *Astrophys. J.* 83 (1936), pp. 23–30. DOI: 10.1086/143697.

[68] M. Schwarzschild. "Mass distribution and mass-luminosity ratio in galaxies". In: *The Astrophysical Journal* 59 (Sept. 1954), p. 273. DOI: 10.1086/107013.

[69] Ray G. Carlberg, H. K. C. Yee, and E. Ellingson. "The Average mass and light profiles of galaxy clusters". In: *Astrophys. J.* 478 (1997), p. 462. DOI: 10.1086/303805. arXiv: astro-ph/9512087.

[70] Matts Roos. "Dark Matter: The evidence from astronomy, astrophysics and cosmology". In: (Jan. 2010). arXiv: 1001.0316 [astro-ph.CO].

[71] Vera C. Rubin, W. Kent Ford Jr., and Norbert Thonnard. "Extended rotation curves of high-luminosity spiral galaxies. IV. Systematic dynamical properties, Sa through Sc". In: *Astrophys. J. Lett.* 225 (1978), pp. L107–L111. DOI: 10.1086/182804.

[72] Vera C. Rubin and W. Kent Ford Jr. "Rotation of the Andromeda Nebula from a Spectroscopic Survey of Emission Regions". In: *Astrophys. J.* 159 (1970), pp. 379–403. DOI: 10.1086/150317.

[73] Stefano Profumo. *An Introduction to Particle Dark Matter*. WORLD SCIENTIFIC (EUROPE), Nov. 2015. DOI: 10.1142/q0001.

[74] K. C. Freeman. "On the disks of spiral and SO Galaxies". In: *Astrophys. J.* 160 (1970), p. 811. DOI: 10.1086/150474.

[75] Masamune Oguri et al. "The Sloan Digital Sky Survey Quasar Lens Search. 3. Constraints on Dark Energy from the Third Data Release Quasar Lens Catalog". In: *Astron. J.* 135 (2008), pp. 512–519. DOI: 10.1088/0004-6256/135/2/512. arXiv: 0708.0825 [astro-ph].

[76] Richard Massey, Thomas Kitching, and Johan Richard. "The dark matter of gravitational lensing". In: *Rept. Prog. Phys.* 73 (2010), p. 086901. DOI: 10.1088/0034-4885/73/8/086901. arXiv: 1001.1739 [astro-ph.CO].

[77] David J. Bacon, Alexandre R. Refregier, and Richard S. Ellis. "Detection of weak gravitational lensing by large-scale structure". In: *Mon. Not. Roy. Astron. Soc.* 318 (2000), p. 625. DOI: 10.1046/j.1365-8711.2000.03851.x. arXiv: astro-ph/0003008.

[78] Nick Kaiser, Gillian Wilson, and Gerard A. Luppino. "Large scale cosmic shear measurements". In: (Mar. 2000). arXiv: astro-ph/0003338.

[79] Ludovic van Waerbeke et al. "Detection of correlated galaxy ellipticities on CFHT data: First evidence for gravitational lensing by large scale structures". In: *Astron. Astrophys.* 358 (2000), pp. 30–44. arXiv: astro-ph/0002500.

[80] David M. Wittman et al. "Detection of weak gravitational lensing distortions of distant galaxies by cosmic dark matter at large scales". In: *Nature* 405 (2000), pp. 143–149. DOI: 10.1038/35012001. arXiv: astro-ph/0003014.

[81] Richard Massey et al. "Dark matter maps reveal cosmic scaffolding". In: *Nature* 445 (2007), p. 286. DOI: 10.1038/nature05497. arXiv: astro-ph/0701594.

[82] Douglas Clowe, Anthony Gonzalez, and Maxim Markevitch. "Weak lensing mass reconstruction of the interacting cluster 1E0657-558: Direct evidence for the existence of dark matter". In: *Astrophys. J.* 604 (2004), pp. 596–603. DOI: 10.1086/381970. arXiv: astro-ph/0312273.

[83] M. Markevitch et al. "A Textbook example of a bow shock in the merging galaxy cluster 1E0657-56". In: *Astrophys. J. Lett.* 567 (2002), p. L27. DOI: 10.1086/339619. arXiv: astro-ph/0110468.

[84] Douglas Clowe et al. "A direct empirical proof of the existence of dark matter". In: *Astrophys. J.* 648 (2006), pp. L109–L113. DOI: 10.1086/508162. arXiv: astro-ph/0608407 [astro-ph].

[85] Scott W. Randall et al. "Constraints on the Self-Interaction Cross-Section of Dark Matter from Numerical Simulations of the Merging Galaxy Cluster 1E 0657-56". In: *Astrophys. J.* 679 (2008), pp. 1173–1180. DOI: 10.1086/587859. arXiv: 0704.0261 [astro-ph].

[86] Greg Madejski. "Recent and future observations in the x-ray and gamma-ray bands: chandra, suzaku, glast, and nustar". In: *AIP Conf. Proc.* 801.1 (2005). Ed. by Tomasz Bulik, Bronislaw Rudak, and Grzegorz Madejski, pp. 21–30. DOI: 10.1063/1.2141828. arXiv: astro-ph/0512012.

[87] Jounghun Lee and Eiichiro Komatsu. "Bullet Cluster: A Challenge to LCDM Cosmology". In: *Astrophys. J.* 718 (2010), pp. 60–65. DOI: 10.1088/0004-637X/718/1/60. arXiv: 1003.0939 [astro-ph.CO].

[88] Robert Thompson, Romeel Davé, and Kentaro Nagamine. "The rise and fall of a challenger: the Bullet Cluster in Λ cold dark matter simulations". In: *Mon. Not. Roy. Astron. Soc.* 452.3 (2015), pp. 3030–3037. DOI: 10.1093/mnras/stv1433. arXiv: 1410.7438 [astro-ph.CO].

[89] A. Mahdavi et al. "A Dark Core in Abell 520". In: *Astrophys. J.* 668 (2007), pp. 806–814. DOI: 10.1086/521383. arXiv: 0706.3048 [astro-ph].

[90] Marusa Bradac et al. "Revealing the properties of dark matter in the merging cluster MACSJ0025.4-1222". In: *Astrophys. J.* 687 (2008), p. 959. DOI: 10.1086/591246. arXiv: 0806.2320 [astro-ph].

[91] R. Herman R. A. Alpher. "Evolution of the Universe". In: *Nature* 162 (Nov. 1948), p. 774.

[92] G. Gamow. "The Evolution of the Universe". In: *Nature* 162 (Oct. 1948), p. 680.

[93] Oliver F. Piattella. *Lecture Notes in Cosmology*. UNITEXT for Physics. Cham: Springer, 2018. DOI: 10.1007/978-3-319-95570-4. arXiv: 1803.00070 [astro-ph.CO].

[94] A. Penzias and R. Wilson. "A Measurement of excess antenna temperature at 4080 Mc/s". In: *Astrophysical Journal* 142 (May 1965), p. 419.

[95] P. Roll D. Wilkinson R. Dicke P. Peebles. "Cosmic Black-Body Radiation". In: *Astrophysical Journal* 142 (May 1965), p. 414.

[96] N. Aghanim et al. “Planck 2018 results. VI. Cosmological parameters”. In: *Astron. Astrophys.* 641 (2020), A6. DOI: 10.1051/0004-6361/201833910. arXiv: 1807.06209 [astro-ph.CO].

[97] Scott Dodelson. *Modern cosmology*. San Diego, CA: Academic Press, 2003. URL: https://cds.cern.ch/record/1282338.

[98] Wayne Hu. “Lecture Notes on CMB Theory: From Nucleosynthesis to Recombination”. In: (Feb. 2008). arXiv: 0802.3688 [astro-ph].

[99] Will J. Percival et al. “The shape of the SDSS DR5 galaxy power spectrum”. In: *Astrophys. J.* 657 (2007), pp. 645–663. DOI: 10.1086/510615. arXiv: astro-ph/0608636 [astro-ph].

[100] Scott Dodelson. “The Real Problem with MOND”. In: *Int. J. Mod. Phys.* D20 (2011), pp. 2749–2753. DOI: 10.1142/S0218271811020561. arXiv: 1112.1320 [astro-ph.CO].

[101] Viatcheslav F. Mukhanov, H. A. Feldman, and Robert H. Brandenberger. “Theory of cosmological perturbations. Part 1. Classical perturbations. Part 2. Quantum theory of perturbations. Part 3. Extensions”. In: *Phys. Rept.* 215 (1992), pp. 203–333. DOI: 10.1016/0370-1573(92)90044-Z.

[102] Volker Springel, Carlos S. Frenk, and Simon D. M. White. “The large-scale structure of the Universe”. In: *Nature* 440 (Apr. 2006), 1137 EP -. URL: http://dx.doi.org/10.1038/nature04805.

[103] R. E. Angulo et al. “Scaling relations for galaxy clusters in the Millennium-XXL simulation”. In: *Mon. Not. Roy. Astron. Soc.* 426 (2012), p. 2046. DOI: 10.1111/j.1365-2966.2012.21830.x. arXiv: 1203.3216 [astro-ph.CO].

[104] Volker Springel et al. “The Aquarius Project: the subhalos of galactic halos”. In: *Mon. Not. Roy. Astron. Soc.* 391 (2008), pp. 1685–1711. DOI: 10.1111/j.1365-2966.2008.14066.x. arXiv: 0809.0898 [astro-ph].

[105] Mark Vogelsberger et al. “Cosmological Simulations of Galaxy Formation”. In: *Nature Rev. Phys.* 2.1 (2020), pp. 42–66. DOI: 10.1038/s42254-019-0127-2. arXiv: 1909.07976 [astro-ph.GA].

[106] Daniel J. Eisenstein et al. “Detection of the Baryon Acoustic Peak in the Large-Scale Correlation Function of SDSS Luminous Red Galaxies”. In: *Astrophys. J.* 633 (2005), pp. 560–574. DOI: 10.1086/466512. arXiv: astro-ph/0501171.

[107] Shadab Alam et al. “The clustering of galaxies in the completed SDSS-III Baryon Oscillation Spectroscopic Survey: cosmological analysis of the DR12 galaxy sample”. In: *Mon. Not. Roy. Astron. Soc.* 470.3 (2017), pp. 2617–2652. DOI: 10.1093/mnras/stx721. arXiv: 1607.03155 [astro-ph.CO].

[108] C. Alcock et al. “The MACHO project: Microlensing results from 5.7 years of LMC observations”. In: *Astrophys. J.* 542 (2000), pp. 281–307. DOI: 10.1086/309512. arXiv: astro-ph/0001272.

[109] Bernard Carr, Florian Kuhnel, and Marit Sandstad. "Primordial Black Holes as Dark Matter". In: *Phys. Rev. D* 94.8 (2016), p. 083504. DOI: 10.1103/PhysRevD.94.083504. arXiv: 1607.06077 [astro-ph.CO].

[110] B. P. Abbott et al. "Observation of Gravitational Waves from a Binary Black Hole Merger". In: *Phys. Rev. Lett.* 116.6 (2016), p. 061102. DOI: 10.1103/PhysRevLett.116.061102. arXiv: 1602.03837 [gr-qc].

[111] Bernard Carr et al. "Constraints on primordial black holes". In: *Rept. Prog. Phys.* 84.11 (2021), p. 116902. DOI: 10.1088/1361-6633/ac1e31. arXiv: 2002.12778 [astro-ph.CO].

[112] M. Milgrom. "A Modification of the Newtonian dynamics as a possible alternative to the hidden mass hypothesis". In: *Astrophys. J.* 270 (1983), pp. 365–370. DOI: 10.1086/161130.

[113] Kris Pardo and David N. Spergel. "What is the price of abandoning dark matter? Cosmological constraints on alternative gravity theories". In: *Phys. Rev. Lett.* 125.21 (2020), p. 211101. DOI: 10.1103/PhysRevLett.125.211101. arXiv: 2007.00555 [astro-ph.CO].

[114] Gianfranco Bertone and Tim Tait M. P. "A new era in the search for dark matter". In: *Nature* 562.7725 (2018), pp. 51–56. DOI: 10.1038/s41586-018-0542-z. arXiv: 1810.01668 [astro-ph.CO].

[115] Wayne Hu, Rennan Barkana, and Andrei Gruzinov. "Cold and fuzzy dark matter". In: *Phys. Rev. Lett.* 85 (2000), pp. 1158–1161. DOI: 10.1103/PhysRevLett.85.1158. arXiv: astro-ph/0003365.

[116] J. Silk et al. *Particle Dark Matter: Observations, Models and Searches*. Ed. by Gianfranco Bertone. Cambridge: Cambridge Univ. Press, 2010. ISBN: 9781107653924. DOI: 10.1017/CBO9780511770739. URL: http://www.cambridge.org/uk/catalogue/catalogue.asp?isbn=9780521763684.

[117] Elisa G. M. Ferreira. "Ultra-light dark matter". In: *Astron. Astrophys. Rev.* 29.1 (2021), p. 7. DOI: 10.1007/s00159-021-00135-6. arXiv: 2005.03254 [astro-ph.CO].

[118] L. Arturo Ureña-López. "Brief Review on Scalar Field Dark Matter Models". In: *Front. Astron. Space Sci.* 6 (2019), p. 47. DOI: 10.3389/fspas.2019.00047.

[119] Frank Wilczek. "Problem of Strong P and T Invariance in the Presence of Instantons". In: *Phys. Rev. Lett.* 40 (1978), pp. 279–282. DOI: 10.1103/PhysRevLett.40.279.

[120] C. A. Baker et al. "An Improved experimental limit on the electric dipole moment of the neutron". In: *Phys. Rev. Lett.* 97 (2006), p. 131801. DOI: 10.1103/PhysRevLett.97.131801. arXiv: hep-ex/0602020.

[121] R. D. Peccei and Helen R. Quinn. "Constraints Imposed by CP Conservation in the Presence of Instantons". In: *Phys. Rev. D* 16 (1977), pp. 1791–1797. DOI: 10.1103/PhysRevD.16.1791.

[122] R. D. Peccei and Helen R. Quinn. "CP Conservation in the Presence of Instantons". In: *Phys. Rev. Lett.* 38 (1977), pp. 1440–1443. DOI: 10.1103/PhysRevLett.38.1440.

[123] Steven Weinberg. "A New Light Boson?" In: *Phys. Rev. Lett.* 40 (1978), pp. 223–226. DOI: 10.1103/PhysRevLett.40.223.

[124] John Preskill, Mark B. Wise, and Frank Wilczek. "Cosmology of the Invisible Axion". In: *Phys. Lett. B* 120 (1983). Ed. by M. A. Srednicki, pp. 127–132. DOI: 10.1016/0370-2693(83)90637-8.

[125] David J. E. Marsh. "Axion Cosmology". In: *Phys. Rept.* 643 (2016), pp. 1–79. DOI: 10.1016/j.physrep.2016.06.005. arXiv: 1510.07633 [astro-ph.CO].

[126] S. S. Gershtein and Ya. B. Zeldovich. "Rest Mass of Muonic Neutrino and Cosmology". In: *JETP Lett.* 4 (1966). Ed. by M. A. Srednicki, pp. 120–122.

[127] R. Cowsik and J. McClelland. "An Upper Limit on the Neutrino Rest Mass". In: *Phys. Rev. Lett.* 29 (1972), pp. 669–670. DOI: 10.1103/PhysRevLett.29.669.

[128] A. S. Szalay and G. Marx. "Neutrino rest mass from cosmology". In: *Astron. Astrophys.* 49 (1976), pp. 437–441.

[129] Benjamin W. Lee and Steven Weinberg. "Cosmological Lower Bound on Heavy Neutrino Masses". In: *Phys. Rev. Lett.* 39 (1977). [,183(1977)], pp. 165–168. DOI: 10.1103/PhysRevLett.39.165.

[130] Simon D. M. White, C. S. Frenk, and M. Davis. "Clustering in a Neutrino Dominated Universe". In: *Astrophys. J. Lett.* 274 (1983). Ed. by M. A. Srednicki, pp. L1–L5. DOI: 10.1086/161425.

[131] M. Acciarri et al. "Determination of the number of light neutrino species from single photon production at LEP". In: *Phys. Lett. B* 431 (1998), pp. 199–208. DOI: 10.1016/S0370-2693(98)00519-X.

[132] Giorgio Arcadi et al. "The waning of the WIMP? A review of models, searches, and constraints". In: *Eur. Phys. J. C* 78.3 (2018), p. 203. DOI: 10.1140/epjc/s10052-018-5662-y. arXiv: 1703.07364 [hep-ph].

[133] J. Aalbers et al. "A search for new physics in low-energy electron recoils from the first LZ exposure". In: (July 2023). arXiv: 2307.15753 [hep-ex].

[134] J. Aalbers et al. "First Dark Matter Search Results from the LUX-ZEPLIN (LZ) Experiment". In: *Phys. Rev. Lett.* 131.4 (2023), p. 041002. DOI: 10.1103/PhysRevLett.131.041002. arXiv: 2207.03764 [hep-ex].

[135] E. Aprile et al. "First Dark Matter Search with Nuclear Recoils from the XENONnT Experiment". In: *Phys. Rev. Lett.* 131.4 (2023), p. 041003. DOI: 10.1103/PhysRevLett.131.041003. arXiv: 2303.14729 [hep-ex].

[136] E. Aprile et al. "Search for New Physics in Electronic Recoil Data from XENONnT". In: *Phys. Rev. Lett.* 129.16 (2022), p. 161805. DOI: 10.1103/PhysRevLett.129.161805. arXiv: 2207.11330 [hep-ex].

[137] Edward W. Kolb, Daniel J. H. Chung, and Antonio Riotto. "WIMPzillas!" In: *AIP Conf. Proc.* 484.1 (1999). Ed. by H. Falomir, R. E. Gamboa Saravi, and F. A. Schaposnik, pp. 91–105. DOI: 10.1063/1.59655. arXiv: hep-ph/9810361.

[138] Kim Griest and Marc Kamionkowski. "Unitarity Limits on the Mass and Radius of Dark Matter Particles". In: *Phys. Rev. Lett.* 64 (1990), p. 615. DOI: 10.1103/PhysRevLett.64.615.

[139] V. Berezinsky, M. Kachelriess, and A. Vilenkin. "Ultrahigh-energy cosmic rays without GZK cutoff". In: *Phys. Rev. Lett.* 79 (1997), pp. 4302–4305. DOI: 10.1103/PhysRevLett.79.4302. arXiv: astro-ph/9708217.

[140] Lev A. Kofman. "The Origin of matter in the universe: Reheating after inflation". In: May 1996. arXiv: astro-ph/9605155.

[141] Edward W. Kolb, Antonio Riotto, and Igor I. Tkachev. "GUT baryogenesis after preheating: Numerical study of the production and decay of X bosons". In: *Phys. Lett. B* 423 (1998), pp. 348–354. DOI: 10.1016/S0370-2693(98)00134-8. arXiv: hep-ph/9801306.

[142] Daniel J. H. Chung, Edward W. Kolb, and Antonio Riotto. "Superheavy dark matter". In: *Phys. Rev. D* 59 (1998), p. 023501. DOI: 10.1103/PhysRevD.59.023501. arXiv: hep-ph/9802238.

[143] George F. Chapline. "Cosmological effects of primordial black holes". In: *Nature* 253.5489 (1975), pp. 251–252. DOI: 10.1038/253251a0.

[144] Suvodip Mukherjee and Joseph Silk. "Can we distinguish astrophysical from primordial black holes via the stochastic gravitational wave background?" In: *Mon. Not. Roy. Astron. Soc.* 506.3 (2021), pp. 3977–3985. DOI: 10.1093/mnras/stab1932. arXiv: 2105.11139 [gr-qc].

[145] Paolo Gondolo and Graciela Gelmini. "Cosmic abundances of stable particles: Improved analysis". In: *Nucl. Phys.* B360 (1991), pp. 145–179. DOI: 10.1016/0550-3213(91)90438-4.

[146] Lars Husdal. "On Effective Degrees of Freedom in the Early Universe". In: *Galaxies* 4.4 (2016), p. 78. DOI: 10.3390/galaxies4040078. arXiv: 1609.04979 [astro-ph.CO].

[147] Gary Steigman, Basudeb Dasgupta, and John F. Beacom. "Precise relic WIMP abundance and its impact on searches for dark matter annihilation". In: *Physical Review D* 86.2 (July 2012). DOI: 10.1103/physrevd.86.023506.

[148] Kim Griest and David Seckel. "Three exceptions in the calculation of relic abundances". In: *Phys. Rev. D* 43 (1991), pp. 3191–3203. DOI: 10.1103/PhysRevD.43.3191.

[149] Takehiko Asaka, Steve Blanchet, and Mikhail Shaposhnikov. "The nuMSM, dark matter and neutrino masses". In: *Phys. Lett. B* 631 (2005), pp. 151–156. DOI: 10.1016/j.physletb.2005.09.070. arXiv: hep-ph/0503065.

[150] Takehiko Asaka and Mikhail Shaposhnikov. "The nuMSM, dark matter and baryon asymmetry of the universe". In: *Phys. Lett.* B620 (2005), pp. 17–26. DOI: 10.1016/j.physletb.2005.06.020. arXiv: hep-ph/0505013 [hep-ph].

[151] Scott Dodelson and Lawrence M. Widrow. "Sterile neutrinos as dark matter". In: *Physical Review Letters* 72.1 (Jan. 1994), pp. 17–20. DOI: 10.1103/physrevlett.72.17. arXiv: https://arxiv.org/abs/hep-ph/9303287 [astro-ph.HE]. URL: https://arxiv.org/abs/hep-ph/9303287.

[152] M. Drewes et al. "A White Paper on keV Sterile Neutrino Dark Matter". In: *JCAP* 1701.01 (2017), p. 025. DOI: 10.1088/1475-7516/2017/01/025. arXiv: 1602.04816 [hep-ph]. URL: https://arxiv.org/pdf/1602.04816.pdf.

[153] Takehiko Asaka, Mikhail Shaposhnikov, and Alexander Kusenko. "Opening a new window for warm dark matter". In: *Phys. Lett. B* 638 (2006), pp. 401–406. DOI: 10.1016/j.physletb.2006.05.067. arXiv: hep-ph/0602150.

[154] Xiang-Dong Shi and George M. Fuller. "A New dark matter candidate: Nonthermal sterile neutrinos". In: *Phys. Rev. Lett.* 82 (1999), pp. 2832–2835. DOI: 10.1103/PhysRevLett.82.2832. arXiv: astro-ph/9810076 [astro-ph].

[155] M. Laine and M. Shaposhnikov. "Sterile neutrino dark matter as a consequence of nuMSM-induced lepton asymmetry". In: *JCAP* 06 (2008), p. 031. DOI: 10.1088/1475-7516/2008/06/031. arXiv: 0804.4543 [hep-ph].

[156] F. R. Klinkhamer and N. S. Manton. "A saddle-point solution in the Weinberg-Salam theory". In: *Phys. Rev. D* 30 (10 Nov. 1984), pp. 2212–2220. DOI: 10.1103/PhysRevD.30.2212. URL: https://link.aps.org/doi/10.1103/PhysRevD.30.2212.

[157] Alexander Kusenko. "Sterile neutrinos: The Dark side of the light fermions". In: *Phys. Rept.* 481 (2009), pp. 1–28. arXiv: 0906.2968 [hep-ph].

[158] Scott Tremaine and James E Gunn. "Dynamical role of light neutral leptons in cosmology". In: *Physical Review Letters* 42.6 (1979), p. 407.

[159] Alexey Boyarsky, Oleg Ruchayskiy, and Dmytro Iakubovskyi. "A Lower bound on the mass of Dark Matter particles". In: *JCAP* 03 (2009), p. 005. DOI: 10.1088/1475-7516/2009/03/005. arXiv: 0808.3902 [hep-ph].

[160] Aurel Schneider. "Astrophysical constraints on resonantly produced sterile neutrino dark matter". In: *JCAP* 04 (2016), p. 059. DOI: 10.1088/1475-7516/2016/04/059. arXiv: 1601.07553 [astro-ph.CO].

[161] Christophe Yèche et al. "Constraints on neutrino masses from Lyman-alpha forest power spectrum with BOSS and XQ-100". In: *JCAP* 06 (2017), p. 047. DOI: 10.1088/1475-7516/2017/06/047. arXiv: 1702.03314 [astro-ph.CO].

[162] Antonella Garzilli, Alexey Boyarsky, and Oleg Ruchayskiy. "Cutoff in the Lyman \alpha forest power spectrum: warm IGM or warm dark matter?" In: *Phys. Lett. B* 773 (2017), pp. 258–264. DOI: 10.1016/j.physletb.2017.08.022. arXiv: 1510.07006 [astro-ph.CO].

[163] Vernon D. Barger, R. J. N. Phillips, and Subir Sarkar. "Remarks on the KARMEN anomaly". In: *Phys. Lett. B* 352 (1995). [Erratum: Phys.Lett.B 356, 617–617 (1995)], pp. 365–371. DOI: 10.1016/0370-2693(95)00486-5. arXiv: hep-ph/9503295.

[164] Robert E. Shrock. "Electromagnetic properties and decays of Dirac and Majorana neutrinos in a general class of gauge theories". In: *Nuclear Physics B* 206.3 (Oct. 1982), pp. 359–379. DOI: 10.1016/0550-3213(82)90273-5.

[165] Kenny C. Y. Ng et al. "New Constraints on Sterile Neutrino Dark Matter from *NuSTAR* M31 Observations". In: *Phys. Rev. D* 99 (2019), p. 083005. DOI: 10.1103/PhysRevD.99.083005. arXiv: 1901.01262 [astro-ph.HE].

[166] Dominic Sicilian et al. "Probing the Milky Ways Dark Matter Halo for the 3.5 keV Line". In: *Astrophys. J.* 905.2 (2020), p. 146. DOI: 10.3847/1538-4357/abbee9. arXiv: 2008.02283 [astro-ph.HE].

[167] Esra Bulbul et al. "Detection of An Unidentified Emission Line in the Stacked X-ray spectrum of Galaxy Clusters". In: *Astrophys. J.* 789 (2014), p. 13. DOI: 10.1088/0004-637X/789/1/13. arXiv: 1402.2301 [astro-ph.CO].

[168] Alexey Boyarsky et al. "Unidentified Line in X-Ray Spectra of the Andromeda Galaxy and Perseus Galaxy Cluster". In: *Phys. Rev. Lett.* 113 (2014), p. 251301. DOI: 10.1103/PhysRevLett.113.251301. arXiv: 1402.4119 [astro-ph.CO].

[169] Alexey Boyarsky et al. "Checking the Dark Matter Origin of a 3.53 keV Line with the Milky Way Center". In: *Phys. Rev. Lett.* 115 (2015), p. 161301. DOI: 10.1103/PhysRevLett.115.161301. arXiv: 1408.2503 [astro-ph.CO].

[170] Shunsaku Horiuchi et al. "Sterile neutrino dark matter bounds from galaxies of the Local Group". In: *Phys. Rev. D* 89.2 (2014), p. 025017. DOI: 10.1103/PhysRevD.89.025017. arXiv: 1311.0282 [astro-ph.CO].

[171] D. Malyshev, A. Neronov, and D. Eckert. "Constraints on 3.55 keV line emission from stacked observations of dwarf spheroidal galaxies". In: *Phys. Rev. D* 90 (2014), p. 103506. DOI: 10.1103/PhysRevD.90.103506. arXiv: 1408.3531 [astro-ph.HE].

[172] Alexey Boyarsky, Oleg Ruchayskiy, and Mikhail Shaposhnikov. "The Role of sterile neutrinos in cosmology and astrophysics". In: *Ann. Rev. Nucl. Part. Sci.* 59 (2009), pp. 191–214. DOI: 10.1146/annurev.nucl.010909.083654. arXiv: 0901.0011 [hep-ph].

[173] Pasquale D. Serpico and Georg G. Raffelt. "Lepton asymmetry and primordial nucleosynthesis in the era of precision cosmology". In: *Phys. Rev. D* 71 (2005), p. 127301. DOI: 10.1103/PhysRevD.71.127301. arXiv: astro-ph/0506162.

[174] Géraldine Servant. "The serendipity of electroweak baryogenesis". In: *Phil. Trans. Roy. Soc. Lond. A* 376.2114 (2018), p. 20170124. DOI: 10.1098/rsta.2017.0124. arXiv: 1807.11507 [hep-ph].

[175] Sebastian Bruggisser et al. "Electroweak Phase Transition and Baryogenesis in Composite Higgs Models". In: *JHEP* 12 (2018), p. 099. DOI: 10.1007/JHEP12(2018)099. arXiv: 1804.07314 [hep-ph].

[176] Iason Baldes, Thomas Konstandin, and Geraldine Servant. "Flavor Cosmology: Dynamical Yukawas in the Froggatt-Nielsen Mechanism". In: *JHEP* 12 (2016), p. 073. arXiv: 1608.03254 [hep-ph].

[177] Carlos Jaramillo. "Reviving keV sterile Neutrino Dark Matter". In: *JCAP* 10 (Oct. 2022), p. 093. DOI: 10.1088/1475-7516/2022/10/093. arXiv: 2207.11269 [hep-ph].

[178] F. Bezrukov, A. Chudaykin, and D. Gorbunov. "Hiding an elephant: heavy sterile neutrino with large mixing angle does not contradict cosmology". In: *JCAP* 06 (2017), p. 051. arXiv: 1705.02184 [hep-ph].

[179] Rasmus S. L. Hansen and Stefan Vogl. "Thermalizing sterile neutrino dark matter". In: *Phys. Rev. Lett.* 119.25 (2017), p. 251305. arXiv: 1706.02707 [hep-ph].

[180] Pasquale Di Bari, Danny Marfatia, and Ye-Ling Zhou. "Gravitational waves from neutrino mass and dark matter genesis". In: (Jan. 2020). arXiv: 2001.07637 [hep-ph].

[181] Valentina De Romeri et al. "Neutrino dark matter and the Higgs portal: improved freeze-in analysis". In: (Mar. 2020). arXiv: 2003.12606 [hep-ph].

[182] Lucien Heurtier and Herve Partouche. "Spontaneous Freeze Out of Dark Matter From an Early Thermal Phase Transition". In: *Phys. Rev. D* 101.4 (2020), p. 043527. arXiv: 1912.02828 [hep-ph].

[183] Michael J. Baker et al. "Dynamic Freeze-In: Impact of Thermal Masses and Cosmological Phase Transitions on Dark Matter Production". In: *JHEP* 03 (2018), p. 114. DOI: 10.1007/JHEP03(2018)114. arXiv: 1712.03962 [hep-ph].

[184] W. Buchmüller, P. Di Bari, and M. Plümacher. "Leptogenesis for pedestrians". In: *Annals of Physics* 315.2 (Feb. 2005), pp. 305–351.

[185] Apostolos Pilaftsis and Thomas E.J. Underwood. "Resonant leptogenesis". In: *Nucl. Phys. B* 692 (2004), pp. 303–345. DOI: 10.1016/j.nuclphysb.2004.05.029. arXiv: hep-ph/0309342.

[186] G. F. Giudice et al. "Towards a complete theory of thermal leptogenesis in the SM and MSSM". In: *Nucl. Phys.* B685 (2004), pp. 89–149. DOI: 10.1016/j.nuclphysb.2004.02.019. arXiv: hep-ph/0310123 [hep-ph].

[187] Iason Baldes, Thomas Konstandin, and Geraldine Servant. "A first-order electroweak phase transition from varying Yukawas". In: *Phys. Lett. B* 786 (2018), pp. 373–377. DOI: 10.1016/j.physletb.2018.10.015. arXiv: 1604.04526 [hep-ph].

[188] Simone Blasi and Alberto Mariotti. "Domain walls seeding the electroweak phase transition". In: (Mar. 2022). arXiv: 2203.16450 [hep-ph].

[189] J. A. Casas and A. Ibarra. "Oscillating neutrinos and $\mu \to e, \gamma$". In: *Nucl. Phys. B* 618 (2001), pp. 171–204. DOI: 10.1016/S0550-3213(01)00475-8. arXiv: hep-ph/0103065.

[190] M. Aker et al. "KATRIN: status and prospects for the neutrino mass and beyond". In: *J. Phys. G* 49.10 (2022), p. 100501. DOI: 10.1088/1361-6471/ac834e. arXiv: 2203.08059 [nucl-ex].

[191] Claudio Giganti, Stéphane Lavignac, and Marco Zito. "Neutrino oscillations: The rise of the PMNS paradigm". In: *Prog. Part. Nucl. Phys.* 98 (2018), pp. 1–54. DOI: 10.1016/j.ppnp.2017.10.001. arXiv: 1710.00715 [hep-ex].

[192] Kerstin Perez et al. "Almost closing the νMSM sterile neutrino dark matter window with NuSTAR". In: *Phys. Rev. D* 95.12 (2017), p. 123002. DOI: 10.1103/PhysRevD.95.123002. arXiv: 1609.00667 [astro-ph.HE].

[193] Benedict von Harling and Geraldine Servant. "Cosmological evolution of Yukawa couplings: the 5D perspective". In: *JHEP* 05 (2017), p. 077. DOI: 10.1007/JHEP05(2017)077. arXiv: 1612.02447 [hep-ph].

[194] Lisa Randall and Raman Sundrum. "A Large mass hierarchy from a small extra dimension". In: *Phys. Rev. Lett.* 83 (1999), pp. 3370–3373. DOI: 10.1103/PhysRevLett.83.3370. arXiv: hep-ph/9905221.